Professorship of Human Spaceflight Technology
TUM School of Engineering and Design
Technical University of Munich

Development of the Atmosphere Management System for the Lunar Agricultural Module – Ground Test Demonstrator LAM -GTD

Master's Thesis by Paul Guastavino

HSP 2024-12

Scientific thesis to obtain the degree

M.Sc Earth Oriented Space Science and Technology

at the TUM School of Engineering and Design of the Technical University of Munich.

Supervisor	**Prof. Dr. Gisela Detrell**
	Human Spaceflight Technology
Task provider	**Dr. Daniel Schubert, Michel Franke, Tobias Korth**
	EDEN Research Group
Submitted by	**Paul Guastavino**
	03740602
Submitted on	**Munich, 31.03.2025**

Professorship of Human Spaceflight Technology
TUM School of Engineering and Design
Technical University of Munich

Task Description Master Thesis
for Paul Guastavino

Development of the Atmosphere Management System for the Lunar Agricultural Module – Ground Test Demonstrator LAM -GTD

Topic Description:
With the future of human space exploration leading us to colonise the Moon and Mars it is imperative to keep developing our capabilities to grow nutritional food outside of our Planet for future explorers. In this thesis, I will give a summary of the current state of the EDEN ISS project deployed in Antarctica. Specifically focusing on the Atmosphere Management System, I will complete a full analysis of the current system in EDEN ISS and design an improved version of the Atmosphere Management System for LAM-GTD, Starting from the inlet (from the habitation module to the Farm module) and ending at the outlet to the vents in the LAM-GTD. This will include calculations to support the sizing of the system, and a 3D model of the entire system.

Tasks:

- Give a summary of the EDEN ISS Project with an in-depth look at its Atmosphere management system (AMS), including each of its components and how they all work together.
- Get a thorough understanding of the current state of LAM-GTD
- Design a new and improved AMS complete with calculations to support my design choices
- Complete a Full CAD/Solidworks/Rhino model of the AMS that could be used for the manufacturing of the system

Supervisor: Prof. Gisela Detrell
External Supervisor: (DLR)

Start of Thesis: 01.10.2024

Submission of Thesis: 01.04.2025

I hereby confirm that I have read and understood the task description and the legal framework for the thesis specified in the General Academic and Examination Regulations (ASPO) and the Departmental Examination and Academic Regulations (FPSO).

Prof. Dr.-Ing. Gisela Detrell (Responsible Professor)	Mr Michel Franke and Mr Tobias Korth (External Supervisor)	Student Signature

Professorship of Human Spaceflight Technology
TUM School of Engineering and Design
Technical University of Munich

Declaration of own work

I hereby declare that I have written the thesis submitted by me independently and have not used any sources and aids other than those specified.

Munich, 31/03/2025

Place, date, signature

This page intentionally left blank

Table of Contents

Abstract

Long-duration space missions and the establishment of permanent extraterrestrial habitats demand robust, sustainable life support systems. Controlled Environment Agriculture is pivotal in meeting both the nutritional and psychological needs of astronauts, while simultaneously contributing to closed-loop life support. This thesis presents a novel design and comprehensive analysis of an advanced Atmosphere Management System (AMS) for the Lunar Agricultural Module – Ground Test Demonstrator, a terrestrial prototype engineered to simulate lunar agricultural conditions.

Building on insights from pioneering projects such as the EDEN ISS Mobile Test Facility and the Advanced Plant Habitat, the proposed AMS integrates enhanced temperature, humidity, and gas regulation strategies to ensure optimal environmental conditions for both plant growth and crew safety. Notable innovations include an optimized dehumidification subsystem, improved air distribution through localized fan arrays, and a modular design that enhances system redundancy and simplifies maintenance. Detailed computational modelling and a full CAD model support the design choices.

The advancements presented in this work address critical challenges such as under-dimensioned cooling capacity, microbial contamination, ethylene detection and improved crop evapotranspiration modelling, thereby contributing to the development of robust Bioregenerative Life Support Systems for future lunar and deep-space missions.

Acknowledgement

I would like to thank Professor Gisela Detrell and Dr. Daniel Schubert for giving me the opportunity to work on such an interesting project. I would also like to express my gratitude towards Michel Fabien Franke and Tobias Korth for their generous support throughout this thesis and for welcoming me into the team.

Additionally, I want to express my immense gratitude towards my parents, Isabelle and Louis, who always encouraged me to study, to dream big and chase those dreams. They gave me the greatest treasure I could have ever wished for: my Brothers and Sisters, Nicolas, Marie, Baptiste, Odette and Pernelle who have always been there to support me no matter what. I could not have done any of this without them.

List of Figures

List of Tables

Nomenclature

List of Abbreviations

- **ACH – Air Changes per Hour**
- **AMS – Atmosphere Management System**
- **APH – Advanced Plant Habitat**
- **BLSS – Bioregenerative Life Support System**
- **CDHS / DHCS – Data Handling and Control System**
- **CEA – Controlled Environment Agriculture**
- **CFM – Cubic Feet per Minute**
- **CHX – Condensing Heat Exchangers**
- **CO_2 – Carbon Dioxide**
- **CQ – Crew Quarters**
- **DLR – German Aerospace Center**
- **EDEN ISS MTF – EDEN ISS Mobile Test Facility**
- **EDEN LUNA – EDEN LUNA Project**
- **EPS – Electrical Power Supply**
- **ET (ET_0) – Evapotranspiration (Reference Evapotranspiration)**
- **FEG – Future Exploration Greenhouse**
- **g_M – Lunar Gravitational Acceleration**
- **HabSim – Habitat Simulator**
- **HEPA – High Efficiency Particulate Air**

- **ILS – Illumination System**
- **IMV – Intermodular Ventilation**
- **ISS – International Space Station**
- **LAM-GTD – Lunar Agriculture Module – Ground Test Demonstrator**
- **LMTD – Log Mean Temperature Difference**
- **LSS – Life Support System**
- **MTF – Mobile Test Facility**
- **NASA – National Aeronautics and Space Administration**
- **NDS – Nutrient Delivery System**
- **O_2 – Oxygen**
- **PCDS – Power Control and Distribution System**
- **PHM – Prognostics and Health Management**
- **PI – Polyimide**
- **PSA/VSA – Pressure or Vacuum Swing Adsorption**
- **RH – Relative Humidity**
- **Re – Reynolds Number**
- **TCS – Thermal Control System**
- **TPMS – Triply Periodic Minimal Surface**
- **UV-C – Ultraviolet-C**
- **VOC – Volatile Organic Compounds**
- **VPD – Vapor Pressure Deficit**

1. Introduction

As Civilizations push the boundaries of space exploration and undertake long-duration missions to explore the Moon and Mars, the development of sustainable life support systems becomes essential. The ability to grow food in extraterrestrial environments not only addresses logistical challenges of resupply but also contributes to crew health, morale, and psychological well-being [2][67]. Controlled Environment Agriculture (CEA) is at the forefront of these developments, offering a method to produce crops efficiently while offering life support in the form of air revitalisation and recycling organic waste in a closed-loop system.

The Lunar Agriculture Module – Ground Test Demonstrator (LAM-GTD) serves as a prototype platform to evaluate the performance of all systems required for future space farms among which an integrated Atmosphere Management System (AMS) will constitute the focal point of this thesis. This thesis presents the design, calculation, and critical analysis of the AMS, which regulates parameters such as temperature, humidity, CO_2, and O_2 concentrations to sustain optimal plant growth conditions.

Atmospheric management in extraterrestrial agriculture is uniquely challenging due to closed-loop dynamics, variable thermal loading, and constrained energy budgets. Factors such as plant transpiration, microbial growth, air quality, and equipment-generated heat necessitate a system that is not only technologically advanced but also highly adaptable. As such, this research builds upon previous systems such as the EDEN ISS Mobile Test Facility (MTF) in Antarctica, the Advanced Plant Habitat (APH) on the ISS, and the Lunar Palace 1 in China. These pioneering efforts provide invaluable insights into CEA operations under isolated, remote conditions.

The specific objectives of this thesis include:

- Get a thorough understanding of previous research into extraterrestrial CEA
- Improve the modelling of crop evapotranspiration to better understand the dehumidifiers requirements
- Design a new and improved AMS complete with calculations to support the design choices
- Develop a detailed CAD model of the system for prototyping and manufacturing purposes.
- Propose scalable improvements for lunar agricultural

2. Theory

2.1. Literature Review: Atmosphere Management and Life Support Systems for Hydroponic Lunar Farms

2.1.1. Life Support System Foundations

In this next chapter, we will be looking at the past work done on sustainable life support systems (LSS) and CEA as they are essential technologies for long-duration missions. LSS are technologies designed to sustain human life in space by managing critical elements like air, water, food, temperature, and waste.
Hydroponic lunar farms are often envisioned as a major part of future extraterrestrial habitats as they can be used in four of the main LSS responsibilities, namely in air revitalization, food production, water recycling and waste recycling. Additionally, many studies show that being in proximity with plants has significant psychological benefits for humans, something which is of great value in extended space missions [67].
Their integration into a space station will mark the continuation of Bioregenerative Life Support Systems (BLSS) which is a critical technology to continue developing closed loop systems, where all available resources are reused/recycled, allowing for longer duration missions and saving on resupply mass and cost. This concept is illustrated below in Figure 2.1.1.

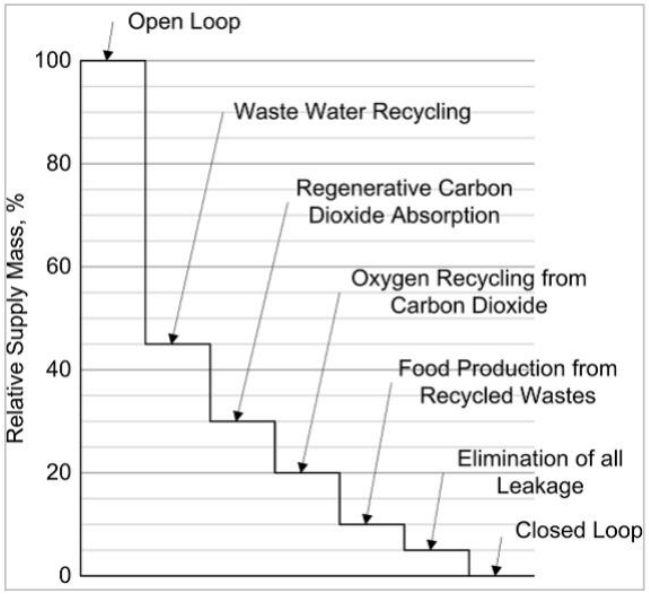

Figure 2.1.1 - Life support system foundation [1]

Closed-loop systems are essential for long term space exploration missions as historically, LSS aboard spacecraft relied heavily on mechanical and chemical processes which were dependant on consumables. For example, The ISS relies on a partially regenerative air revitalization system comprising electrolysis-based oxygen generation, pressure swing adsorption for CO_2 removal, trace contaminant filtration, and Sabatier reactors for limited water recovery. While effective for near-Earth missions, this system still depends on periodic resupply [68]. The aim of closed-loop systems is to eliminate resupply as the further away we get from Earth the more impractical and expensive they become.

2.1.2. The Role of Controlled Environmental Agriculture in Space exploration

CEA employs controlled growing environments, such as hydroponics, aeroponics, and advanced substrate based growing techniques, to cultivate edible plants under regulated conditions involving light, temperature, humidity, and nutrients. The integration of CEA into LSS on spacecraft or extraterrestrial habitats, such as space, lunar or Martian colonies is known as biological life support system (BLSS), this technology presents considerable advantages. Firstly, plants actively support air revitalization through photosynthesis, converting exhaled carbon dioxide back into breathable oxygen, thus reducing reliance on electrochemical oxygen generators [68]. Additionally, plants contribute significantly to water recycling through phytofiltration, a natural process whereas the water passes through the plant it is filtered by the roots and xylem ultimately evaporating pure water, which is the collected and recirculated in the system [88]. Lastly on very long-term missions composting the grown non-edible organic matter in conjunction with other organic waste can be used to enrich extraterrestrial substrates in order to create more potential growing space [54].

NASA's Vegetable Production System (Veggie), installed on the International Space Station, demonstrates CEA's feasibility in space environments. This system has successfully grown crops such as lettuce, kale, and even flowers, providing astronauts with essential nutrients and psychological benefits from tending to living organisms [2] [3]. The Advanced Plant Habitat (APH), also aboard the ISS, advances this capability by offering precise environmental controls, including lighting, temperature, and humidity, creating optimal conditions for plant growth experiments aimed at future missions to the Moon and Mars [10].

Despite these successes, several challenges remain. Plants in microgravity environments experience issues such as impaired root development and nutrient delivery anomalies. Ongoing research continues to tackle these hurdles, as evidenced by experiments such as NASA's TROPI-1 and TROPI-2, designed to study how gravity or lack thereof affects plant orientation and growth patterns [69].

Looking ahead, the integration of CEA into LSS is increasingly seen as essential. BLSS create closed-loop ecological systems where plants, algae, microbes, and human habitats mutually benefit and sustain each other, significantly reducing the need for external resupply missions [68].

2.2. Existing Space Farm Projects

2.2.1. Veggie Plant Growth System (NASA, 2014–Present)

History

The Veggie Plant Growth System shown in Figure 2.2.1 was developed collaboratively by NASA and Orbital Technologies Corporation (ORBITEC). It marked a significant advancement in space agriculture when it launched aboard SpaceX CRS-3 in 2014. Following its successful deployment on the ISS, Veggie undertook the task it was specifically engineered for; to cultivate crops in microgravity environments using minimal resources. This made it an ideal technological demonstrator for future long-duration space exploration missions. Initial experiments successfully produced red romaine lettuce, zinnias which served as a model for studying flowering processes in microgravity. Subsequent iterations of Veggie expanded crop capabilities further, successfully testing more complex plants such as radishes and chili peppers and mustard greens.

Notable Achievements

Veggie made history by cultivating red romaine lettuce, becoming the first edible crop grown in space and consumed by astronauts in 2015. This milestone demonstrated the feasibility of supplementing traditional astronaut diets with fresh produce grown directly in space. Furthermore, Veggie showcased its versatility by expanding crop variety to include zinnias, radishes, and chili peppers, confirming that a range of plants can successfully be cultivated under microgravity conditions. Additionally, astronauts reported significant psychological benefits from interacting with live plants, underscoring the value of space-grown crops beyond nutritional supplementation. These interactions enhanced crew morale and provided emotional support during extended missions.

Lessons Learned

The implementation of Veggie provided valuable insights into managing resources effectively in space. Early challenges highlighted the importance of sophisticated water management systems, specifically emphasizing the necessity of controlled wicking techniques and specially designed growth substrates to ensure optimal water distribution in microgravity. Additionally, initial experiments brought attention to the critical importance of maintaining sterile environments to mitigate microbial contamination, mold, and other potential health risks. Finally, active engagement with the plant growth system demonstrated clear psychological advantages, as astronauts exhibited improved morale and mental health through interactions with fresh, space-grown plants, reinforcing the all-inclusive benefits of integrating agriculture into human space exploration [2] [3].

Figure 2.2.1 - Veggie Plant Growth System [72]

2.2.2. EDEN ISS Mobile Test Facility (EDEN ISS MTF) (European Union, 2015–2024)

History

The EDEN ISS facility, shown in Figure 2.2.2, was developed by the DLR in close collaboration with numerous international partners, designed explicitly to evaluate plant cultivation technologies in extreme and isolated environments. Situated in Antarctica, EDEN ISS served as an effective terrestrial analogue, simulating the challenging conditions anticipated in space habitats, including lunar and Martian bases. Equipped with advanced hydroponic systems, energy-efficient LED lighting, and sophisticated atmosphere management systems, the facility provides a realistic platform for testing and validating space-bound agricultural solutions. Since its initial operation in 2018, EDEN ISS has conducted numerous experiments throughout multiple Antarctic overwintering seasons, generating valuable insights into sustainable food production for future space exploration missions.

Notable Achievements

EDEN ISS achieved remarkable crop yields, successfully producing 269 kilograms of fresh vegetables in its first year and over one tonne over its whole deployment, all of this under harsh Antarctic conditions. Notably, the crops included a diverse selection, such as cucumbers, tomatoes, and various leafy greens, demonstrating significant agricultural productivity in an isolated and resource-limited environment. Moreover, EDEN ISS effectively demonstrated the integration of advanced atmospheric control measures within a closed-loop environment. These measures encompassed comprehensive air filtration, precise carbon dioxide (CO2) regulation, and meticulous humidity management, all crucial for sustaining plant growth and productivity. Furthermore, EDEN ISS developed critical operational protocols and maintenance routines, valuable analogues for potential procedures in future lunar or Martian missions, showcasing practical approaches for crop handling and system upkeep under extreme isolation.

Lessons Learned

Operational experiences from the EDEN ISS MTF facility underscored several critical lessons for extraterrestrial agriculture. First and foremost, maintaining precise environmental control emerged as essential for ensuring consistent plant health and crop yield. This emphasised the necessity for redundancy in atmosphere management systems, allowing continued plant productivity despite potential component failures or environmental fluctuations. Secondly, observations from crop cultivation revealed that while crops such as tomatoes, cucumbers, and leafy greens were highly successful, each plant variety required distinct nutrient formulations and specific environmental settings to thrive optimally. These insights emphasized the importance of tailored approaches for diverse crop types within controlled agricultural systems. Lastly, experiences involving failures in power systems highlighted the imperative for robust backup systems and comprehensive maintenance protocols, particularly vital in isolated or remote settings where immediate external support may not be feasible, reinforcing the significance of resilience and redundancy in system design for space missions [4] [5].

Figure 2.2.2 - EDEN ISS Mobile Test Facility [5]

2.2.3. Lunar Greenhouse (University of Arizona, NASA, 2009–2013)

History

The Lunar greenhouse shown in figure 2.2.3 emerged from the broader goal of achieving self-sufficiency for long-term extraterrestrial habitats. Early research, built on lessons from terrestrial closed-loop system experiments like Biosphere 2 [73], to develop a controlled-environment agriculture for the Moon's extreme conditions. This led to the development of a multi-crop lunar greenhouse prototype

Notable Achievements

One of the most significant technical accomplishments was the adaptation of the energy cascade model for a multi-crop setting. This model provided critical insights into managing the interdependent flows of light, heat, and other forms of energy, ensuring that the greenhouse could operate with maximum efficiency even under lunar constraints. This data driven approach allowed for precise calculation regarding, daily biomass increase, water consumption, CO_2 consumption and power consumption. The Lunar Greenhouse ultimately achieved an average of 24g of edible biomass per kWh.

The prototype also demonstrated the feasibility of cultivating a diversity of crops in a single closed system which is a key requirement for sustaining a crew on long-duration missions. This diversity is essential not only for nutritional balance but also for maintaining ecological stability within the greenhouse. The prototype used principles learned from Earth-based closed systems to implement advanced techniques for recycling water, nutrients, and waste.

Lessons Learned

The Lunar Greenhouse project's development process provided valuable insights into the challenges and practicalities of extraterrestrial agriculture. One key takeaway was the necessity of an integrated design that addresses energy input, resource recycling, and crop production simultaneously. The interplay between light, temperature, and plant metabolism must be carefully managed for a sustainable

operation. Additionally, the Lunar greenhouse studies highlight the need for automation, not only to reduce crew workload but also to maintain optimal environmental conditions continuously. Automated control of lighting, temperature, and nutrient delivery is critical for long-duration missions. Finaly, the move toward a multi-crop, modular greenhouse has reinforced the value of designing systems that can be expanded or adapted over time. As mission parameters evolve, the greenhouse must be able to adjust its operations and scale its output accordingly. [6] [7].

Figure 2.2.3 - Lunar Greenhouse [6]

2.2.4. Lunar Palace 1 (China, 2013–2018)

History

Lunar Palace 1 shown in figure 2.2.4 is a pioneering BLSS developed by Beihang University to advance sustainable human habitation technologies for space exploration. The facility consists of two dedicated plant cultivation modules and an integrated living area designed to support human occupants. Through extensive experimental campaigns, Lunar Palace 1 has rigorously evaluated closed-loop life support capabilities, notably conducting significant trials lasting 105 days and a groundbreaking 365-day mission. These long-duration experiments aimed to demonstrate the feasibility of sustained human life in isolated and resource-limited environments, closely simulating conditions expected in future extraterrestrial settlements.

Notable Achievements

A hallmark achievement of Lunar Palace 1 was the completion of the longest continuous bioregenerative life support experiment to date, successfully supporting three crew members for an entire 365-day cycle. This trial decisively demonstrated the long-term viability of closed-loop ecological systems for sustaining human life, significantly advancing the field of space habitation technology. Remarkably, Lunar Palace 1 achieved a near-perfect efficiency in recycling critical resources. The system

accomplished 100% recycling of oxygen and carbon dioxide through the integrated use of higher plants and photobioreactors. Additionally, it achieved an impressive 85% recycling rate of water and solid waste, demonstrating exceptional resource efficiency. The facility also proved highly versatile, successfully cultivating a diverse range of 35 types of plants, including essential staple crops such as wheat and a variety of fruits and vegetables, providing balanced nutrition for its human inhabitants in a completely enclosed environment.

Lessons Learned

One of the primary insights was the critical need for maintaining a precise balance among all subsystems. Small imbalances in one area (e.g., nutrient cycles or microbial populations) can have cascading effects on the entire ecosystem, underscoring the need for robust monitoring and control systems. Additionally, the system highlighted the importance of incorporating redundancy and adaptive management strategies. These design principles are essential to cope with unforeseen challenges, ensuring that critical life support functions can be maintained even if one component fails.
Most importantly the successful operation of the facility served as a proof-of-concept that long term closed-loop systems are a viable concept for space exploration, with some models predicting that this BLSS could last an estimated 52 years (with a 95% confidence interval) under normal operation and maintenance. [8] [9] [75]

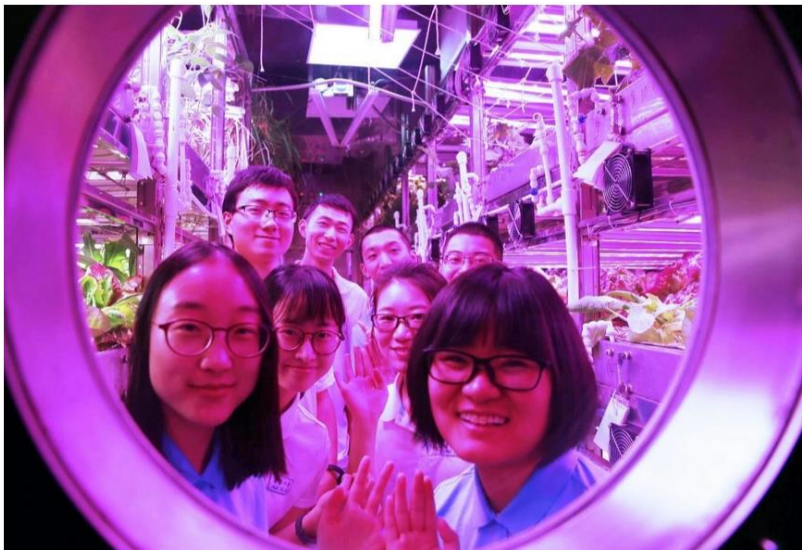

Figure 2.2.4 - Lunar Palace 1 [74]

2.2.5. Advanced Plant Habitat (NASA, 2017–Present)

History

The APH, shown in figure 2.2.5, installed aboard the ISS in 2017, represents NASA's most sophisticated and largest plant cultivation chamber to date. Engineered to facilitate meticulous research in plant biology under microgravity conditions, the APH provides unparalleled precision in environmental controls. It allows rigorous regulation of crucial parameters including temperature, humidity, oxygen, and carbon dioxide concentrations, as well as precise control over lighting intensity and photoperiod. The initial experiments utilizing APH primarily focused on model organisms like Arabidopsis,

widely recognized in biological studies, as well as economically important crops such as wheat, aiming to uncover foundational biological responses to space environments.

Notable Achievements

One of the defining achievements of the APH system has been its ability to maintain a highly precise, automated environment, ensuring detailed control over environmental conditions critical for plant growth and development. This precision has facilitated in-depth investigations into plant responses to microgravity and space conditions. Through carefully managed experiments, APH contributed significantly to scientific knowledge, identifying genetic and epigenetic modifications in Arabidopsis and wheat resulting from exposure to microgravity. These findings are pivotal, enhancing our fundamental understanding of plant biology and adaptation mechanisms relevant to future space agriculture. Moreover, the APH has set new benchmarks for data collection in space agriculture, employing advanced sensor technology to generate extensive real-time data on plant growth dynamics. This unprecedented level of data collection significantly improves the scientific community's ability to analyse and interpret plant behaviour in space.

Lessons Learned

Experiences from the APH have yielded valuable insights into the genetic and epigenetic impacts of microgravity on plants, highlighting significant adaptive mechanisms at a molecular level. These insights are essential for the development of resilient plant varieties suited for future extraterrestrial agricultural systems. Furthermore, the APH's highly automated and sophisticated remote sensing capabilities have underscored the benefits of robust data collection systems, enabling scientists to capture comprehensive datasets that surpass the capabilities of previous plant growth platforms. Lastly, the complexity and high precision requirements of the APH emphasized the necessity for modular design strategies. Modular systems facilitate easier maintenance and quicker replacement or repair of components in the event of system failures, essential for maintaining continuous, reliable operations during long-duration space missions [10] [11].

Figure 2.2.5 - Advanced Plant Habitat [100]

2.2.6. Overarching Themes Across Projects

Analysing these space centric CEA projects allows us to pinpoint several overarching themes which have consistently emerged, highlighting critical considerations for the development and implementation of CEA systems for future long term space missions.

Redundancy and Reliability

A key lesson observed in all controlled environment agriculture projects for space applications is the extreme importance of redundancy and reliability. Due to the isolated and resource-constrained conditions typical of space environments, robust backup systems and redundancy protocols become indispensable. Systems must be designed with multiple layers of fail-safes, enabling rapid recovery from unexpected failures to ensure continuous operation. Whether managing atmospheric controls, nutrient delivery, or lighting systems, redundancy significantly enhances the reliability and resilience of the agricultural systems, which will ensure the safety and longevity of the crew in harsh extraterrestrial locations.

Robust Monitoring and Control Systems

A very important takeaway was that fact that maintaining a precise balance among all subsystems is crucial to ensure nominal operation of the BLSS over long-term missions. Small imbalances in any one area could lead to increasingly negative effects on the entire ecosystem, underscoring the need for a robust monitoring and control systems to deal with a problem as soon as it arises.

Customization for Crops

Another prominent theme identified is the necessity of tailored cultivation approaches for different crops. Each plant species possesses unique requirements concerning lighting intensity and spectral composition, nutrient availability, water distribution, and airflow management. The flexibility and adaptability of agricultural system designs are therefore essential. Proper care must be taken to design a schedule that can enable varying plants to thrive together to create a more diverse ecosystem. Additionally, systems must be capable of precise adjustments in environmental parameters to accommodate varying plant needs, optimizing crop yield and quality. This customization ensures sustainable food production, providing balanced nutrition and enhancing dietary variety for astronauts on extended missions.

Psychological Benefits

The psychological advantages of plant cultivation in space environments have also been consistently highlighted across various projects. Access to fresh, self-grown food significantly improves dietary quality and provides essential nutrients that pre-packaged space foods often lack. Additionally, engaging directly with plants has demonstrated measurable mental health benefits for astronauts and analogue participants. These interactions with living organisms offer emotional support, reduce stress, and combat feelings of isolation and confinement, ultimately enhancing overall crew morale and mental well-being.

Energy Efficiency

Energy efficiency remains an ongoing challenge in CEA systems designed for space habitats. High demands from essential components such as artificial lighting and climate control systems require significant energy inputs. Advancements in efficient LED lighting technologies, optimized power management systems, and innovative thermal management solutions have become critical to the success of BLSS. Improving energy efficiency not only reduces the reliance on limited external resources but also facilitates the practical implementation of agricultural systems within constrained power budgets, crucial for sustained long-term space habitation.

Conclusion

Across the diverse range of CEA systems studied, significant advancements have been made toward achieving sustainable agricultural production in extraterrestrial environments. Each of these systems has played a pivotal role as an integral component of life support by effectively integrating food production, air revitalization, water recycling, and waste management in closed-loop or semi-closed-loop settings.

Moving forward, the lessons learned from these pioneering space farming projects must inform the design and implementation of the next generation of extraterrestrial agricultural systems. By synthesizing insights related to redundancy, customization, psychological impact, and energy efficiency, future space farms can become even more resilient, productive, and supportive of long-duration missions. Ultimately, the ongoing refinement of CEA as a BLSS will significantly enhance humanity's capacity for sustained space exploration, paving the way for permanent human presence on the Moon, Mars, and beyond.

2.3. Benefits of Space research for humanity and Terrestrial Applications of Vertical Farming

A common misconception promoted by mainstream media is the idea that funding dedicated to space research diverts resources away from fundamental human needs; however, this perspective is inaccurate. In reality, investments in the space industry have significantly enhanced everyday life, positively impacting various aspects of human society. Below are several examples:

2.3.1. Health and Medicine

Technologies originally designed for space missions have significantly advanced medical imaging and diagnostic capabilities on Earth. Innovations such as infrared ear thermometers, which provide rapid and accurate temperature readings, and enhanced imaging techniques like MRI and CT scans have improved diagnostic precision and healthcare quality. Additionally, materials and robotics initially created for space environments have been successfully adapted into sophisticated prosthetic limbs and advanced rehabilitation equipment, offering improved comfort, functionality, and mobility for amputees and individuals undergoing physical therapy [13].

2.3.2. Environmental Monitoring and Management

Environmental Monitoring and Management Space technology has greatly contributed to environmental monitoring and resource management. Satellites now provide critical and comprehensive data

regarding climate change, pollution levels, deforestation, and natural disaster patterns, aiding global environmental protection efforts and informed decision-making. Additionally, innovations in water recycling technology developed for use aboard spacecraft have been adapted for terrestrial applications. These water purification systems now offer effective solutions to provide clean drinking water in regions that previously lacked access to reliable water sources, thus greatly improving public health outcomes [13][14].

2.3.3. Technology and Consumer Products

Research conducted in microgravity environments has facilitated the development of advanced materials characterized by increased strength and reduced weight. These innovations have been effectively integrated into consumer products, such as durable sports equipment, lightweight and sturdy household items, and even more efficient vehicles. Furthermore, protective coatings originally engineered for space applications have been adapted for terrestrial use, resulting in the creation of highly durable, scratch-resistant lenses for eyewear, significantly enhancing their longevity and usability [13].

2.3.4. Communication and Navigation

Communication and Navigation Satellite technology has dramatically transformed global communication and navigation infrastructure. Advances in satellite communications have enabled comprehensive global connectivity, allowing for precise GPS navigation, reliable satellite television broadcasting, and widespread internet access, even in remote and previously underserved areas. Moreover, satellites play a crucial role in disaster management by providing vital data for predicting and tracking natural disasters, facilitating effective emergency preparedness, and improving response strategies to safeguard human lives and mitigate damage [14][15].

2.3.5. Economic and Educational Impact

The growth of the space industry has spurred significant economic development through the creation of high-tech jobs and fostering new sectors and technological innovations. The continuous expansion and investment in space-related activities stimulate economic productivity and encourage new business opportunities. Additionally, the achievements and challenges associated with space exploration serve as powerful educational inspirations, motivating students and individuals to pursue education and careers in Science, Technology, Engineering, and Mathematics (STEM) fields. This influence cultivates a culture of scientific curiosity, innovation, and creativity, essential for addressing future technological and societal challenges [14][16].

2.3.6. Vertical Farms

This thesis explores CEA which is essential to vertical farming, highlighting the broad array of spin-off technologies and applications associated with this innovative approach. While vertical farming is critically important for supporting human exploration beyond Earth, it simultaneously offers profound benefits for improving sustainability in terrestrial urban environments. The implementation of vertical farming techniques yields numerous substantial advantages:

1. **Year-Round Crop Production:** Vertical farming systems operate within precisely controlled indoor environments, allowing continuous, year-round cultivation of high-quality crops.

Unlike conventional agriculture, vertical farms remain unaffected by seasonal fluctuations, adverse weather conditions, droughts, floods, or extreme temperatures. This reliability ensures stable and predictable food supplies irrespective of external climate variability.

2. **Efficient Space Utilization:** A hallmark feature of vertical farming is its efficient use of limited space by vertically stacking multiple layers of crops. This stacking capability significantly enhances crop yield per unit area, making vertical farming especially suitable for densely populated urban areas with scarce or expensive land resources. Consequently, vertical farms can significantly increase food production capacity within urban centers without requiring additional land clearance or expansion.

3. **Water Conservation:** Vertical farms commonly employ hydroponic or aeroponic systems, which utilize nutrient-rich water solutions or mist to nourish plants directly. These advanced systems substantially reduce water consumption, often achieving water savings of up to 90% compared to traditional farming methods. In such closed-loop systems, water is continually recycled and reused, dramatically reducing the environmental impact and resource consumption associated with food production.

4. **Reduced Pesticide Use:** Due to their enclosed and highly controlled environments, vertical farms are inherently protected from common agricultural pests and diseases. This natural isolation significantly minimizes or even eliminates the need for chemical pesticides. The reduction in pesticide use not only results in healthier, chemical-free produce but also contributes to safer working conditions for farm staff and a reduced ecological footprint.

5. **Proximity to Urban Centers**: Vertical farms can be strategically located near or within urban areas, significantly reducing the distance between food production sites and consumers. This proximity minimizes transportation requirements, cutting down both transportation costs and associated carbon emissions. As a result, urban populations gain access to fresher, more nutritious produce, enhancing food security and reducing the environmental impacts of traditional food logistics.

6. **Environmental Sustainability:** Vertical farming offers significant ecological advantages by relieving pressure on conventional farmland, thus providing opportunities for reforestation, biodiversity conservation, and natural habitat restoration. By producing food efficiently in urban areas, vertical farming contributes directly to reducing agricultural land usage, mitigating deforestation, and supporting the broader health of ecosystems. Ultimately, this practice promotes greater ecological balance and sustainability, enhancing overall environmental resilience [17].

2.4. Challenges of Controlled Environmental Agriculture for Extraterrestrial Farm Development

2.4.1. Altered Gravity

One of the primary challenges of establishing extraterrestrial farms is altered gravity conditions. For instance, on the Moon, gravity is approximately one-sixth that of Earth, significantly impacting biological and physical processes vital for agriculture. On Earth, gravity facilitates natural convection currents driven by temperature-induced density variations, effectively distributing heat and gases. Under reduced gravity conditions, such natural convection currents are severely suppressed, disrupting the typical dispersion of gases such as carbon dioxide. Without carefully engineered ventilation systems,

exhaled carbon dioxide may accumulate around astronauts, presenting significant health risks such as respiratory difficulties or even carbon dioxide poisoning. To mitigate these risks, it becomes essential to design and implement robust artificial air circulation systems capable of effectively mixing and redistributing atmospheric gases. This engineered ventilation not only ensures air quality but also helps regulate internal temperature, humidity, and the removal of potentially harmful trace gases within the habitat [21].

2.4.2. Radiation Exposure

Another substantial challenge is the elevated exposure to ionizing radiation beyond Earth's protective atmosphere. High radiation levels in space environments, including cosmic rays and solar flares, can severely damage plant cellular structures, harm DNA, and disrupt critical biological processes, potentially reducing crop yield or viability [19]. To safeguard plant life and ensure successful cultivation, effective shielding strategies must be employed. One practical solution involves using lunar regolith, the loose layer of soil and rock fragments on the Moon's surface, as a protective barrier. Studies indicate that constructing a lunar base beneath a regolith covering of at least 50 centimeters significantly reduces radiation exposure, creating a safer environment for both crops and crew. Additionally, this regolith layer provides a dual functionality by offering protection against micrometeoroids, small high-velocity space debris that poses significant risks to structures and life in extraterrestrial settings [20] [70].

2.4.3. Resource Availability and Cultivation Techniques

Resource scarcity presents another critical challenge for extraterrestrial agricultural development. Essential resources such as water, nutrients, sunlight, and carbon dioxide, which are abundant or readily accessible on Earth, become severely constrained in space environments. Every resource must be viewed as precious and meticulously conserved, recycled, and efficiently utilized. Addressing these constraints requires advanced solutions, including closed-loop recycling systems capable of capturing, purifying, and reusing water and nutrients with minimal loss. Heat recovery systems further enhance resource efficiency by harnessing and redistributing thermal energy within habitats. Additionally, the limited availability of natural sunlight, particularly during the Lunar night or with Martian habitats, necessitates the integration of advanced lighting technologies such as LEDs optimized for plant growth while minimizing energy consumption. Moreover, optimized power distribution systems become critical to ensure the sustainable operation of resource-intensive agricultural modules. Cultivation techniques must also evolve, embracing innovative approaches such as vertical hydroponics and aeroponics, which maximize space utilization and water efficiency, thus enabling the sustainable production of food under resource-limited extraterrestrial conditions [9] [54].

2.5. Lunar Agriculture Module - Ground Test Demonstrator (LAM-GTD)

The LAM-GTD is a cutting-edge project developed to simulate, test, and advance technologies for future lunar agriculture modules. It is designed as a testbed for the Lunar Agriculture Module (LAM) to mature technologies and operational concepts for growing plants in a controlled environment on the Moon [22]. LAM-GTD aims to build on the past successes of EDEN ISS MTF to achieve the following objectives:

- Demonstrate ground-based bio-regenerative life support with independent fresh food production for humans.
- Provide a high level of autonomy (using robotic support).
- Support related terrestrial applications in harsh environments.
- Advance research on microbiomes, crop growth modeling, and technical-biological interactions.
- Include contributions from global institutional and industry partners.
- Provide a minimum of 10% of calorie intake for a three-person crew at the end of the demonstrator mission.

The current concept would place the inauguration of the LAM-GTD in about 2028, after which it would be operated for at least three years enabling the development of an actual LAM.

2.5.1. Design Methodology

A key foundation of the current design is a Concurrent Engineering (CE) study conducted in March 2024 at the Concurrent Engineering Facility (CEF) of the German Aerospace Center (DLR) in Bremen, Germany, following an initial study in September 2022 [79]. A comprehensive overview of the CE process used by DLR is available in [77], with additional insights into the broader design approach detailed in [78].

The CE process is iterative and collaborative, combining moderated sessions focused on key topics with offline work, during which participants tackle individual tasks or engage in smaller, specialized discussions to address specific design challenges.

The design team includes domain experts, engineers, scientists, and students, ensuring that all relevant perspectives are incorporated. A shared data model helps align the team's understanding of the system and allows early identification of potential issues, such as power requirements or spatial constraints.

Following the CE study, the design process has continued through trade-off analyses, refinement of system requirements, and adjustments to the module's layout, supported by ongoing collaboration between all involved experts.

LAM-GTD will comprise of 8 main subsystems to make it fully operational, these are the following**:**

2.5.2. Atmosphere Management System (AMS)

- **Purpose**: Maintains optimal atmospheric conditions, including temperature, humidity, and gas composition (CO_2, O_2, etc.), ensuring plant growth and human safety.
- **Component**s: Dehumidifier, HEPA filters, VOC scrubbers, UV-C Lamps, fans, sensors and a gas interface to the habitat.
- **Metrics**: Airflow (1000 m^3/h), Air speed (0.3 – 0.7 m/s), Operating Pressure (57 kPa to 101.13 kPa), Operating Temperature (16 ^oC to 27 ^oC)

2.5.3. Thermal Control System (TCS)

- **Purpose**: Manages heat within the module to maintain stable temperatures.
- **Components**: Active liquid cooling for LEDs, air management, and heat rejection units.

2.5.4. Nutrient Delivery System (NDS)

- **Purpose**: ensure a continuous supply of water and nutrients to plants via hydroponic systems.
- **Components**: Pumps, nutrient storage tanks, dosing systems, and trays.
- **Metrics**: Preliminary power usage is estimated at ~570W during operations

2.5.5. Illumination System (ILS)

- **Purpose**: Provides light spectra optimized for plant photosynthesis using LEDs.
- **Components**: Red, white, and far-red LED arrays with cooling systems.
- **Metrics**: 9700 W of heat load generated

2.5.6. Data Handling and Control System (DHCS)

- **Purpose**: Centralized control and monitoring of subsystems.
- **Components**: Sensors, data acquisition systems, and computational units for automation.
- **Metrics**: Integrated with sensors for temperature, humidity, gas and VOC concentrations, and system performance

2.5.7. Power Control and Distribution System (PCDS)

- **Purpose**: The PCDS divides and supplies the incoming power from the habitat to the different subsystems providing voltage regulation, AC/DC conversion, filtering, stabilization and surge protection.
- **Components**: wires, sensors, switches, fuses, batteries

2.5.8. Structural Systems

- **Purpose**: Supports the physical integrity of the module under operational conditions, including storage.
- **Components**: Primary and secondary structures, storage solutions.
- **Metrics**: Mass and volume constraints are defined within the system's mass budget

2.5.9. Habitat Simulator (HabSim)

- **Purpose**: Simulates habitat interfaces for integrated testing.
- **Components**: Environmental interfaces, subsystems for atmosphere and nutrient exchange.

2.5.10. General Overview of how the Components work together

Figures 2.5.10.1 and 2.5.10.2 show a preliminary design of how all the systems work together: The NDS is responsible for the perfectly adjusted mix ratio of the nutrient solutions and the continuous supply of the plants with it. The incoming power from the habitat is divided and spread to the different subsystems by the PCDS. The TCS will regulate the temperature of all subsystems inside LAM-GTD within a defined range. All systems are controlled and monitored via DHCS. All data gathered by the sensors and cameras will also be processed by the DHCS. The ILS will provide light to the whole LAM-GTD, with the main area of importance being the cultivation area. The task of the AMS is to guarantee defined atmospheric conditions in the greenhouse module. Firstly, the air is treated by UV lights, then the air is filtered and dehumidified, then heated and then distributed. The air filtration and VOC scrubbing system is decoupled from the AMS in order to limit pressure losses in the system. The CO_2 and O_2 levels are monitored via the DHCS and a balance is done via the air exchange system between the modules. The Structural system holds the whole system together and gives us the geometrical constraints while the HabSim will act as our simulated crew module with which we will have a gas interface.

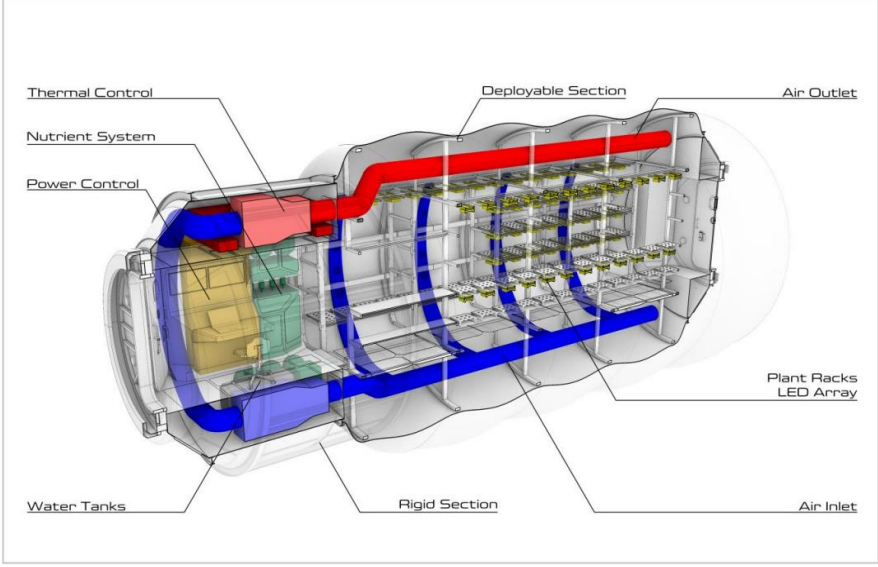

Figure 2.5.10.1 - Preliminary LAM-GTD Design 1 [80]

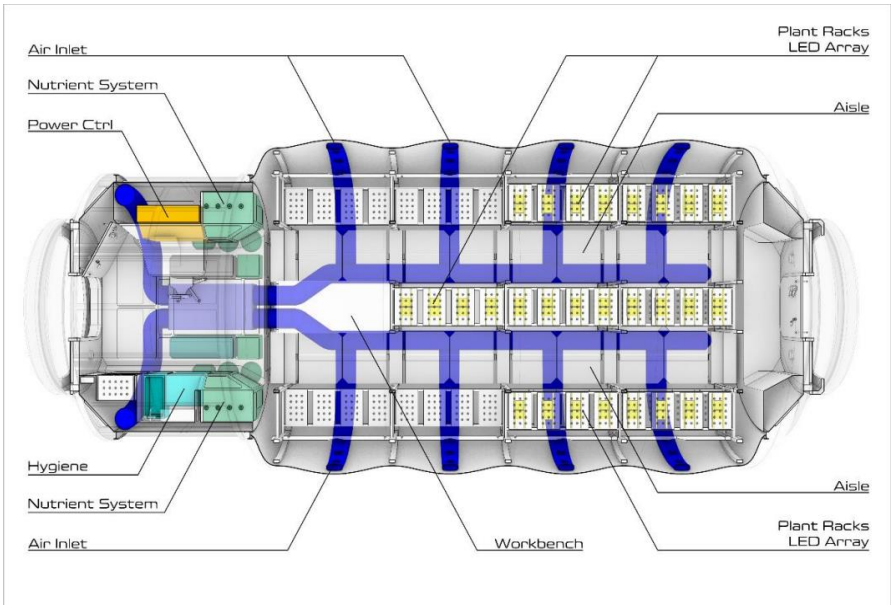

Figure 2.5.10.2 - Preliminary LAM-GTD Design 2 [80]

2.5.11. The AMS of EDEN ISS MTF

This thesis is focused on designing the next generation of AMS for LAM-GTD. In order to build on past progress inspiration will be taken from EDEN ISS MTF. The AMS in EDEN ISS MTF was divided into two sections, the first section was located in the service section container, its purpose was to monitor and control the atmospheric conditions in the cultivation area of the future exploration greenhouse (FEG). The second part was responsible for the air distribution and dimensioning in the cultivation area.

Figure 2.5.11.1 shows the first section located in the service section.

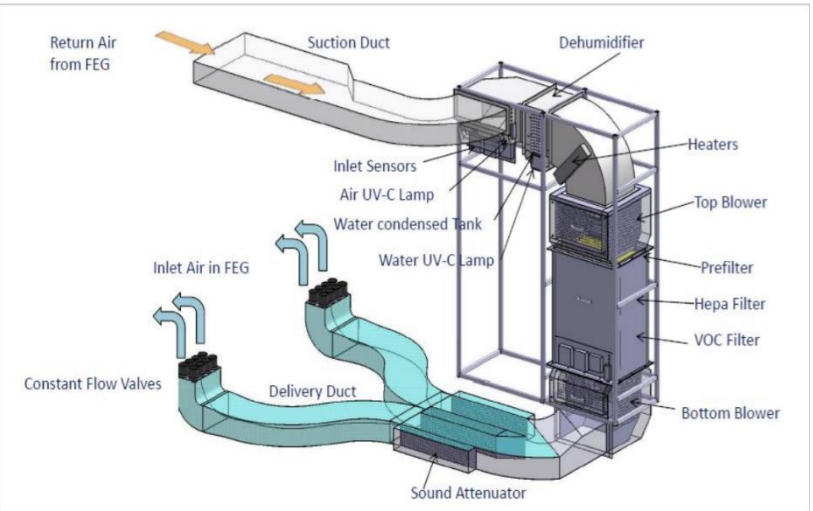

Figure 2.5.11.1 - EDEN ISS MTF AMS Service Section [80]

The return air from the FEG first passes through a UV-C lamp, which prevents microbial growth. Next, the air flows through a dehumidifier, where it is cooled to a temperature that causes water condensation. The condensed water is collected in a storage tank and also treated with UV-C light for disinfection.

Following dehumidification, the cooled air is reheated using heaters, with temperature sensors at both the FEG air inlet and outlet determining how much heating power is required to reach the desired setpoint. To ensure continuous air circulation, two fans operate constantly, one positioned before and one after the filter block.

The filter block consists of a pre-filter, HEPA filter, and VOC filter, which work together to remove dust, pollen, fine particles, and volatile organic compounds (e.g., ethylene). After the second fan, the filtered and conditioned air is split into two ducts and directed toward the outer walls of the container.

Oxygen levels are measured at the FEG outlet to monitor O_2 production, while CO_2 levels are tracked at both the inlet and outlet. If CO_2 levels fall below a specified threshold, CO_2 from a gas cylinder is automatically injected at the FEG inlet to maintain optimal conditions [12]. Figure 2.5.11.2 shows the section located in the FEG.

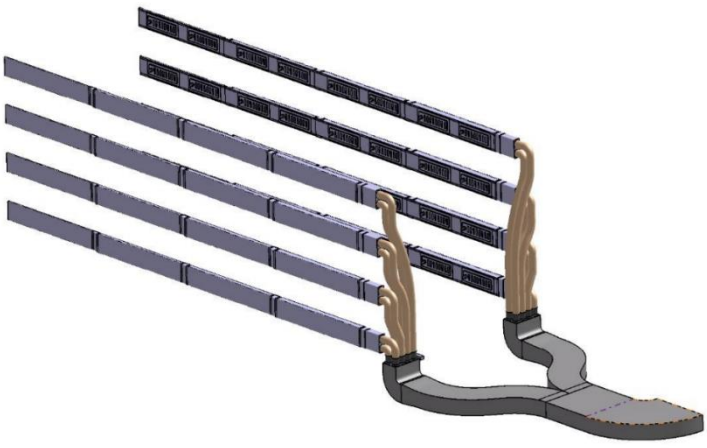

Figure 2.5.11.2 - EDEN ISS MTF AMS Future Exploration Greenhouse [80]

As the air entered back into the FEG it was split between the two main air ducts and then further divided into four smaller ducts, allowing the revitalized air to be introduced into the FEG at four different vertical levels. To ensure balanced air distribution, the horizontal ducts are tapered, gradually narrowing toward their ends. This design promotes even airflow throughout the system.

The ventilation rate, and consequently the air distribution, can be manually adjusted by partially or fully closing the louvers facing inward, enabling the creation of zones with varying airflow intensities. Additional airflow distribution is achieved through overhead fans installed on both sides of the aisle, with a total of eight tangential fans (four per side) in operation [12].

Over the past years of operating the MTF prototype in Antarctica, significant knowledge has been gained, and numerous lessons learned. As a result, several optimizations and improvements have already been implemented to enhance the performance, reliability, and usability of the technology.

These lessons are displayed in Table 2.5.11 below [80]:

Table 2.5.11: Lessons Learned with EDEN ISS MTF

ID	Lesson Learned	Consequence for LAM-GTD
LL-AMS-01	Heat exchanger performance too small. Since the water load was larger than originally anticipated not enough water could be recovered.	Transpiration data from EDEN ISS MTF will be used to get a better estimate for total transpired water per day. Additionally, effort to more accurately model the plant transpiration using more current techniques will be undertaken.
LL-AMS-02	Sensors for monitoring trace contaminants make the work at the greenhouse module safer.	several sensors to monitor trace contaminants should be applied.
LL-AMS-03	Microbial loads are a major problem. Especially at the heat exchanger microbial growth is critical and the applied UV-C lamp was not sufficient. In addition, the access to clean the heat exchanger from microbial growth was difficult due to the interfaces with the secondary structure.	The UV-C Lamps should be redesigned to ensure proper removal of unwanted microbes and pathogens. Additionally, the CHX should have an antimicrobial coating and its maintenance should be simplified
LL-AMS-04	Humid air has a negative effect in the efficiency of the charcoal filter.	Charcoal Filters should be located downstream of the heat exchanger
LL-AMS-05	No actual use to regulate the air dimensioning of the air supplying ducts at the four different levels.	No adjustable louvers are applied anymore.

3. Methodology

3.1. System Analysis

3.1.1. Design Philosophy

The design philosophy for the AMS is based on a clear and methodical process: identifying the specific requirements of the LAM-GTD, using mathematical models to define their upper bounds and designing a compact, efficient and fail-safe AMS to fulfill them.

Although LAM-GTD is a precursor to the LAM, it is important to note that it will be operated under Earth-based conditions. This brings both benefits and limitations. While the absence of reduced gravity limits the accuracy of certain validation efforts for lunar applications, the terrestrial setup also allows for thorough testing of the system under controlled conditions. This makes it possible to push the system to its limits, identify potential failure points, and refine solutions before deployment in a space environment.

Figure 3.1.1 below illustrates the spatial allocation for the AMS, which consists of cylindrical ducts measuring 3.51 meters in length and 0.5 meters in diameter. These ducts form the backbone of the system and house essential components such as blowers, filters, dehumidifiers, UV-C lamps, and sensors.

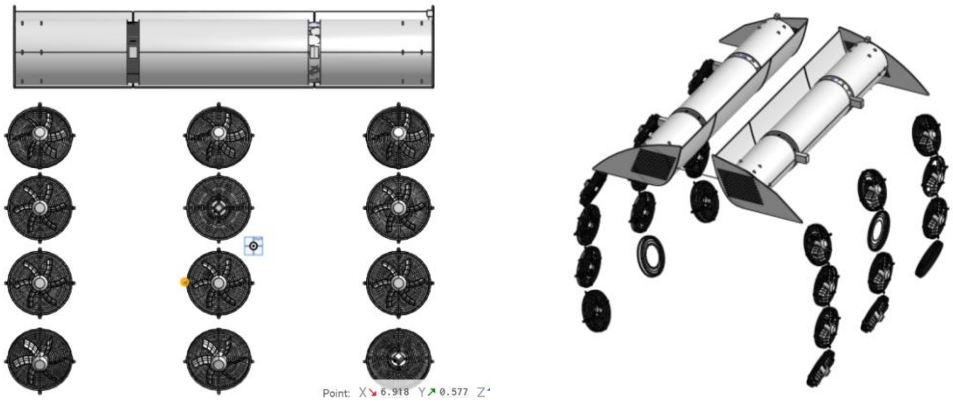

Figure 3.1.1 - Preliminary LAM-GTD AMS

The design draws inspiration from key principles used in previous BLSS, particularly the emphasis on redundancy. Each cylindrical module is designed to independently meet the AMS performance requirements, providing a built-in level of redundancy in case of subsystem failures. Additionally, maintenance and ease of operation have been central design considerations, ensuring that components are accessible, so that the system remains reliable over time.

3.1.2. Assumptions and Requirements

In order to design the AMS for the LAM-GTD some assumptions must be determined. These will be shown in Table 3.1.2.1 below:

Table 3.1.2.1 : Assumptions For The AMS

ID	Assumption	Reason
A-ASM-01	Due to a protective regolith layer the mean ambient temperature of the pressurized agricultural module will be assumed to be constant at $T_a = 254\ K$	Due to regolith having strong insulating capabilities it will be used as a thermal shield for the LAM-GTD [20] [70].
A-AMS-02	The regolith layer will be such that the radiation levels inside the LAM-GTD will be safe for humans	Regolith also have strong radiation shielding properties A layer of >0.8m is considered to give extremely good radiation shielding [20] [70].
A-AMS-03	Heat transfer with the outside of LAM-GTD will be done only via radiation.	The negligible atmosphere on the moon makes this a good assumption as the heat transferred via convection and conduction will be so small it can be neglected.
A-AMS-04	Internal thermal loads inside LAM-GTD will be estimated by scaling known values from previous project such as EDEN ISS MTF	In order to give our estimates, the best accuracy data collected from the previous iterations of this project will be used.
A-AMS-05	The AMS shall be designed to exchange O2 and CO2 with the habitat.	Being a BLSS, LAM will ultimately be tasked with receiving the CO_2 from the habitat while injecting O_2 enriched greenhouse air into the habitat. This exchange shall close the loop further.
A-AMS-06	The AMS modular design shall allow easy access to each equipment group to guarantee quick maintenance.	The easy access to each equipment group facilitates and speeds up maintenance and replacement of parts. The downtime of the AMS is shortened, and plant growth is not affected.
A-AMS-07	Unexpected thermal loads will be buffered by the TCS	The TCS will be the main component in charge of thermal loads
A-AMS-08	Pressure losses are neglected, the atmospheric pressure inside LAM-GTD is guaranteed by the AMS and the structural design of LAM-GTD	The seal in LAM-GTD will be effective enough to maintain constant pressure

Next, we will look at the design requirements of the AMS. These requirements will be shown in 3.1.2.2 below:

Table 3.1.2.2: Requirements For The AMS

ID	Title	Description	Rational	Verification Method
R-AMS-001	Temperature Control	The Temperature of the LAM-GTD will be kept between 16 and 27 degrees Celsius accurate to ± 1 degree Celsius	The temperature must remain within these set values to ensure the crops grow optimally and that human operators remain comfortable	Analysis and testing
R-AMS-002	Humidity Control	The AMS shall keep the relative humidity within 45% and 85% accurate to ± 5%	The relative humidity is a crucial value for plant growth and must be monitored and controlled to ensure optimal plant growth as well as comfort for human operators	Analysis and testing
R-AMS-003	Air pressure	The air pressure inside the LAM-GTD shall be kept between 57 kPa and 101.135 kPa with a nominal operation pressure of 70.3kPa	The air pressure is crucial for the well-being of plants and humans, and it should be monitored and controlled to ensure optimal operating conditions for the farm	Analysis and Testing
R-AMS-004	Carbon Dioxide Concentration	The Carbon Dioxide concentration inside the LAM-GTD shall be kept at between 350ppm and 5000ppm at (101.135 kPa)	Carbon Dioxide is an important resource for plant growth, and it is detrimental to human well-being in high doses. An efficient air exchange needs to be in place to ensure optimal growing conditions for the plants and optimal working conditions for the astronauts	Analysis and Testing
R-AMS-005	Oxygen Concentration	The oxygen concentration in the LAM-GTD shall be kept between 19% and 24% at (101.135 kPa)	Oxygen is a vital resource for both plants and humans. Controlling and monitoring it is crucial to ensure the well-being of astronauts and plants	Analysis and Testing
R-AMS-006	Ethylene Concentration	The ethylene concentration shall remain under 20ppb	Ethylene is a plant hormone which is important to control to ensure optimum growing conditions	Analysis and testing
R-AMS-007	Air flow rate	The air flow rate in the LAM-GTD shall stay below 1000 $\frac{m^3}{h}$	This airflow rate is high comparing to the ISS. Keeping it under this threshold simulates realistic operating conditions	Analysis and testing
R-AMS-008	Air flow speed (out)	The air flow speed inside the LAM-GTD (specifically around the crops) shall remain between 0.1 and 1 m/s with a nominal operating air speed of 0.5 m/s	Plants need airflow to grow effectively, however too much can be damaging. This range is optimum for healthy growth	Analysis and testing
R-AMS-009	Life expectancy	The AMS will be designed to have a life expectancy of 3 years for the ground test demonstrator and 10 years for the Lunar Agricultural Module	LAM-GTD is expected to be operational for 3 years before the development of LAM.	Analysis and Testing
R-AMS-010	Weight	The AMS shall be less than 500kg	The allocated weight for the AMS in the LAM-GTD project is 500 kg	Analysis and Testing

3.2. AMS components

3.2.1. Air Entering LAM-GTD

LAM-GTD will be sealed atmospherically from the other modules in the lunar habitat. The gas interface between the habitation module and LAM will be done via the standardized valve systems when keeping the modules separate. In order to constantly remove CO2 from the habitation module we shall use pressure swing adsorption (PSA).
PSA is a gas separation technology that removes specific gases (like CO_2) from a gas mixture by exploiting the difference in adsorption properties of gases under varying pressures. It works by cycling between adsorption (high pressure) and desorption (low pressure or vacuum) phases using a special material (usually zeolite) that selectively adsorbs CO_2 from the air. Typical PSA systems have 2 or more beds to allow continuous operation [40].

The Step-by-Step process looks like this:

1. Cabin air (containing CO_2, oxygen, nitrogen, etc.) is passed into a sorption bed filled with zeolite or another adsorbent material.
2. Under high pressure, the adsorbent traps CO_2 molecules because CO_2 adheres more strongly to the material than O_2 or N_2.
3. The remaining CO_2-depleted air (clean air) is sent back into the cabin or downstream systems.
4. Over time, the adsorbent reaches its capacity and can no longer remove CO_2 effectively.
5. At this point, the system needs to regenerate the bed to keep working efficiently.
6. The bed is isolated from the air stream and connected to a low-pressure or vacuum source.
7. Pressure is reduced, causing the CO_2 molecules to release (desorb) from the zeolite surface.
8. The desorbed CO_2 is then vented to LAM-GTD.
9. While Bed A is being regenerated, Bed B (which was previously regenerated) takes over the adsorption process.
10. The system swings back and forth between beds in a timed sequence to ensure continuous CO_2 removal.

3.2.2. Blowers

The required Air Changes per Hour (ACH) is a value that will influence our design a lot. For our assumptions we will take inspiration from the ISS as well as commercial vertical farming companies. The ISS has $900m^3$ of usable pressurised volume for the astronauts to live in [25] with the air flow around the ISS varying. The mean air flow in the ISS is $420m^3/h$ to $460m^3/h$ which is equal to 0.46 to 0.51 ACH [27]. Each of the ISS modules are connected via the Intermodular Ventilation (IMV) system, this system can recirculate all the air in the ISS in about 2-3 hours [24]. Finally, the crew quarters (CQ) have an air flow rate of 96-$162m^3/h$ which is equivalent to an ACH of 44-77. The reason for this

is that the CQ are quite small, roughly 2.1m^3 and so require a higher volumetric flow rate to make sure that there is no build-up of CO_2 and other trace gases.

However, it must be noted that commercial CEA operations recommend an ACH of up to 30 [95]. The higher ACH offers advantages and disadvantages listed below:

Advantages:

- Improved temperature Control: more effectively removes excess heat generated by lighting systems, creates more uniform temperature distribution throughout growing spaces, reduces hot-spots that can stress plants
- Humidity management: Prevents excessive humidity buildup around plant canopies, reduces condensation on surfaces and plants, Lowers disease pressure, particularly fungal pathogens like powdery mildew
- Enhanced Gas Exchange: Better distribution of supplemental CO_2, Removal of plant-produced ethylene (which can accelerate ripening/aging), prevention of oxygen depletion in dense growing area
- Pest and Disease Prevention: Moving air disrupts the lifecycle of certain pests (e.g., fungus gnats, thrips), creates less favorable conditions for bacterial and fungal pathogens, can help distribute beneficial biological control agents

Disadvantages:

- Increases energy consumption significantly
- Too much air movement can stress plants
- Could reduce relative humidity too much in certain scenarios

Such a high ACH is unrealistic when dealing with a pressurised lunar habitat, therefore a compromise is necessary. For this paper an average of 11.5 air exchanges per hour will be used with further research needed to check if it could be reduced. This is to take advantage of LAM-GTD being on the ground, therefore we can push the system to its upper limits to see how it functions and where points of failure are. Having a modular design enable this to be changed on the fly as more data is gathered from running LAM-GTD.

Calculate Required Airflow Rate (Q):

Where Q is the flow rate, V is the volume of LAM-GTD and ACH is the air changes per hour

$$Q = V * ACH = 87m^3 * 11.5 \approx 1000 \frac{m^3}{h} \approx 0.0.28 \frac{m^3}{s}$$

Total pressure loss $\Delta P = 250\ Pa$

Blower efficiency $\eta \approx 60$

Power= Q×ΔP/η = $0.28 \frac{m^3}{s}$×250/0.6≈116.6 W

Commercial Option:

Figure 3.2.2.1 taken from Annex 1.1 give us the performance curves of different models of the Radi-Pac line offered by ebm-papst a leading manufacturer in high end wind circulation devices. From the chart we see that model A will give us the flow rate required with a static pressure of 500 Pa. This blower weighs around 6kg and consumes 0.5 kW at maximum power. This model measure 380mm*245mm*380mm as shown in figure 3.2.2.2. Two of these blowers will be used in the AMS, one at the entrance and one at the exit, this will provide redundancy while allowing the blowers to run below their max rated power.

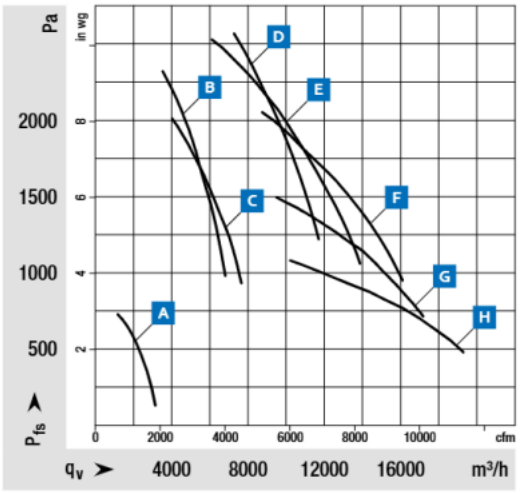

Figure 3.2.2.1 - Performance Graphs of RadiPac

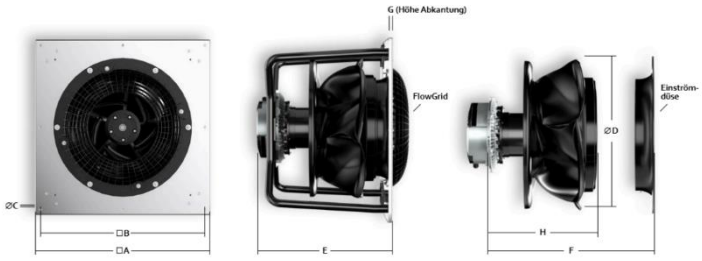

Abmessungen

Baugröße	□A	□B	ØC	ØD	E*	F	G	H	Einströmdüse Bestellnummer	FlowGrid Bestellnummer
280	380	330	11	289	245	202	15	172	8217102230	20280-2-2957

Figure 3.2.2.2 - Dimension of RadiPac

3.2.3. Fans

It was decided to use multiple small fans to create localized airflow around plants rather than one central unit. This was done to limit any single point of failure and give LAM-GTD increased flexibility in its localised air circulation. Additionally, many separate airflows would favour turbulent flow which is better for mixing air in LAM-GTD while avoiding air pockets.
Because gravity is required for density differences to occur, convection-based heat transfer is not possible in microgravity environments such as space. As a result, air pockets can form within the cultivation area, leading to localized heat buildup. These pockets can cause temperatures to rise above the defined threshold, potentially affecting system performance [89].

Additionally, airflow is critical for plants as it reduces condensation and the risk of fungal diseases, it encourages evaporation of moisture through the leaves thus increasing their moisture/nutrient uptake and the movement caused by airflow encourages strong stem growth [90].

The main design features these fans need to satisfy is that they need to be compact, reliable, quiet, provide stable airflow and be energy efficient. Compact diagonal fans are chosen as they generate a cone-shaped airflow and so provide greater air distribution [80]. Additionally, diagonal fans produce higher pressure and greater airflow compared to axial fans. At the same time, they operate more quietly than centrifugal fans, as they can achieve the same performance at lower rotational speeds [91].

For this task the DV 6224 from ebm papst is selected. Its specification can be seen below in Figure 3.2.3. The growing area will be split into 30 growing zones, in order to keep good airflow on the plants it is suggested to use one fan per 2 zones [81]. At a weight of 820g per fan and with a power consumption of 40W per fan this system will consume 600W while weighing 12.3kg. More information on this fan is available in Annex 1.2

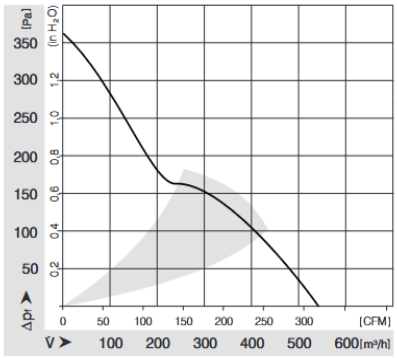

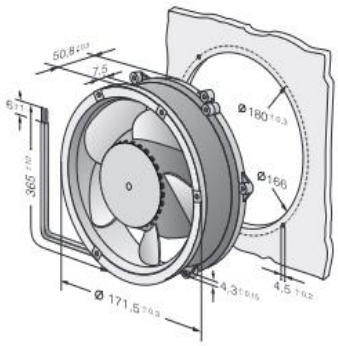

Typ	DV 6224	
Nennspannung	VDC	24
Nennspannungsbereich	VDC	16 .. 28
Drehzahl	min-1	4300
Leistungsaufnahme	W	40,0
Min. Umgebungstemperatur	°C	-20
Max. Umgebungstemperatur	°C	75
Volumenstrom	m³/h	540
Schallleistungspegel	B	7,1
Schalldruckpegel	dB(A)	63

Figure 3.2.3 - Performance of DV 6224 [42]

3.2.4. UV-C Lamps

UV lights will be used to provide germicidal irradiation to reduce airborne pathogens. The chamber is designed with reflective surfaces to ensure uniform exposure.

UV-C Dosage Calculation

Target UV-C Dose(D): 5000 μW·s/cm² [44]

Airflow Rate (Q): 0.28 m³/s

Duct Diameter: 0.5m

Duct Cross sectional area (A_d): 0.196 m^2

Air Velocity (v):$v = Q * A_d$ = 0.28 * 0.196 m^2 = 1.427 m/s

Assuming UV-C section length (L) = 0.45 meters

Irradiation Time (t): $t = \frac{L}{v}$ = 0.3m / 1.427 m/s = 0.31 seconds

Required UV-C Intensity (I): $I = \frac{D}{t}$ = 5000 μW·s/cm^2 / 0.2 s = 15851 μW/cm^2

Circumference of duct (C_d): $C_d = \pi * D$ =π * 0.5 m≈1.57 m

Duct Cross-Sectional Area (A_{duct}): A_{duct} = 1.57*0.45 = 0.7065 m^2 = 7065 cm^2

Total UV-C Power Required: 15851 μW/cm^2 * 7065 cm^2 = 111994048.5 μW = 111.9 W

The NL-T8 UV 25W/254 G13 [43] produces 8.2 W of effective UV-C power (See Annex 1.3). This means that with 14 lamps we could get rid of all the pathogens. However, as we learnt from the experience of EDEN ISS MTF, microbial loads were a significant problem. Therefore, a safety factor of 2 will be used here, meaning 28 lamps will be used. This will give the system greater redundancy while allowing tests to be done on the ground to see how much UV-C power is required in practice. At 70g per light and with a power consumption of 25W this system will weigh 1.96 kg and consume 700W.

3.2.5. Pre-Filter and HEPA Filter

To minimise the fowling of the dehumidifier while reducing microbial load a pre-filter and a HEPA filter will be used. The pre-filter will be a modified OPR-G7-610x610x292-P-PS from camfil weighing 7.7 kg and having an approximate pressure drop of 40 Pa at 1000 m^3/hr [92]. For the HEPA filter a modified VGXXL14-610x610x292-P-PS from camfil will be used. This particular filter weighs 9.6 kg while having a pressure drop of 50 Pa at 1000 m^3/hr [93]. This puts the total weight and pressure drop of this filtration system at 17.3 kg and 90 Pa pressure drop. More information on these filters is available in the Annex. 1.4

3.2.6. Duct Design

For the AMS ducting system, 1 mm aluminum with a Heresite coating has been selected [96]. Aluminum naturally forms a protective oxide layer when exposed to air, making it inherently corrosion-resistant without the need for additional treatments. It is also significantly lighter than steel, typically weighing 50% less, which is a major advantage when launching mass-sensitive missions to the Moon. Its high thermal conductivity allows the ducting to equilibrate quickly with ambient temperatures,

reducing the risk of condensation during system cycling. Additionally, aluminum's low thermal mass enables faster thermal response, further minimizing condensation formation. From a hygiene perspective, aluminum surfaces are less hospitable to microbial growth due to their smooth finish, which makes it harder for biofilms to establish. These benefits are further enhanced by the Heresite coating, which provides exceptional resistance to corrosion, microbial contamination, and long-term environmental degradation, contributing to a more durable and reliable ducting system [84].

The total weight for the 3.51m aluminum duct will be 14.88 kg with negligible pressure drop (less than 1.5 Pa)

3.2.7. Dehumidifier

Table 3.2.7 : Heat Load of Components [81]

Subsystem	*Components*	*Heat Load*	*Coverred by AMS*	*Transferred by Coolant*	*Transferred by Air*
		[W]	[%]	[W]	[W]
ICS	LEDs	9700	70	2910	6790
NDS	Pumps, UV Lamps, Switches, Sensors	570	20	456	114
AMS	Blowers, Fans, Heater, UV Lamp, Sensors	1940	100	0	1940
Structure	Mechanisms	50	100	0	50
DHCS	Data Interfaces, Electric Box	200	20	160	40
TCS	Heat Exchanger, Pump, Valves, Sensors	200	20	160	40
EPS	Converters, transistors, re-lays	1000	20	800	200
PHM	Sensors	500	100	0	500
Robotics	Rail, Motors, Computer, Sensors	976	100	0	976
Human Factors	Metabolism	200	100	0	200
Miscellaneous	Ceiling Lamps etc.	150	100	0	150
Total		**15486**			**11000**

3.2.8. Crop Transpiration and Environmental Modelling

Transpiration rate will be calculated using assumptions from previous EDEN ISS MTF and EDEN LUNA research as well as research done on plants growing in reduced atmospheres. From internal design documents we get a transpiration rate of 6.8 $kg/(m^2 * day)$ [32] while NASA baseline values suggest a transpiration rate between 1.74 – 11.79 $kg/(m^2 * day)$[31]. From previous research we also know that while the pressure remains over 10kPa radish and spinach transpiration varies by about 15% [30]. Historically in EDEN ISS MTF testing it was also found that the dehumidifier was often underdesigned, putting all these things together we will air on the side of caution and assume a transpiration rate of 8.5 $kg/(m^2 * day)$ or roughly 200kg of water per day on a 23.5 m^2 grow area.

This thesis is intended to serve as a reference point for future designs and iterations of the LAM-GTD. As such, the development of a reliable computational model to predict crop-specific transpiration rates represents a valuable contribution to the project. To achieve this, a Python script was developed based on the FAO56 guidelines [45][46] (see Annex 1.5). The script estimates the transpiration rates for four key crop types; peppers, tomatoes, cucumbers, and leafy greens, and provides graphical visualizations of the results. A detailed explanation of the script's functionality is provided below.

1. Crop Coefficient (Kc) Interpolation

For each crop, the growth cycle is divided into stages. In each stage, a crop coefficient is specified at the beginning and end. When the coefficient is not constant, a linear interpolation is used:

$$K_c(d) = K_{cstart} + \frac{(d - d_{start})}{(d_{end} - d_{start})} * (K_{cend} - K_{cstart})$$

Where K_{cstart} is the crop coefficient at the start of growth and K_{cend} is the crop coefficient at the end of the growth cycle. The days are represented by d, where d_{start} and d_{end} are the first and last day of the growth cycle.

2. Adjustment of Reference ET (ET_o) for Ambient Pressure

This simplified correction assumes that evapotranspiration is inversely proportional to the ambient pressure relative to the standard atmospheric pressure (101.3 kPa)

$$ET_{O\ adjusted} = ET_o * \frac{101.3\ kPa}{Chosen\ Ambient\ Pressure\ (kPa)}$$

A base ET_o is chosen at 6mm/day this is higher than the calculated ET_o (around 4.5 mm/day) using the FAO-56 Penman Monteith method as it is known to underestimate the reference evapotranspiration[45].

3. Daily and Cumulative ET

Here we will calculate the daily evapotranspiration given in Liters per m^2.

$$\boldsymbol{ET_{daily}} = ET_{O\ adjusted} * \boldsymbol{K_c}$$

With the first part of the script, we are able to more accurately model the evapotranspiration of each crop at any given part of its growth cycle. Below will be displayed the evapotranspiration for some common plants to grow in a hydroponic system, such as tomatoes, peppers, cucumbers and leafy greens. The growth area is taken as 23.5 meters squared. [81]

Table 3.2.8: Evapotranspiration per crop

Crop	Tomatoes	Peppers	Cucumbers	Leafy Greens
Total Growth Cycle (days)	120	100	80	30
Adjusted ET_O (mm/day)	8.68	8.68	8.68	8.68
Total Water loss (Liters)	24332	19323	14574	3928
Total water loss per day (Liters)	202.8	193.2	182.2	130.9
Total CO_2 uptake during growth cycle [49] (kg)	53.61	44.68	34.74	13.4

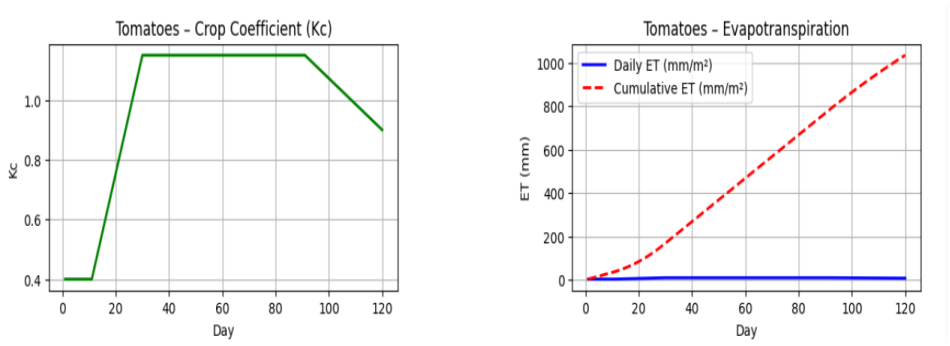

Figure 3.2.8.1 - Tomato Crop Coefficient (Kc) and Cumulative Evapotranspiration

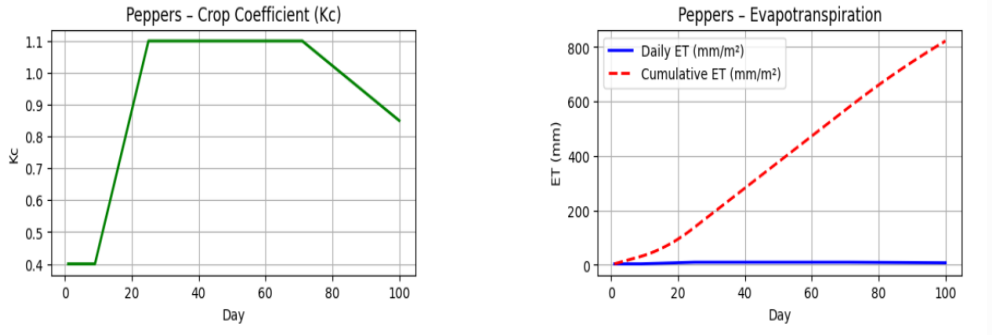

Figure 3.2.8.2 - Peppers Crop Coefficient (Kc) and Cumulative Evapotranspiration

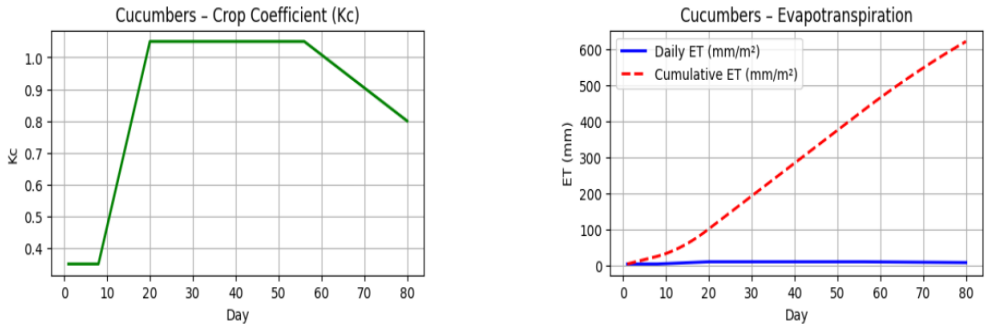

Figure 3.2.8.3 - Cucumbers Crop Coefficient (Kc) and Cumulative Evapotranspiration

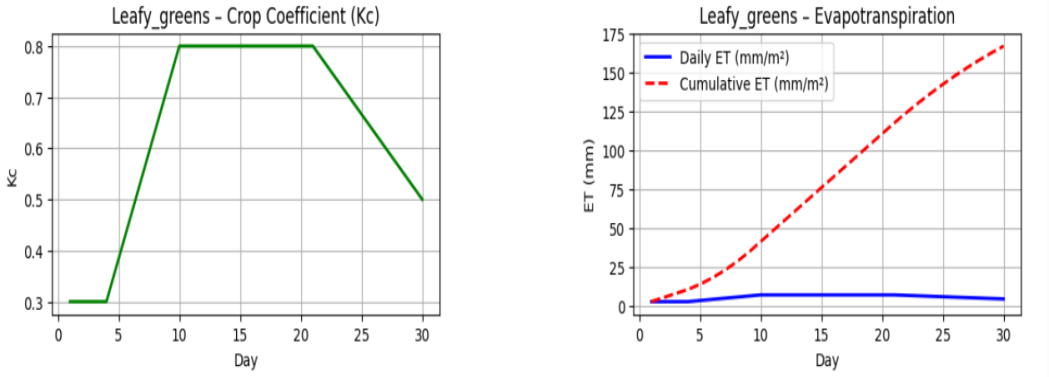

Figure 3.2.8.4 – Leafy Greens Crop Coefficient (Kc) and Cumulative Evapotranspiration

3.2.9. HVAC Energy Load Calculation

1. Sensible Cooling Load

Given that all equipment produces a constant 11 kW of sensible heat, the sensible cooling load is:

11kW * 24h = 264 kWh

2. Latent Cooling Load

Latent cooling is required to remove water vapor released by the crops. The latent cooling is calculated as:

$$Latent\ cooling\ (kWh/day)\ =\ Daily\ ET\ (liters/day)\ *\ 0.68\ kWh\ /liter$$

Where 0.68 kWh/liter is derived from the latent heat of vaporization of water. Assuming 1 Liter of water is roughly 1 kg:

Latent heat ≈ 2450 kJ/kg and 1kWh = 3600 kJ => $\frac{2450}{3600} = 0.68 \frac{kWh}{liter}$

3. Net Power Consumption

The net power consumption is the sum of the sensible cooling and latent cooling loads:

Net Power (kWh/day) = Sensible Cooling + Latent Cooling

3. HVAC Air Process and Power Consumption Model

1. Air Process Interpolation

Air mass: $m_{da} = Density * Volume$

2.Equipment Sensible Load

This converts the power rating from kW to kJ/h

$$Q_{eq,hour} = equipmentLoadKw * 3600$$

3. Potential Enthalpy Increase: $\Delta h = \frac{Q_{eq,hour}}{m_{da}}$

4. Water Addition from ET:
water_added_hourly=$\frac{daily\_ET\_area}{24}$

This Spreads the daily water loss evenly over each hour.

5. Increase in Humidity Ratio:
Δw=$\frac{water\_added\_hourly}{m_{da}}$
This calculates how much the water content per unit mass of air increases hourly.

6. Latent Energy Load:
latent_hourly_kWh = $\frac{water\_added\_hourl}{24}$

This will convert the energy required to remove the added water (via condensation) into kilowatt-hours.

7. Daily Latent Load:

latent_daily= latent_hourly_kWh * 24

This will sum the hourly latent loads over the entire day.

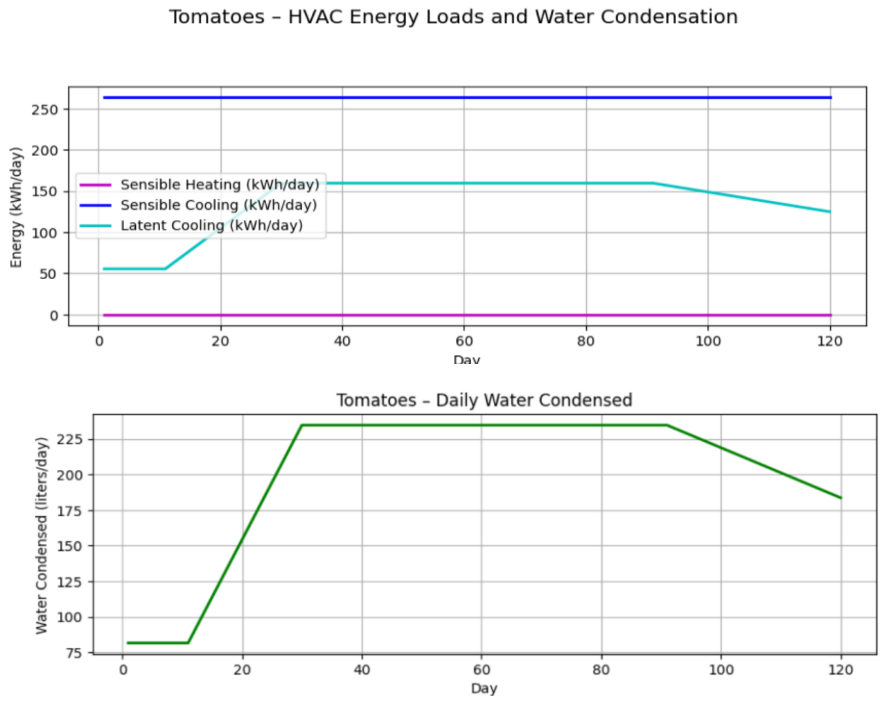

Figure 3.2.9.1 - Tomatoes - HVAC Energy Loads and Water Condensation

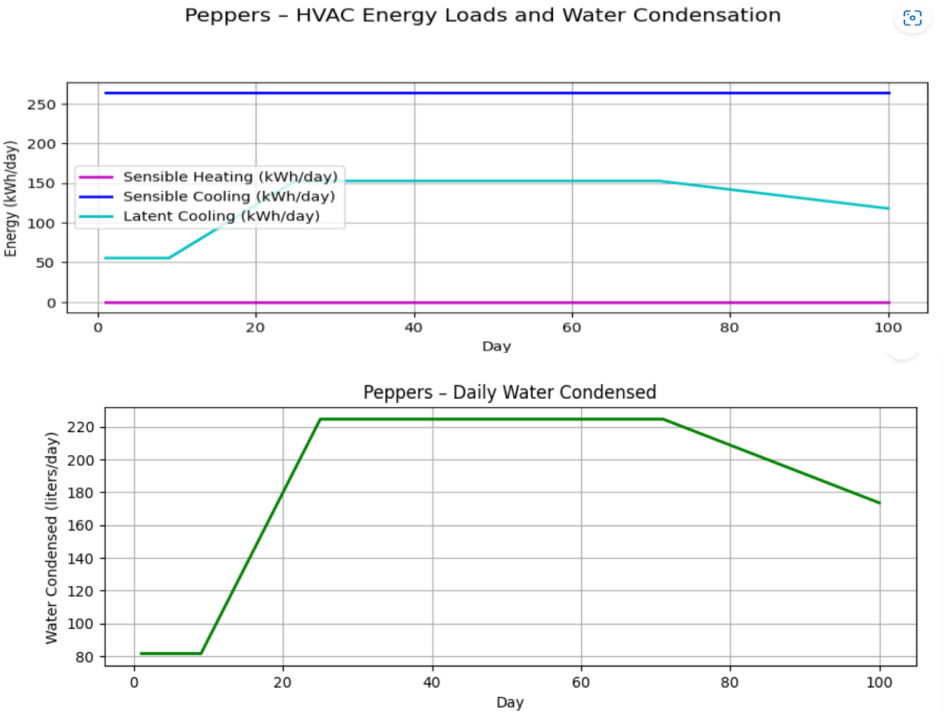

Figure 3.2.9.2 - Peppers - HVAC Energy Loads and Water Condensation

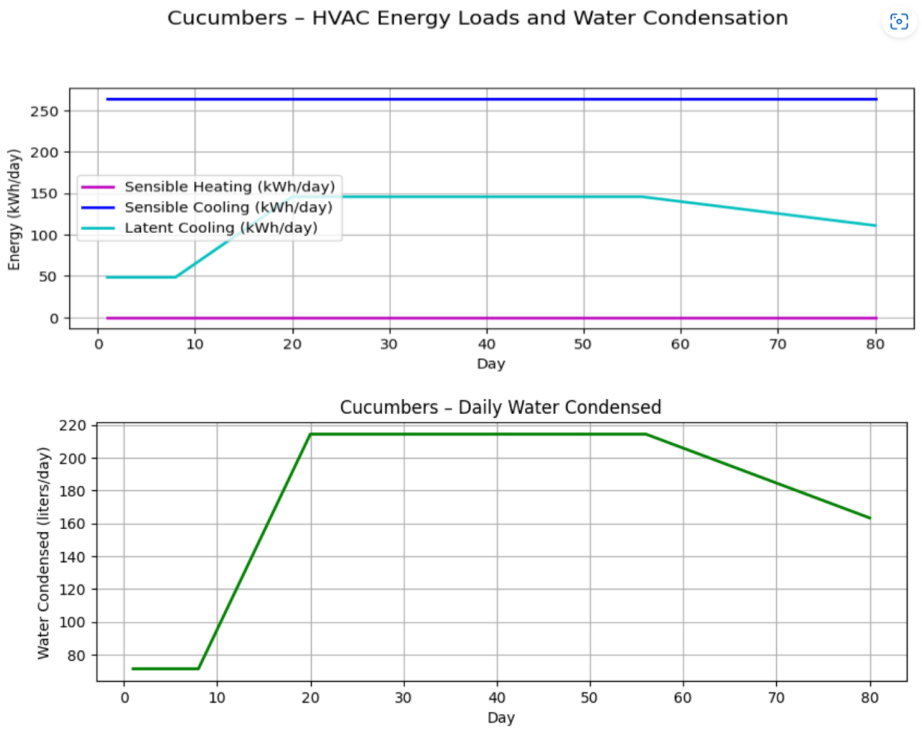

Figure 3.2.9.3 - Cucumbers - HVAC Energy Loads and Water Condensation

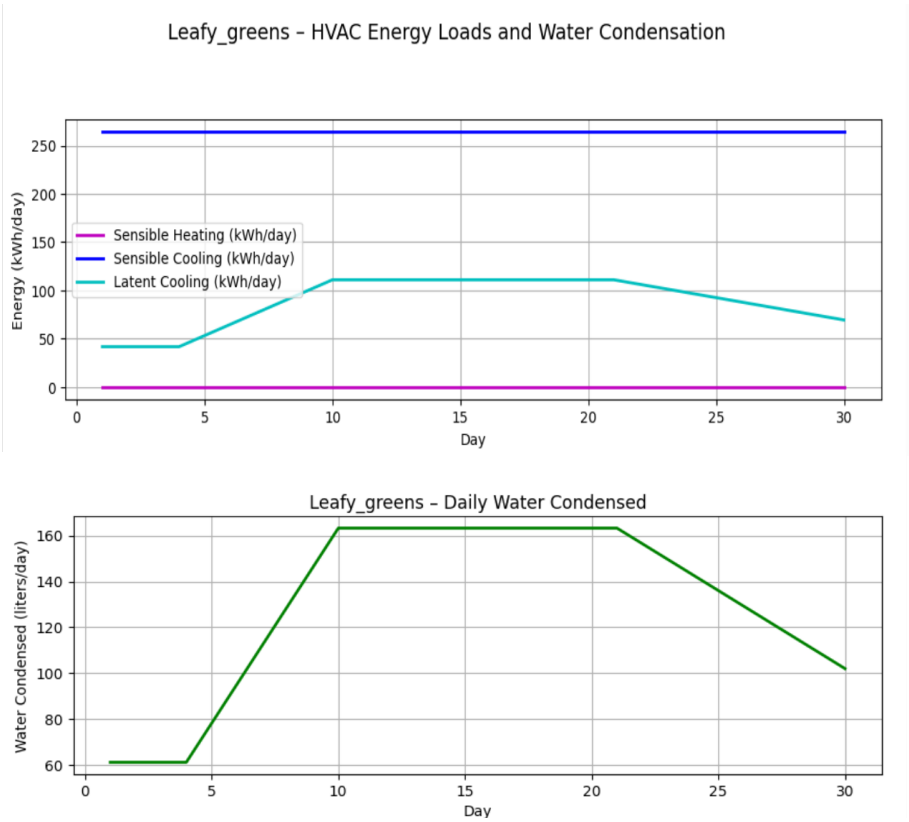

Figure 3.2.9.4 - Leafy Greens - HVAC Energy Loads and Water Condensation

Table 3.2.9: Power Requirements to condense transpiration of each crop

Crop	Tomatoes	Peppers	Cucumbers	Leafy Greens
Total Growth Cycle (days)	120	100	80	30
Grow Area (m^2)	23.5	23.5	23.5	23.5
Sensible Heating (kWh)	0	0	0	0
Sensible Cooling (kWh)	31680	26400	21120	7920
Latent Cooling to maintain RH ≤ 65% (kWh)	16546	13139	9910	2670
Net Power Usage over Growth cycle (kWh)	48226	39539	31030	10590
Average Daily power Usage (kWh)	401.9	395.4	387.9	353
Average Daily Power Usage with safety factor (20%) (kWh)	482.3	474.5	465.5	423.6
Total Cooling power required (kW)	20.1	19.8	19.4	17.7

3.2.10. HVAC Energy Load Calculation Using Psychometric Charts

In order to extract the water from the air we are required to go below the dew point of water, this point differs based on the atmospheric pressure and cooling and heating loads will be determined with the help of the following psychometric charts (figure 3.2.10.1, figure 3.2.10.2)

- **Water removal Capacity Required:** Growing Area * Transpiration Rate= 23.52m^2*8.5 $kg/(m^2 * day)$ ≈ 200 kg/day of water
- Load at 101kPa:
  - Starting Enthalpy: h_{start}=77 kJ/kg
  - Target Enthalpy: h_{target}=29 kJ/kg
  - ΔEnthalpy: Δh = (77-29)kJ/kg=48kJ/kg
- Cooling Capacity (kW): $\dot{V} * \rho * c_p * \Delta h = \frac{1000}{3600} * 1.2 * 1.005 * 48 = 16.08\ kW$

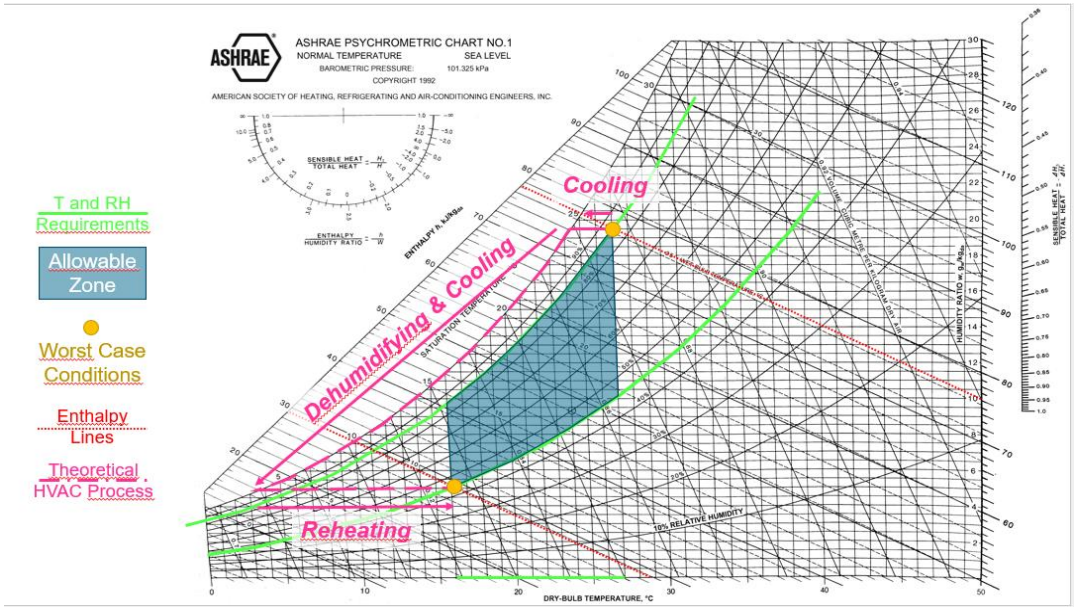

Figure 3.2.10.1 – ASHRAE Psychrometric chart 101.325 kPa [102]

- Load at 70kPa:
  - Starting Enthalpy: h_{start}=100 kJ/kg
  - Target Enthalpy: h_{target}=35 kJ/kg
  - ΔEnthalpy: Δh = (100-35)kJ/kg=65kJ/kg
- Cooling Capacity: $\dot{V} * \rho * c_p * \Delta h = \frac{1000}{3600} * 0.83 * 1.005 * 65 = 15.06\ kW$

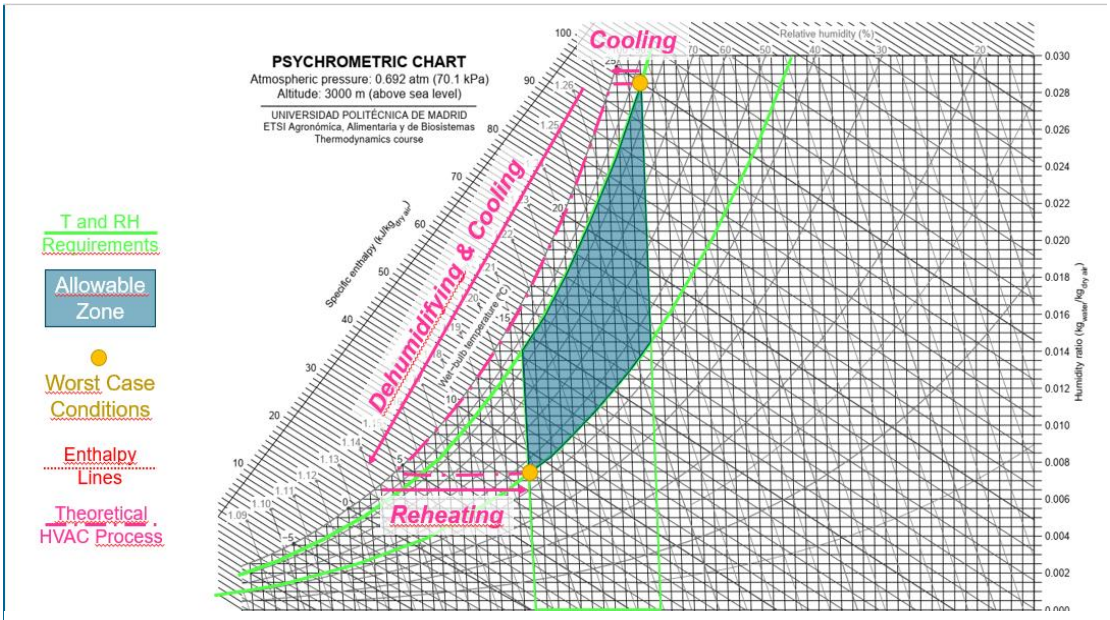

Figure 3.2.10.2 - ASHRAE Psychrometric chart 70.1 kPa [102]

A comparison of the two methods shows that the psychrometric charts estimate a lower cooling requirement. However, to ensure safety and account for uncertainties in this demonstration prototype, this thesis adopts the higher cooling load estimate of 20.1 kW as the design baseline.

Commercial Options

The VEAB CFK 315-2,5 has dimensions 553mm*639mm*462mm, weighs 16kg and can provide 10.6kW of cooling power with a pressure drop of 35 Pa while dealing with an airflow of 1000 m^3/hr with no modification. Its specifications can be seen in figure 3.2.10.3 [47].
Stacking two in succession one after the other would satisfy our cooling requirements. This system gives us a lot of redundancy and flexibility, by having two modules and having dual heating and cooling functions. Additionally, the drip trays will collect the condensate and recirculate it to the NDS. This dehumidification system will weigh a total of 32 kg with a pressure drop of 70 Pa while consuming roughly 21.2 kW of power at its peak. (See Annex 1.6)

Performance Data		**Heating**	**Cooling**
Model	CFK 315-3-2,5		
Art. no	210825		
Capacity	kW	11.0	10.6

Air Side Data		**Heating**	**Cooling**
Atmospheric Pressure / Altitude	Pa / m	101325.00 / 0.00	
Volumetric Flow	m³/h	1000	1000
Mass Flow	kg/h	1221.30	1162.55
Density	kg/m³	1.22	1.16
Surface Velocity	m/s	1.46	1.46
Air Inlet Temperature	°C	15.0	27.0
Inlet Humidity	%	45.0	85.0
Air Outlet Temperature	°C	47.2	15.2
Outlet Humidity	%	7.1	100.0
Pressure Drop	Pa	20	35

Figure 3.2.10.3 - Performance of the VEAB CFK 315-2,5 [47]

Custom Option:

As the dehumidifier is such an important part of the system efforts were made to find more innovative and efficient solutions. With the advent of 3D printing, complex geometries for heat exchangers have become possible to manufacture at reasonable prices. One such geometry which shows a lot of promise as a heat exchanger is the Gyroid.

Gyroid heat exchangers:

A gyroid is a type of three-dimensional (3D) triply periodic minimal surface (TPMS). These geometric properties allow it to have a high surface-area-to-volume ratio which is crucial when designing a compact heat exchanger. The triply periodic minimal surface refers to the fact that this geometry repeats without self-intersection and maintains a continuous curvature. Fluid flowing through these channels benefits from:

1. **Lower Pressure Drops:** Unlike sharp turns or narrow channels, gyroid passages can be smoother and more continuous, potentially reducing pumping power requirements.
2. **Efficient Mixing:** The convoluted pathways promote better mixing and more uniform heat distribution, avoiding localized hot or cold spots. [35]

Beyond thermal performance, gyroid lattices also offer favourable mechanical properties, such as high stiffness-to-weight and strong load-bearing capabilities. They can even be incorporated into multifunctional components where thermal management is combined with structural support.

1. **Resistance to Thermal Stress:** The continuous nature of a gyroid helps mitigate stress concentrations, reducing the chance of cracking under wide temperature swings on the Moon (daytime to nighttime can vary by hundreds of degrees Celsius).
2. **Load-Bearing Heat Exchangers:** In many lunar-farm designs, structural supports and thermal-control systems can merge. A single gyroid module might act as both a supporting truss and a heat exchanger.
3. **Contamination Control:** The closed-cell or partially open-cell nature of certain gyroid designs can help isolate fluids and prevent unwanted leaks into the plant-growth chamber. [35][36]

With these facts in hand, it is possible to write code (See Annex 1.7) to design a heat exchanger that is more compact and efficient that traditional plate heat exchangers [37].

First, we will define some equations that we will use later. These will be the Tetens's Formula [61], the Reynolds Number [63], Gyroid Hydraulic Diameter and Gyroid Pressure Drop [65] and Gyroid coolant pressure drop [87].

Tentens's Formula: $Saturation\ Vapour\ Pressure\ (e_{sat}) = 10^{\frac{7.5*T}{(T+237.3)}}$

Where T is the Temperature

Reynolds Number: $Re = \frac{\rho v D_h}{\mu}$

Where ρ is the fluid density (kg/m^3), v is the velocity (m/s), D_h is the hydraulic diameter (m) and μ is the dynamic viscosity (Pa*s).

Gyroid Hydraulic Diameter: $D_h = \frac{4*\varepsilon}{S_v}$

Where ε is the porosity and S_v is the specific surface area (m^2/m^3)

Gyroid Pressure Drop: $\Delta P = a * Re^b * \frac{L}{0.04}$

Where *a* and *b* are constants derived from research papers on gyroids [65]. *L* is the length of the gyroid.

Gyroid Coolant Pressure Drop: $\Delta P_{cool} = \left(\frac{f*L_{path}*\rho_{cool}*v^2}{2*D_h}\right) * C_f$

Where *f* is the friction factor, L_{path} is the coolant path length, ρ_{cool} is the coolant density and C_f is the complexity factor of the gyroid structure, in this case 2.

Next, we tackle the Log-Mean Temperature Difference. Using the worst-case scenario determined above where 27ºC at 85% RH gets cooled down to 14ºC and 45% RH we see that we need a cooling power of 20.1 kW. We assume that on the waterside the coolant enters at 5ºC and leaves at 13ºC. Then the air "sees" a temperature difference of about 14°C at the inlet (27–13) and about 11°C at the outlet (16–5). The log–mean temperature difference (LMTD) is then about 9.1°C.

1. **<u>Temperature Differences and LMTD</u>**

Temperature of water at inlet T_{water}:5ºC

Temperature difference at inlet ($\Delta T_1 = T_{air\_in} - T_{water}$): 14 K

Temperature difference at outlet ($\Delta T_2 = T_{dew} - T_{water}$): 11 K

Log mean temperature difference LMTD = $\frac{\Delta T_1 - \Delta T_2}{ln\frac{\Delta T_1}{\Delta T_2}} = 12.4K$

2. With this and assuming an overall heat–transfer coefficient of U = 120 W/m²K, [37] we can use the following equation to determine the surface area required.

$$A_{req} = \frac{Q_{tot}}{U * LMTD} = \frac{20100}{120 * 12.4} = 13.5\ m^2$$

Next, we will calculate the vapour pressure deficit (VPD). We use this approach as RH only tells you how "full" the air is with water vapor as a percentage, but it doesn't directly tell you how much moisture the air can still hold.

3. VPD represents the difference between the amount of moisture in the air and the amount it can hold at saturation (saturation vapor pressure). This is a more absolute measure of the air's drying power or moisture demand. The VPD is calculated using Tetens formula for saturation pressure [52].

Vapour Pressure Deficit: $\text{VPD} = e_{sat} * (1 - RH)$

4. Next, we calculate the coolant flow rate by doing an energy balance calculation [53]. For our coolant we will be using distilled water as this is what is used in the ISS [34], which gives us a specific heat capacity (J/kg*K) of 4180 J/kg*K and a density of 1000 kg/m^3.

$$Q_{cool} = \dot{m}_{cool} * C_p * \Delta T \Rightarrow \dot{m}_{cool} = \frac{Q_{cool}}{c_p \Delta T} = \frac{20100}{4180 * 8} = 0.601\ kg/s$$

5. Having a geometrical constraint of using a 0.5m duct for our AMS give us a duct area of:

$$A_{duct} = \pi * r^2 = \pi * 0.25^2 = 0.196\ m^2$$

This design will be using two gyroid geometries offset to allow a hollow section for the coolant to flow through We will be using a gyroid cell of period L = 4.5 cm which will have a surface area of about $3.1*L^2$ per cell and a volume of $0.5*L^3$ [55].

$$A_{cell} = 3.1 * L^2 = 0.00628 m^2$$

$$V_{cell} = 0.5 * L^3 = 0.0000456\ m^3$$

With this in hand we are able to calculate the specific surface area per volume of the gyroid:

$$S_v = \frac{A_{cell}}{V_{cell}} = 137.78\ m^2/m^3$$

Using the required area calculated above allows us to then calculate the total gyroid volume as well as the length of the dehumidifier:

$$V_{gyroid} = \frac{A_{req}}{S_v} = 0.098\ m^3$$

$$L_{tube} = \frac{V_{gyroid}}{A_{duct}} = 0.498\ m$$

Note: this is assuming that the gyroid is fully packed in the tube, in practice this will likely not be the case, therefore we expect the dehumidifier to be roughly 10% longer.

$$L_{tube} = 0.55\ m$$

Now we will calculate the porosity of the gyroid based on its periodicity and wall thickness [64]

Level Set parameter (c) : $c = \frac{t_{wall} * \pi}{L_{cell}} = 0.4189$

Solid Fraction (S_f) : $S_f = 0.65 * c = 0.2723$

Porosity (ε): $\varepsilon = 1 - S_f = 0.7277$

Volume of Air Channel $\left(V_{air_{channel}}\right)$: $V_{air_{channel}} = V_{tube} * \varepsilon = 0.0857\ m^3$

Volume of Gyroid Wall (V_{wall}): $V_{wall} = V_{cell} * S_f = 0.0291\ m^3$

Volume of Coolant Channel ($(V_{coolant_{channel}}$): $V_{wall_{channel}} = \frac{V_{wall}}{2} = 0.0146 m^3$

Effective Area for Air (A_{aireff}): $A_{aireff} = \varepsilon * A_{tube} = 0.1429\ m^2$

We then call our previously defined equations to determine the pressure drop of the air as well as its Average Air velocity.

Hydraulic Diameter for air ($D_{h_{air}}$) : $D_{h_{air}} = \frac{4*\varepsilon}{S_v}$ = 21.13mm

Average Coolant Velocity (V_{air}): $V_{cool} = \frac{\dot{m}_{cool}}{\frac{V_{channel}}{L_{tube}}} = 1.94 m/s$

Reynolds Number: $Re_{air} = \frac{\rho_{air} V_{air} D_h}{\mu_{air}} = 188$

Air Pressure Drop: $\Delta P_{cool} = a * Re_{cool}^{b} * \frac{L}{0.04} = 452.2\ Pa$

We then calculate the coolant pressure drop using Darcy-Weisbach previously declared as Gyroid Coolant Pressure drop.

Volumetric Flow rate of coolant $(\dot{V})$: $\dot{V} = \frac{\dot{m_{cool}}}{\rho_{cool}} = 6.0 * 10^{-4} \frac{m^3}{s}$

Unit Cell Count in Gyroid (U_c) : $U_c = \frac{\pi r^2 * L_{tube}}{0.5 * L_{cell}^3} = 2789\ cells$

Surface Area of Gyroid wall ($SA_{GyroidWall}$) : $SA_{GyroidWall} = \left(3.1 * L_{cell}^2 * U_c\right) * 0.92 = 16.1\ m^2$

Flow Area for coolant (A_{flow}) : $A_{flow} = SA_{GyroidWall} * Channel_{gap} = 0.048\ m^2$

Hydraulic Diameter for Coolant ($D_{h_{cool}}$) : $D_{h_{cool}} = 4 * Channel_{gap}$ = 12mm

Coolant Velocity ($v_{coolant}$) : $v_{coolant} = \frac{A_{flow}}{\dot{V}} = 0.012 m/s$

Coolant Reynolds Number: $Re_{cool} = \frac{\rho_{cool} V_{cool} D_h}{\mu_{cool}} = 149.3$

Friction factor for coolant (f_{cool}): $f_{cool} = \frac{64}{f_{cool}}$ = 0.428

Path length of coolant (L_{path}): $L_{path} = L_{tube} * pathLengthFactor$ = 1.29m

Total Gyroid Coolant Pressure Drop: $\Delta P_{cool} = \left(\frac{f * L_{path} * \rho_{cool} * v^2}{2 * D_h}\right) * Complexity\_Factor$ = 6 Pa

With this information we are then able to plot our gyroid cell in 3D as well as the full gyroid in the cylindrical duct in 3D. These are displayed in figure 3.2.10.4 and figure 3.2.10.5

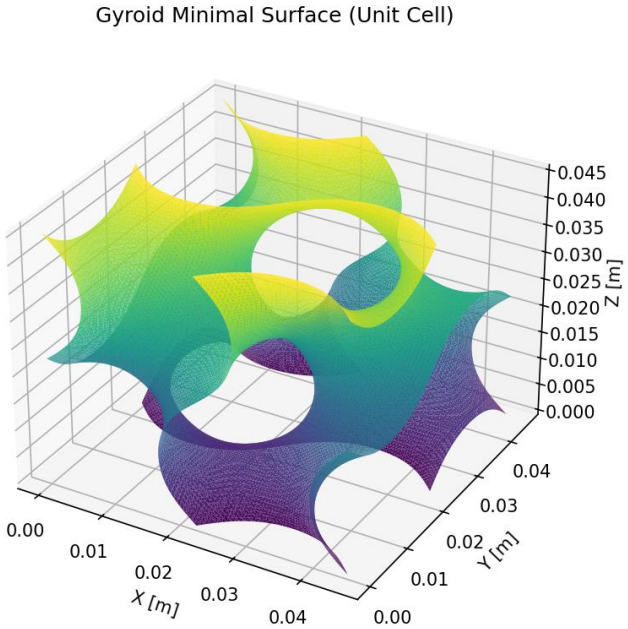

Figure 3.2.10.4- Gyroid Minimal Surface (Unit Cell)

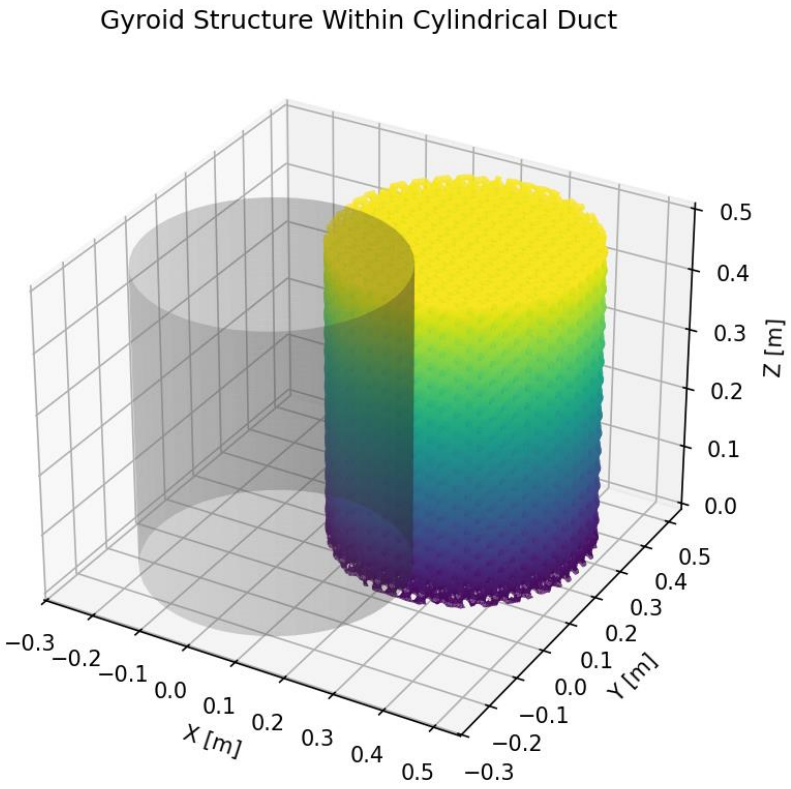

Figure 3.2.10.5 - Gyroid Structure Within Cylindrical Duct

This system would be 0.55m long, 0.5m diameter and it would weigh roughly 36.6 kg if made out of copper plated aluminium. The complexity that this system for the reduction in space it offers is likely not worth the ease of using COTS, however LAM-GTD is at the forefront of innovation, and it remains a possible solution.

In both systems the then condensed water would then be treated with UV-C via the 9D PearlAqua before being recycled into the NDS system [94]. The 9D PearlyAqua is rated for 10000 hours of continuous use and can deal with flow rates of 1.5 liter per minute. Additionally, its easily replaceable LED lamp module make it align with the redundant and easily maintainable design philosophy of this AMS.

3.2.11. Heater

Based on the psychrometric charts, it is evident that air must be cooled in order to achieve condensation. To maintain a comfortable ambient temperature for both plants and personnel, the system should therefore incorporate a heating element. In the identified worst-case scenario, it is assumed that reheating will be required from 16°C to 22°C. The required heating power can then be determined using the energy balance equation.

Mass flow rate $\dot{m} = \rho * \frac{1000\frac{m}{s}}{3600\frac{s}{hr}} = 0.825 * 0.278 = 0.231\ kg/s$

Energy equation: $Q = \dot{m} * C_p * \Delta T$ = 0.231* 1005 * 6 = 1392 Watts

Assuming a heater of 70% efficiency: $Power = \frac{1392}{0.7} = 1988\ Watts$

The VEAB CV31-315-230 VAC1 heater has a weight of 16 kg and dimensions of 375 mm * 397 mm * 340 mm. It delivers a heating output of 2000 W with a theoretical 5 Pa pressure drop (see Annex 1.8). Additionally, the unit is equipped with integrated sensors that allow for precise temperature regulation.

3.2.12. VOC Filter

Compared to the earlier design of the AMS, the decision to decouple the Volatile Organic Compound (VOC) filter unit from the core system architecture enables a significant reduction in pressure drop while also improving system compactness.

To remove VOCs and ethylene, we draw inspiration from the Trace Contaminant Control Subassembly (TCCS) ISS. The TCCS employs a granular activated carbon bed for VOC adsorption, followed by a thermal catalytic oxidizer to remove residual gaseous compounds such as methane and carbon monoxide. Additionally, a lithium hydroxide (LiOH) bed is integrated downstream to capture acid gases generated during the oxidation process. Notably, the TCCS operates at a relatively low volumetric flow rate of approximately 15.3 m³/h, as it is not required to process the entire cabin air volume simultaneously. Instead, it gradually removes trace contaminants, maintaining air quality within Spacecraft Maximum Allowable Concentration (SMAC) thresholds. This design strategy achieves a balance between minimizing system mass and energy consumption while ensuring effective contaminant control [50].

Adopting a similar design philosophy, our system operates at lower volumetric flow rates for efficient removal of trace gases in a compact configuration. However, recognizing that LAM-GTD will present a more biologically active environment, the system must be capable of accommodating higher flow rates to ensure comprehensive VOC and ethylene removal. To meet this requirement, we propose integrating the Levoit Core® 400S Smart Air Purifier, which supports a flow rate of 442 m³/h (equivalent

to 5 air changes per hour [ACH]) and features modular filter capability. This modularity allows flexible deployment of filtration media tailored to specific contaminants. In conditions where ethylene concentrations exceed acceptable limits, potassium permanganate filters can be deployed in conjunction with activated carbon filters for enhanced removal efficiency.

The proposed air purification unit has physical dimensions of 27.4 × 27.4 × 52 cm, a total weight of 6.4 kg, and an average power consumption of 38 W. (See Annex 1.9)

3.2.13. Data Handling Control System

For the LAM-GTD, the DHCS is responsible for managing all subsystems, including AMS, nutrient delivery, and thermal control. The sensors shown below will be placed at the entrance and exit of the AMS while constantly communicating with the DHCS to adjust all components of the AMS to maintain optimum conditions. The DHCS follows a decentralized architecture, reducing the complexity of the main computing unit.

Baseline Design**:**

The DHCS consists of two redundant electronic boxes containing:

- Main computer board
- Acquisition and interface boards
- Mass storage & backplane
- Connectors & harnesses

All subsystems are designed to have their own computing intelligence, reducing dependency on a single unit. These can be seen in Table 3.2.13. More information can be found on the sensors in Annex 1.10

Table 3.2.13: Sensors Integrated into the DHCS

Sensor	**Commercial Option**	**Power Consumption (W)**	**Weight (kg)**
Volumetric Flow Rate	EE650 [60]	4.1	0.25
Carbon Dioxide, Temperature & Humidity	EE850 [60]	0.36	0.25
Differential pressure measurement	EE600 [60]	0.1	0.25
Oxygen	FDO2 [59]	0.03	0.01
Ethylene	GASERA ONE [58]	75	13

System Redundancy & Fail-Safe Mechanisms:

- The system is one-failure tolerant, ensuring continuous AMS operations even if a component fails.
- Automatic solenoid valves, airflow redundancy, and CO_2 injection backup are implemented to maintain stable atmospheric conditions.

Interfaces & Control:

- The DHCS interfaces with robotic arms, mission control, and secondary payloads like the C.R.O.P. filtration system.
- The system manages data flow between the AMS, power, and thermal control subsystems

3.2.14. Excess CO_2

An astronaut generates approximately 1 kg of CO_2 per day. Based on this rate and our previous calculations, it is clear that CO_2 accumulation will exceed plant uptake. Over a 120-day period, astronauts would produce around 120 kg of CO_2 per astronaut, while a crop of tomatoes with a typical 120-day growth cycle would only absorb approximately 54 kg of CO_2.

To help balance this excess, a photobioreactor (PBR) measuring 50 cm × 50 cm × 50 cm and filled with *Chlorella vulgaris* could contribute to CO_2 mitigation. Assuming a CO_2 fixation rate between 3.6 kg CO_2/m^3/day and 7.2 kg CO_2/m^3/day, this system could potentially capture between 54 kg – 108 kg of CO_2 over the same 120-day period [97].

In addition to its role in atmospheric CO_2 control, *Chlorella vulgaris* is a nutrient-dense microalgae that offers several advantages as a food source. It contains 50–60% complete protein by dry weight and is rich in essential vitamins (including active B12), minerals like iron and magnesium, and antioxidants such as chlorophyll. Its ability to produce oxygen and absorb CO_2 makes it ideal for closed-loop systems like space missions, where it can serve both as a food source and a life support component [98].

It should be noted that this is a generalized estimate, as algal growth and CO_2 fixation are influenced by environmental variables such as light intensity, temperature, and nutrient availability. Further experimental validation is recommended. The LAM-GTD facility would be an ideal environment to test the performance and feasibility of this integrated life support technology.

3.2.15. Air Exiting LAM-GTD

To function as a BLSS, LAM-GTD must be capable of supplying oxygen-rich air back to the crew module. One viable approach is the integration of Mixed Matrix Membranes (MMMs). Recent studies indicate that MMMs incorporating Metal-Organic Frameworks (MOFs) exhibit high O_2/N_2 selectivity while maintaining high oxygen permeability, making them well-suited for efficient air separation.

These membranes could be integrated into the gas exchange interface between LAM-GTD and the crew module, enabling a continuous supply of oxygen-enriched air to the crew [57] [82]. A key advantage of these systems is their compatibility with standard human-rated environmental conditions, with the primary requirement being elevated operating pressure (typically 2–30 bar). As such, the only additional system requirement would be a compressor to pressurize the air before passing it through the membrane.

4. Analysis and Discussion

4.1. AMS Component Calculations

4.1.1. Blowers

The required airflow within the LAM-GTD was determined based on a target of 11.5 ACH for a total module volume of 87 m^3, resulting in an airflow requirement of approximately 1000 m^3/h. This ACH value represents a deliberate compromise between energy efficiency and effective air mixing, informed by performance data from both the ISS and commercial CEA systems. To meet this requirement, the RadiPac commercial blower was selected for its ability to deliver the necessary airflow while offering a modular design, high performance, low noise output, and minimal maintenance demands.

At around 70 dBA when operating at max power these blowers are in line with the 70 dBA recommended by NASA [101]. Additionally, the fans have space in the AMS for some noise dampening which would further reduce their noise levels.

4.1.2. Localized Fans for Air Mixing

To ensure homogeneity of air distribution around the crops and prevent localized CO_2 build-up, 15 small fans are used to ensure constant airflow on the growing area. This setup ensures uniform transpiration rates, avoiding microclimates around crops, and contributing to overall system redundancy. The selected fans provide compact, low-power, and efficient airflow solutions and are easily replaceable, enhancing system maintainability.

4.1.3. UV-C Lamps

The use of UV-C lamps ensures airborne pathogen control within the AMS. Calculations were based on a target UV-C dose of 5000 $\mu W \cdot s/cm^2$. With an airflow velocity of 1.43 m/s and a duct length of 0.45 meters, the exposure time per air parcel was calculated to be approximately 0.31 seconds. Consequently, the required UV-C intensity was approximately 15,851 $\mu W/cm^2$.
To achieve this, 14 NL-T8 UV 25W/254 G13 lamps were deemed sufficient to meet the necessary germicidal power (total UV-C output of ~114.8 W). However, as we know from EDEN ISS MTF microbial build up was a big problem, as this duct can accommodate more UV-C lights and that their power consumption is not excessive it is recommended to start off with 28 NL-T8 UV 25W/254 G13 lamps to be certain that all unwanted pathogens are eliminated. As LAM-GTD is operated tests can be run to determine how many UV-C lamps are truly necessary. Additionally reflective surfaces within the air duct should be installed to enhance radiation uniformity and disinfection efficiency.

4.1.4. Dehumidifier

The dehumidifier plays a pivotal role in the AMS of the LAM-GTD by maintaining the relative humidity within the specified range of 45% to 85%. Effective humidity regulation is essential not only for optimal plant transpiration and gas exchange but also to prevent microbial growth and protect other system components like filters and electronic equipment.

The high energy requirements of the dehumidifier make it a crucial part of the AMS and its design will be crucial to the mission's success. In this thesis two options were proposed: The VEAB CFK 315-2,5

with 10.6 kW of cooling power and dimensions of 553mm*639mm*462mm and the Gyroid Heat exchanger with a theoretical cooling power of 20.1 kW and dimensions of 550mm long and 500mm diameter.

The VEAB CFK 315-2,5 is a safe choice, with VEAB being a Swedish company with a great track record, this heat exchanger would be easy to acquire and install. Although bulkier than the Gyroid heat exchanger its proven track record is hard to overstate when dealing with future lunar habitats.

The Gyroid heat exchanger is an innovative but unproven design. While the literature suggests that this technology could provide substantial savings in space it lacks the maturity of existing heat exchanger technologies. With space coming at a premium in space exploration, LAM-GTD could be the perfect place to test this innovative design. If the practice validates the theory, then this technology could bring about significant improvements to the AMS.

Regardless of which solution is chosen it should be noted that in EDEN ISS MTF it was observed that microbial loads were always a major problem when dealing with the dehumidifier. Therefore, it is recommended to coat the dehumidifiers internal component with Heresite.

Heresite coatings offer exceptional protection for heat exchangers and HVAC systems, combining corrosion resistance, microbial resistance, and long-term durability. They create a smooth, non-porous surface that prevents the buildup of mold, bacteria, and biofilms, reducing the risk of microbiologically influenced corrosion (MIC) and improving air quality. Their ultra-thin application maintains excellent heat transfer efficiency while shielding metal components from salt spray, chemicals, ammonia, and acidic gases, making them ideal for harsh or humid environments. Heresite coatings also withstand aggressive cleaning agents, enabling easier maintenance and extending equipment lifespan. Overall, they reduce system breakdowns, lower maintenance costs, and deliver lasting performance in even the most demanding conditions [84].

4.1.5. Heater

The heater is one of the major power consumers of the AMS, however with proper data handling and control it may not be necessary. If the temperature of the air can be properly monitored and controlled it would be possible to keep the air at the nominal temperature using the 11 kW of sensible heat generated by the equipment in LAM-GTD. Additionally proper control of the air temperature would also reduce the cooling requirements leading to a more efficient system.
For the sake of this design it is included to make sure every requirement is checked, however when LAM-GTD is deployed and tested it may be deemed unnecessary.

4.1.6. VOC Filter

As pressure drop through VOC filters increases exponentially with air flow rate, it was a major improvement to decouple the filters from the AMS in this project. The ACH necessary to filter out the unwanted VOC is much lower than what LAM-GTD requires for nominal operation. This enabled the AMS to be made much more compact while reattaining its efficiency. Additionally moving the VOC filter system to a standalone unit allows for the replacement of filters to be much easier. The Levoit Core® works great for this case allowing for many different filters to suit the needs of the system. Particularly the potassium permanganate filters will be crucial in filtering out the ethylene [85].

4.1.7. Sensors

The sensors selected for this project are already in use at the current EDEN test site in Bremen, with two notable exceptions. The FDO2, while new to this setup, brings a strong track record from its

deployment on the Mars 2020 Rover, lending it significant credibility. The GASERA One, on the other hand, is a novel addition. Detecting ethylene has historically been difficult due to the need for sensitivity in the parts-per-billion (ppb) range. However, the GASERA One utilizes photoacoustic spectroscopy and is expected to provide the necessary sensitivity to detect subtle changes in ethylene concentration [58].

4.1.8. Where to get the cooling power

Regardless of the type of heat exchanger selected, it remains clear that the cooling load for LAM-GTD will be substantial. To maximize both efficiency and safety, our approach mirrors proven methodologies used on the ISS. Specifically, it is recommended to use water as the primary coolant within the LAM-GTD module due to its high heat capacity, non-toxicity, and overall safety for human interactions.

To minimise the reliance on solar panels and batteries this thesis recommends to complement the internal water loop, with an external liquid ammonia loop, leveraging ammonia's exceptional thermal conductivity and heat transfer capabilities. This ammonia loop would be routed through radiators positioned externally to the LAM, efficiently dissipating heat into the cold vacuum of space. The use of this dual-loop system provides several key advantages, including enhanced thermal management capability, increased redundancy, and reduced risks associated with ammonia leakage inside human habitats.

Implementing this hybrid water-ammonia cooling system would significantly decrease reliance on solar-generated power, thereby minimizing overall energy consumption and operational complexity. This approach enables the AMS and associated cooling hardware to be more compact and efficient. Additionally, utilizing resources potentially available on the Moon, such as water ice, supports sustainable and self-sufficient long-term operation of extraterrestrial habitats, aligning with broader mission objectives of resource efficiency and minimal resupply from Earth [34].

4.1.9. Operational Redundancy and Maintainability

To ensure long-term operational stability, the AMS design incorporates redundancy in fans, sensors, and control systems. Modular COTS allows rapid replacement, while remote diagnostics via the DHCS reduce the need for manual interventions. Maintenance protocols derived from EDEN ISS MTF best practices will be adapted for LAM-GTD, focusing on minimizing crew time, ensuring resilience to part failures, and enabling real-time system adaptation.

Standardized cartridges for filters and UV-C bulbs, plug-and-play sensor modules, and openings enabling easy access to the components reducing the frequency and complexity of maintenance tasks. An example of this is the large hatch shown in Figure 4.1.9 that enables access to the inner components of the AMS.

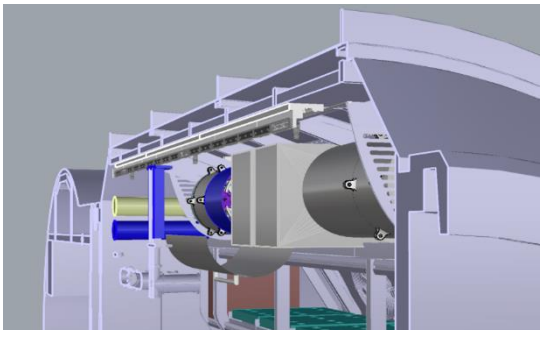

Figure 4.1.9- Hatch for ease of maintenance

4.1.10. Final system

Table 4.1.10.1 and Table 4.1.10.2 lists all AMS components along with their weight, power consumption, and pressure drop. It presents two configurations: one using entirely COTS components, and the other incorporating the gyroid structure.

Table 4.1.10.1 AMS with COTS Components

Component	Power (W)	Weight (kg)	Pressure Drop (Pa)
Blower	500	6	0
Sensors	80	14	0
Fans	600	12.3	0
UV-C Lights	700	1.96	10
Pre-Filter	0	7.7	40
HEPA-Filter	0	9.6	50
VEAB Dehumidifier	20100	32	70
VEAB Heater	1988	16	5
Blower	500	6	0
Duct	0	15.13	5
VOC filter	38	6.4	0
Total for one AMS Module	4406	127.1	166.5
Total For Entire AMS	8774	247.78	166.5

Table 4.1.10.2: AMS with Gyroid dehumidifier

Component	Power (W)	Weight (kg)	Pressure Drop (Pa)
Blower	500	6	0
Sensors	80	14	0
Fans	600	12.3	0
UV-C Lights	700	1.96	10
Pre-Filter	0	7.7	40
HEPA-Filter	0	9.6	50
Gyroid Dehumidifier	20100	36.6	70
VEAB Heater	1988	16	5
Blower	500	6	0
Duct	0	15.13	5
VOC filter	38	6.4	0
Total for one AMS Module	4406	131.7	548.7
Total For Entire AMS	8774	257	548.7

The two tables show that both system configurations are broadly similar. The gyroid-based dehumidifier is more compact but comes with a slight increase in weight and a significantly higher pressure drop. Nonetheless, the total weight of both systems remains well below the 500 kg allocation for the AMS, and the increased pressure drop can be effectively managed by the selected blowers.

The two different system are shown below. Figure 4.1.10.1 shows the COTS AMS and Figure 4.1.10.2 the Gyroid AMS.

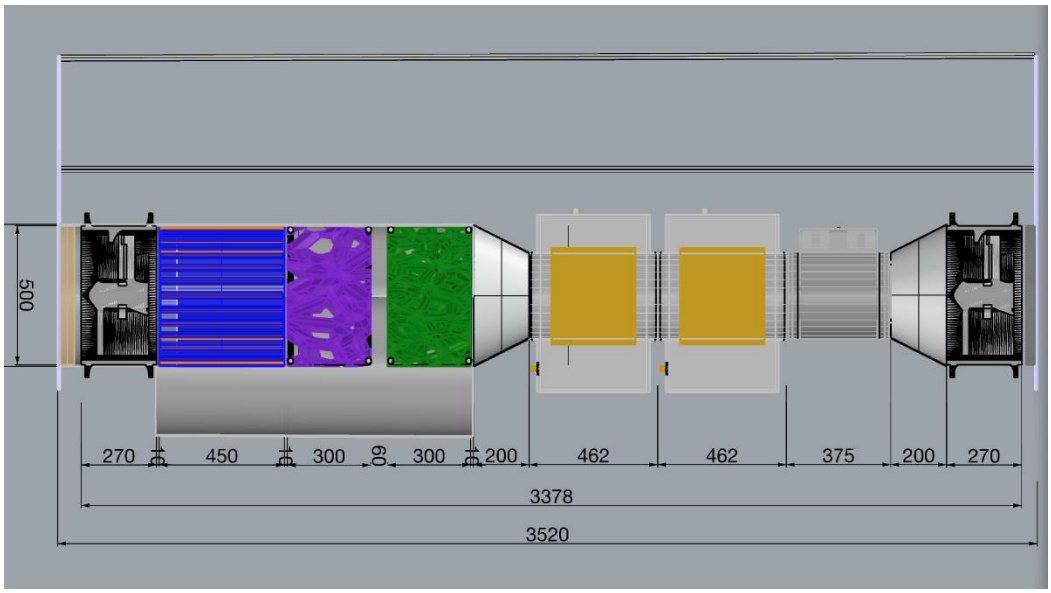

Figure 4.1.10.1 - COTS AMS

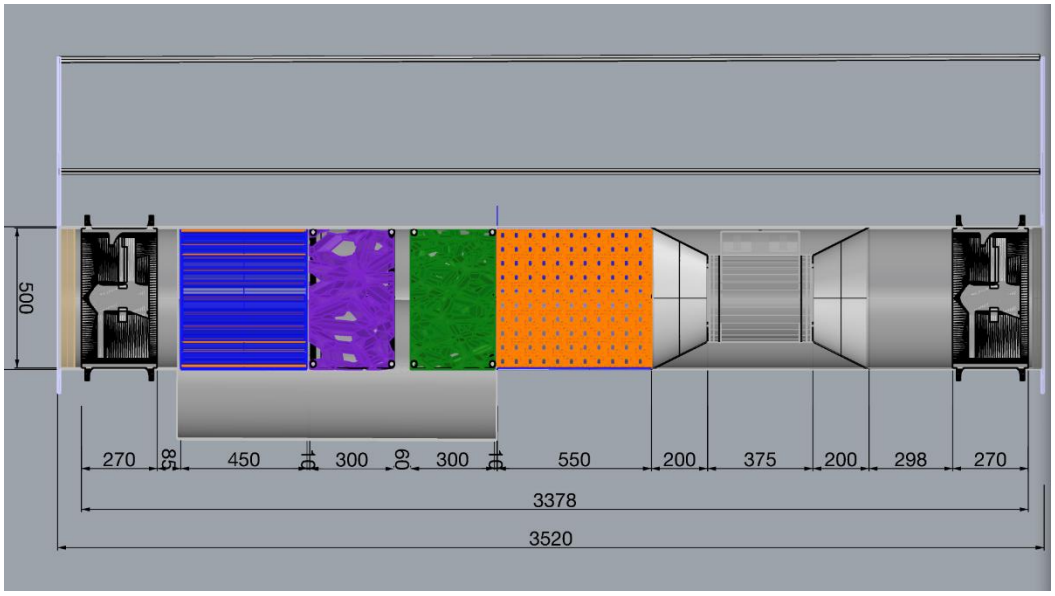

Figure 4.1.10.22 - Gyroid AMS

From left to right, the components of the AMS are: blower, UV-C light, pre-filter, HEPA filter, VEAB or gyroid dehumidifier, heater, and a second blower. When comparing the two configurations, the integration of the gyroid heat exchanger reduces the overall length of the AMS by approximately 30 cm.

Figure 4.1.10.3 illustrates the complete AMS setup complete with side fans using only COTS components.

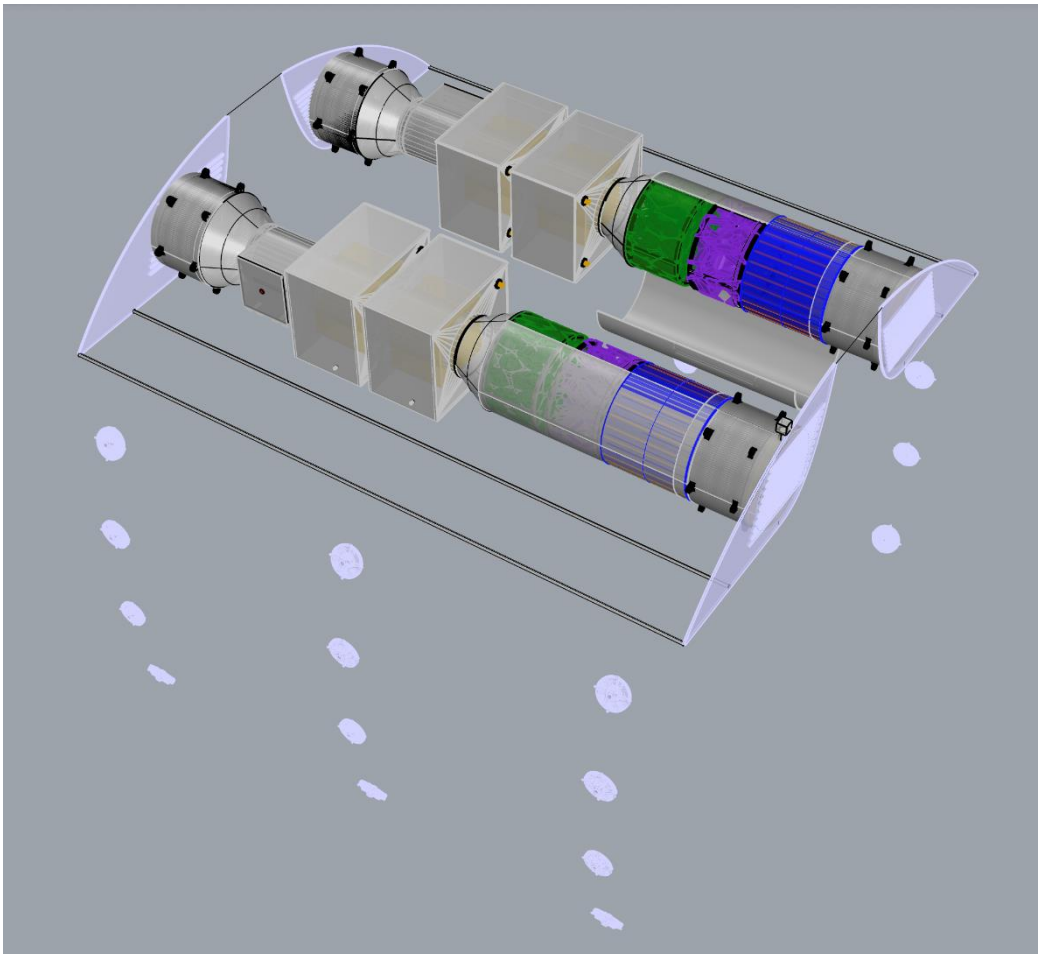

Figure 4.1.10.3 - Whole COTS AMS

Here you can see that a hatch has been designed to allow easy access to the components of the AMS to ensure long-term operational stability by having ease of maintenance. Additionally, you can see each of the fans used to maintain airflow on the crops. In Figure 4.1.10.4 and Figure 4.1.10.5 below the entire AMS is shown integrated to LAM-GTD.

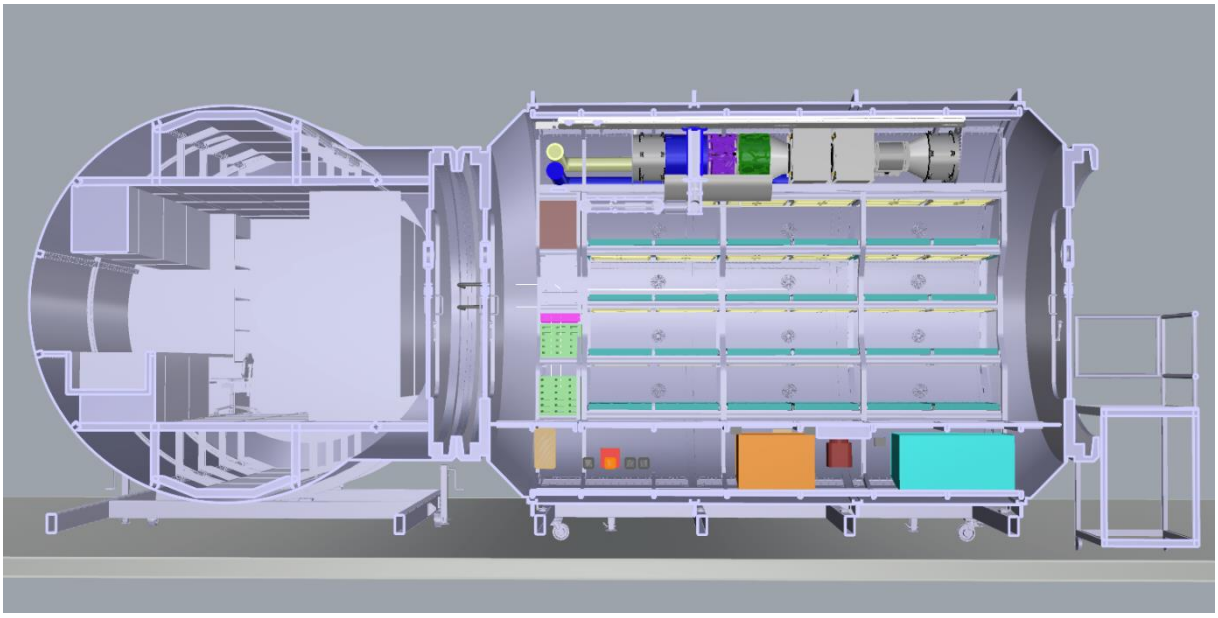

Figure 4.1.10.4- Integrated AMS Front View

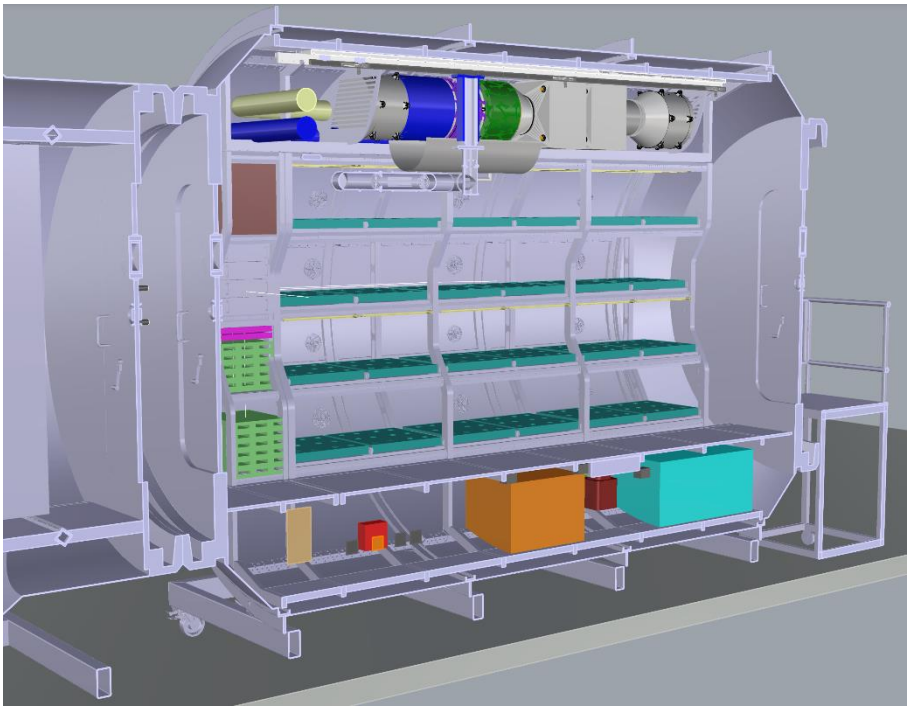

Figure 4.1.10.5- Integrated AMS Angled View

5. Conclusions and future work

As humanity moves closer to establishing permanent extraterrestrial settlements, the development of robust and scalable life support systems is becoming increasingly vital. This thesis has explored the design and optimization of an AMS for the LAM-GTD, contributing to the broader field of BLSS. The work presented here bridges existing technological developments in CEA with the unique demands of off-Earth environments, specifically the Moon.

The AMS is central to creating a viable agricultural module in space, as it regulates temperature, humidity, CO_2/O_2 levels, air filtration, and trace contaminants, all of which are essential for plant health and human safety. Drawing from lessons learned in terrestrial analogues like EDEN ISS MTF, Lunar Palace 1, and the APH aboard the ISS, the design proposed in this thesis integrates critical improvements in energy efficiency, modularity, maintenance accessibility, and microbial resilience.

Special attention was given to the dehumidification subsystem, identified as a historically weak point in earlier prototypes due to under-dimensioned cooling capacity and microbial contamination. This thesis evaluated both conventional COTS and advanced gyroid-based dehumidifier designs, ultimately demonstrating that while the gyroid structure increases pressure drop, it reduces the system's spatial footprint.
Both configurations remained well below the allocated weight limit of 500 kg, and their pressure drops are within the handling capacity of the selected blowers.

A modular approach was used to design the AMS, allowing for redundancy and ease of maintenance. Plug-and-play sensor modules, standardized cartridges for filters and UV-C lamps, and a centralized control system reduce the need for crew time and support rapid diagnostics and repair. The system was also designed with scalability and adaptability in mind, ensuring it can operate effectively in closed-loop terrestrial test beds and future lunar deployments.

Throughout the design process, rigorous engineering analysis was conducted, including airflow calculations, pressure drop estimations, UV-C dosage modelling, and heat load balancing. Additionally, two python scripts were developed, one to improve the evapotranspiration modelling capabilities of the project and one to enable rapid iteration of the gyroid dehumidifier.

This yielded an AMS system with a vastly improved dehumidification system, increased microbial control, improved sensors specifically with regards to ethylene detection, and a decoupled VOC system allowing for lower pressure drops.

Ultimately, this thesis offers a validated design framework and practical insights for future AMS iterations, contributing to the field of space agriculture. As the LAM-GTD prepares for its anticipated deployment, the AMS design presented here lays the groundwork for long-term, closed-loop, biologically regenerative farming systems on the Moon and beyond.

The next phase in the development of the LAM-GTD will involve conducting a comprehensive computational fluid dynamics analysis of the proposed system to further validate the design parameters and performance projections outlined in this paper. If the computational fluid dynamics analysis results corroborate these findings, the project can proceed with the acquisition and construction phase. Once the LAM-GTD is operational, critical data collection efforts can begin, focusing on system performance, environmental stability, and failure response under controlled testing conditions.

Bibliography

[1] W. Hallmann, *Handbuch der Raumfahrttechnik: Grundlagen - Nutzung, Raumfahrtsysteme - Produktsicherung u. Projektmanagement*. München: Hanser, 1988.

[2] "Plant Pillow Preparation for the Veggie Plant Growth System on the International Space Station," *ResearchGate*. [Online]. Available: https://www.researchgate.net/publication/343129660_Plant_Pillow_Preparation_for_the_Veggie_Plant_Growth_System_on_the_International_Space_Station. [Accessed: Oct. 1, 2024].

[3] "Veggie Plant Growth System Factsheet," *NASA*, 2019. [Online]. Available: https://www.nasa.gov/wp-content/uploads/2019/04/veggie_fact_sheet_508.pdf. [Accessed: Oct. 1, 2024].

[4] "EDEN ISS Greenhouse Returns to Bremen and Has a New Destination," *DLR*, 2023. [Online]. Available: https://www.dlr.de/en/latest/news/2023/03/eden-iss-greenhouse-returns-to-bremen-and-has-a-new-destination#:~:text=Over%20the%20course%20of%20the%20mission%2C%20more%20than%20one%20tonne,ingredients%20and%20herbs%20were%20harvested.&text=Most%20recently%2C%20NASA%20guest%20scientist,she%20returned%20in%20spring%202022 [Accessed: Oct. 1, 2024].

[5] "EDEN ISS Project," *EDEN ISS*. [Online]. Available: https://eden-iss.net. [Accessed: Oct. 1, 2024].

[6] G. Giacomelli, "Lunar Greenhouse Prototype for Bioregenerative Life Support System," *University of Arizona*, 2012. [Online]. Available: https://cales.arizona.edu/lunargreenhouse/Documents/2012-07-20_01_Giacomelli.pdf. [Accessed: Oct. 4, 2024].

[7] G. Boscheri et al., "Modified energy cascade model adapted for a multicrop Lunar greenhouse prototype," *Advances in Space Research*, 2012. [Online]. Available: https://www.sciencedirect.com/science/article/pii/S0273117712003705. [Accessed: Oct. 4, 2024].

[8] J. Hu, S. Li, H. Liu, and D. Hu, "Reliability and lifetime estimation of bio-regenerative life support system based on 370-day closed human experiment of lunar palace 1 and Monte Carlo simulation," *Acta Astronautica* , 2023. [Online]. Available: https://www.sciencedirect.com/science/article/pii/S0094576522006294. [Accessed: Oct. 4, 2024].

[9] Y. Fu et al., "A case for supporting human long-term survival on the moon: 'Lunar Palace 365' mission," *Acta Astronautica* , 2025. [Online]. Available: https://www.sciencedirect.com/science/article/pii/S0094576524007343. [Accessed: Oct. 7, 2024].

[10] K. H. Hasenstein and S. P. John et al., "Assessing Radish Health during Space Cultivation by Gene Transcription," *Plants*, vol. 12, no. 19, p. 3458, 2023. [Online]. Available: https://www.mdpi.com/2223-7747/12/19/3458. [Accessed: Oct. 7, 2024].

[11] O. Monje and J. T. Richards et al., "Hardware Validation of the Advanced Plant Habitat on ISS: Canopy Photosynthesis in Reduced Gravity," *Frontiers in Plant Science*, 2020. [Online]. Available: https://www.frontiersin.org/journals/plant-science/articles/10.3389/fpls.2020.00673/full. [Accessed: Oct. 7, 2024].

[12] G. Bonzano and V. Vrakking, "D3.7 – Environmental Control Design Document," DLR, [Online]. Available: https://zenodo.org/records/3229763 [Accessed: Oct. 10, 2024].

[13] "NASA Spinoff," *NASA*. [Online]. Available: https://spinoff.nasa.gov. [Accessed: Oct. 10, 2024].

[14] "Everyday Benefits of Space Exploration," *Canadian Space Agency*. [Online]. Available: https://www.asc-csa.gc.ca/eng/about/everyday-benefits-of-space-exploration/. [Accessed: Oct. 10, 2024].

[15] "Here's how space technology affects our daily lives," *World Economic Forum*, 2024. [Online]. Available: https://www.weforum.org/stories/2024/09/4-surprising-ways-space-technology-shapes-our-everyday/. [Accessed: Oct. 10, 2024].

[16] "Why Go to Space?," *NASA*. [Online]. Available: https://www.nasa.gov/humans-in-space/why-go-to-space/. [Accessed: Oct. 10, 2024].

[17] "The 10 Biggest Advantages of Vertical Farming," *CambridgeHOK*. [Online]. Available: https://cambridgehok.co.uk/news/the-10-biggest-advantages-of-vertical-farming. [Accessed: Oct. 10, 2024].

[18] "Environmental Control and Life Support System," *NASA*, 2007. [Online]. Available: https://ntrs.nasa.gov/api/citations/20070016582/downloads/20070016582.pdf. [Accessed: Oct. 14, 2024].

[19] S. De Pascale et al., "Biology and crop production in Space environments: Challenges and opportunities," *Science Direct*, 2021. [Online]. Available: https://www.sciencedirect.com/science/article/pii/S2214552421000183. [Accessed: Oct. 14, 2024].

[20] "Moon is Safe for Long-Term Human Exploration," *Science.org*. [Online]. Available: https://www.science.org/content/article/moon-safe-long-term-human-exploration-first-surface-radiation-measurements-show. [Accessed: Oct. 14, 2024].

[21] M. von Einem, R. Groll, and C. Heinicke, "Computational modeling of a ventilation concept for a lunar habitat laboratory," *Acta Astronautica* , 2022. [Online]. Available: https://www.sciencedirect.com/science/article/pii/S2468896722000106. [Accessed: Oct. 14, 2024].

[22] V. Maiwald et al., "Lunar Agriculture Module Ground Test Demonstrator – An International Approach for Realizing Plant-based Bio-regenerative Life Support," presented at the *75th*

***International Astronautical Congress*, 2024. [Online]. Available: https://elib.dlr.de/207197/1/IAC-24%2CD3%2C2A%2C2%2Cx86994.pdf. [Accessed: Oct. 19, 2024].**

[23] V. Maiwald, V. Vrakking, P. Zabel, D. Schubert, R. Waclavicek, M. Dorn, L. Fiore, B. Imhof, T. Rousek, V. Rossetti and C. Zeidler, "From ice to space: a greenhouse design for Moon or Mars based on a prototype deployed in Antarctica," *CEAS Space Journal*, 2020. [Online]. Available: https://link.springer.com/article/10.1007/s12567-020-00318-4 [Accessed: Oct. 19, 2024].

[24] M. R. Georgescu et al., "Numerical and Experimental Study of the ISS Crew Quarters Ventilation," *Journal of Building Engineering*, vol. 41, 2021. [Online]. Available: https://www.sciencedirect.com/science/article/abs/pii/S2352710221005726. [Accessed: Oct. 19, 2024].

[25] "Operating an Outpost," 2018. *NASA*, [Online]. Available: https://www.nasa.gov/wp-content/uploads/2018/04/iss-operating_an_outpost-tagged.pdf. [Accessed: Oct. 20, 2024].

[26] "International Space Station," *NASA*. [Online]. Available: https://www.nasa.gov/reference/international-space-station. [Accessed: Oct. 20, 2024].

[27] "International Space Station Bacteria Filter Element Service Life Evaluation," *NASA*, 2005. [Online]. Available: https://ntrs.nasa.gov/api/citations/20050215100/downloads/20050215100.pdf. [Accessed: Oct. 20, 2024].

[28] "Ventilation on the ISS," *AIVC*. [Online]. Available: https://www.aivc.org/sites/default/files/members_area/medias/pdf/Conf/2001/Raatschen%20Ventilation%20on%20the%20ISS.pdf. [Accessed: Oct. 22, 2024].

[29] T. Kozai, G. Niu, and M. Takagaki, Plant Factory: An Indoor Vertical Farming System for Efficient Quality Food Production. *Academic Press*, 2016.

[30] M. Stasiak et al., "Radish (Raphanus sativa L. cv. Cherry Bomb II) growth, net carbon exchange rate, and transpiration at decreased atmospheric pressure and/or oxygen," *Gravitational and Space Research*, vol. 26, no. 1, 2012. [Online]. Available: https://cordis.europa.eu/docs/results/272/272520/final1-radish-2012.pdf [Accessed: Oct. 25, 2024].

[31] M. S. Anderson, M. K. Ewert, and J. F. Keener, "Life Support Baseline Values and Assumptions Document," NASA, Houston, 2018.

[32] M. F. Franke and T. Korth, "S/S Design Description," *DLR*, Bremen, 2024.

[33] K. Iwabuchi and K. Kurata, "Effects of Low Pressure on Gas Exchange in Spinach," *Advances in Space Research*, vol. 31, pp. 241–244, 2003.

[34] "ISS ATCS Overview," *NASA*, 2021. [Online]. Available: https://www.nasa.gov/wp-content/uploads/2021/02/473486main_iss_atcs_overview.pdf. [Accessed: Oct. 25, 2024].

[35] F. Chen et al., "Heat transfer efficiency enhancement of gyroid heat exchanger based on multidimensional gradient structure design," *International Journal of Heat and Mass Transfer*, 2023. [Online]. Available: https://www.sciencedirect.com/science/article/abs/pii/S073519332300516X. [Accessed: Oct. 27, 2024].

[36] O. Alketan, D.-W. Lee, and R. Abu Al-Rub, "Mechanical Properties of Gyroidal Stochastic Cellular Materials," *Research Gate*, 2021. [Online]. Available: https://www.researchgate.net/publication/355786933_Mechanical_Properties_of_Additively-Manufactured_Sheet-Based_Gyroidal_Stochastic_Cellular_Materials. [Accessed: Oct. 27, 2024].

[37] K. Kus, M. Wójcik, Z. Malecha, and Z. Rogala, "Numerical and Experimental Investigation of Gyroid Heat Exchanger," *International Journal of Heat and Mass Transfer*, 2024. [Online]. Available: https://www.sciencedirect.com/science/article/pii/S0017931024007130. [Accessed: Nov. 1, 2024].

[38] "Dew Point Calculator for Moisture," *GasQuip*. [Online]. Available: https://gasquip.com/dew-point-calculator-for-mois-tu-re/. [Accessed: Nov. 1, 2024].

[39] "SPC Online Coil Selector," *POA-SPC*. [Online]. Available: https://poa-spc.com. [Accessed: Nov. 1, 2024].

[40] K. M. Gilk and S. L. Olson, "Evaluation of the Oxygen Concentrator Prototypes: Pressure Swing Adsorption Prototype and Electrochemical Prototype," *NASA*, 2015. [Online]. Available: https://ntrs.nasa.gov/api/citations/20150011038/downloads/20150011038.pdf. [Accessed: Nov. 1, 2024].

[41] "RadiPac Product Brochure," *ebm-papst*. [Online]. Available: https://www.ebmpapst.com/content/dam/ebm-papst/gated-content/product-campaigns/Broschuere_neuer_RadiPac_de.pdf. [Accessed: Nov. 1, 2024].

[42] " DV 6224 Axial Fan," *ebm-papst*. [Online]. Available: https://img.ebmpapst.com/products/datasheets/DC-Diagonalventilator-DV6224-GER.pdf. [Accessed: Nov. 1, 2024].

[43] "Radium Lighting Product Catalog," *Radium*. [Online]. Available: https://www.radium.de/de/radium_product_catalog/pdf/55341. [Accessed: Nov. 3, 2024].

[44] "Ultraviolet Germicidal Irradiation Handbook," *Research Gate*, 2011. [Online]. Available: https://www.researchgate.net/publication/278717381. [Accessed: Nov. 3, 2024].

[45] L. Wang, E. Iddio, and B. Ewers, "Introductory overview: Evapotranspiration (ET) models for controlled environment agriculture (CEA)," *Agriculture and Forest Meteorology*, 2021.

[Online]. Available: https://www.sciencedirect.com/science/article/pii/S0168169921004646. [Accessed: Nov. 3, 2024].

[46] "Irrigation Reference," *FAO*. [Online]. Available: https://www.fao.org/4/x0490e/x0490e00.htm. [Accessed: Mar. 26, 2025].

[47] "AIR CALC Brochure," *VEAB*. [Online]. Available: https://veab.com/en/customer%20files/files/brochures/cwdx-gb.pdf. [Accessed: Nov. 3, 2024].

[48] "Heating and Cooling Calculator" *VEAB*. [Online]. Available: https://electric-calculation.veab.com/ [Accessed: Nov. 3, 2024]

[49] E. A. Ainsworth, "What Have We Learned from 15 Years of FACE?," *New Phytologist*, 2005. [Online]. Available: https://nph.onlinelibrary.wiley.com/doi/10.1111/j.1469-8137.2004.01224.x. [Accessed: Nov. 5, 2024]

[50] JL Perry "Trace Contaminant Control for the International Space Station" *NASA*, 2017. [Online]. Available: https://ntrs.nasa.gov/api/citations/20170005170/downloads/20170005170.pdf. [Accessed: Nov. 5, 2024]

[51] "Core 400S HEPA Air Purifier," *Levoit*. [Online]. Available: https://levoit.com/collections/air-purifiers/products/core-400s-smart-true-hepa-air-purifier. [Accessed: Nov. 5, 2024].

[52] "Frost Protection: Fundamentals, Practice, and Economics, Vol. 1," *FAO*. [Online]. Available: https://www.fao.org/4/y7223e/y7223e0i.htm. [Accessed: Nov. 7, 2024].

[53] *Fundamentals of Engineering Thermodynamics*, 7th Ed. [Online]. Available: https://archive.org/details/FundamentalsOfEngineeringThermodynamics7thEdition/page/n79/mode/2up?view=theater&q=coolant+flow+rate. [Accessed: Nov. 8, 2024].

[54] "Lunar Soil Enrichment for Plant Production: WILD (Waste Improved Lunar Dirt)," *NASA*. [Online]. Available: https://techport.nasa.gov/projects/156897 [Accessed: Nov. 8, 2024].

[55] J. Iyer, T. Moore, D. Nguyen, P. Roy, and J. Stolaroff, "Heat transfer and pressure drop characteristics of heat exchangers based on triply periodic minimal and periodic nodal surfaces," *International Journal of Heat and Mass Transfer*, 2022. [Online]. Available: https://www.sciencedirect.com/science/article/pii/S135943112200148X. [Accessed: Nov. 8, 2024].

[56] H. Peng, F. Gao, and W. Hu, "Design, Modeling and Characterization of Triply Periodic Minimal Surface Heat Exchangers with Additive Manufacturing," *Research Gate*, 2019. [Online]. Available: https://www.researchgate.net/publication/340077269_DESIGN_MODELING_AND_CHARACTERIZA-TION_OF_TRIPLY_PERIODIC_MINIMAL_SURFACE_HEAT_EXCHANGERS_WITH_ADDITIVE_MANUFACTURING. [Accessed: Nov. 12,

2024].

[57] "JESTEC Journal Article," *Journal of Engineering Science and Technology*, vol. 11, no. 7, 2016. [Online]. Available: https://jestec.taylors.edu.my/Vol%2011%20issue%207%20July%202016/11_7_8.pdf. [Accessed: Nov. 14, 2024].

[58] "GASERA ONE Gas Analyzer," *Gasera.* [Online]. Available: https://gasera.fi/product/gaseraone/. [Accessed: Mar. 26, 2025]. [Accessed: Nov. 15, 2024].

[59] "PyroScience DO_2 Sensors," *PyroScience*. [Online]. Available: https://www.pyroscience.com/en/products/all-meters/fdo2. [Accessed: Nov. 16, 2024].

[60] "E+E Elektronik Product Catalog," *E+E Elektronik*. [Online]. Available: https://www.epluse.com/products/. [Accessed: Nov. 17, 2024].

[61] "Tetens' Formula," *American Meteorological Society*. [Online]. Available: https://glossary.ametsoc.org/wiki/Tetens%27s_formula. [Accessed: Nov. 18, 2024].

[62] "Packed Beds Fluid Mechanics Tutorial," *University of Washington*. [Online]. Available: http://faculty.washington.edu/finlayso/Fluidized_Bed/FBR_Fluid_Mech/packed_beds_fbr.htm. [Accessed: Nov. 18, 2024].

[63] "Reynolds Number Calculator," *Engineering ToolBox*. [Online]. Available: https://www.engineeringtoolbox.com/reynolds-number-d_237.html. [Accessed: Nov. 21, 2024]

[64] I. Hussain et al., "Design and Prototyping of Modular Grippers," *The International Journal of Robotics Research*, 2020. [Online]. Available: https://journals.sagepub.com/doi/10.1177/0278364920907697. [Accessed: Nov. 21, 2024].

[65] M. Beer and R. Rybár, "Numerical Study of Fluid Flow in a Gyroid-Shaped Heat Transfer Element," *Research Gate, 2024*. [Online]. Available: https://www.researchgate.net/publication/380416487_Numerical_Study_of_Fluid_Flow_in_a_Gyroid-Shaped_Heat_Transfer_Element. [Accessed: Nov. 21, 2024]

[66] AH Schoen "Infinite periodic minimal surfaces without self-intersections," *NASA*, 1970. [Online]. Available: https://ntrs.nasa.gov/citations/19700020472. [Accessed: Nov. 22, 2024]

[67] "How Plants Promote Better Mental Health," *UKRI*. [Online]. Available: https://www.ukri.org/what-we-do/iyph2020/how-plants-promote-better-mental-health-and-well-being. [Accessed: Nov. 22, 2024]

[68] "Environmental Control and Life Support System (ECLSS): Human-Centered Approach " *NASA* 2022. [Online]. Available: https://www.nasa.gov/wp-content/uploads/2023/07/eclss-technical-brief-ochmo.pdf. [Accessed: [Accessed: Nov. 22, 2024]

[69] "Tropi-2 STS-130," *NASA*, Ames Research Center. [Online]. Available: https://www.nasa.gov/ames/space-biosciences/tropi-2-sts-130/. [Accessed: Nov. 23, 2024]

[70] C. Zhou et al., "Properties and Characteristics of Regolith-Based Materials for Extraterrestrial Construction," *Journal of Materials in Civil Engineering*, 2024. [Online]. Available: https://www.sciencedirect.com/science/article/pii/S2095809924000511. [Accessed: Nov. 26, 2024].

[71] G. D. Massa et al., "Growth Chambers on ISS for Large Plants," *NASA*, 2016. [Online]. Available: https://ntrs.nasa.gov/api/citations/20160006558/downloads/20160006558.pdf [Accessed: Nov. 27, 2024].

[72] "Mission Commander Thrives as Space Gardener," *NASA*, 2023. [Online]. Available: https://www.nasa.gov/humans-in-space/mission-commander-thrives-as-space-gardener/. [Accessed: Nov. 30, 2024].

[73] "Lessons Learned from Biosphere 2 and Laboratory Biosphere Closed Systems Experiments for the Mars On Earth Project," *Research Gate*, 2013. [Online]. Available: https://www.researchgate.net/publication/242368741_Lessons_Learned_from_Biosphere_2_and_Laboratory_Biosphere_Closed_Systems_Experiments_for_the_Mars_On_Earth_Project. [Accessed: Dec. 1, 2024].

[74] "Lunar Palace 1: To the Moon and Beyond," *Beihang University*, 2020. [Online]. Available: https://ev.buaa.edu.cn/info/1103/2695.htm. [Accessed: Dec. 1, 2024].

[75] T. Zhao, G. Liu, D. Liu, Y. Yi, B. Xie, and H. Liu, "Water recycle system in an artificial closed ecosystem – Lunar Palace 1: Treatment performance and microbial evolution," *Science of The Total Environment*, 2021. [Online]. Available: https://www.sciencedirect.com/science/article/pii/S0048969721064482. [Accessed: Dec. 1, 2024].

[76] "Science in Space: Week of July 10, 2023 - Plant Science," *NASA*, 2023. [Online]. Available: https://www.nasa.gov/missions/station/iss-research/science-in-space-week-of-july-10-2023-plant-science/. [Accessed: Dec. 3, 2024].

[77] A. Martelo Gomez, S. Jahnke, A. Braukhane, D. Quantius, V. Maiwald, and O. Romberg, "Statistics and evaluation of 60+ concurrent engineering studies at DLR," in 68th *International Astronautical Congress*, Adelaide, Australia, 2017. [Online]. Available: https://elib.dlr.de/114620/. [Accessed: Dec. 1, 2024].

[78] V. Maiwald, K. Kim, V. Vrakking, and C. Zeidler, "From Antarctic prototype to ground test demonstrator for a lunar greenhouse," *Acta Astronautica*, vol. 212, pp. 246-260, 2023. [Online]. Available: https://www.sciencedirect.com/science/article/pii/S0094576523004101. [Accessed: Dec. 4, 2024].

[79] V. Maiwald, K. Kim, C. Philpot, D. Schubert, and V. Vrakking, "Lunar Eden: Roadmap and Demonstrator Design of a Lunar Greenhouse Based on an Antarctic Prototype," in 73rd *International Astronautical Congress (IAC)*, Paris, France, 2022. [Online]. Available: https://www.researchgate.net/publication/363753257_Lunar_Eden_Roadmap_and_Demonstrator_Design_of_a_Lunar_Greenhouse_Based_on_an_Antarctic_Prototype. [Accessed: Dec. 7, 2024].

[80] J. Schroth, "Development of the Atmosphere Management System of the EDEN Next Gen greenhouse module for long-term space missions (Diplomarbeit)," *Technische Universität Dresden, Dresden*, 2021. [Online]. Available: https://elib.dlr.de/143252/. [Accessed: Dec. 7, 2024]

[81] V. Maiwald, D. Schubert, and J. Stoochnoff, "Lunar Agriculture Module – Ground Test Demonstrator CE-Study," *DLR*, 2023.

[82] R. Singh, B. Prasad, and Y.-H. Ahn, "Recent developments in gas separation membranes enhancing the performance of oxygen and nitrogen separation: A comprehensive review," *Chemical Engineering Journal*, 2024. [Online]. Available: https://www.sciencedirect.com/science/article/pii/S2949908924000529. [Accessed: Dec. 8, 2024]

[83] Y. A. Lim, M. N. Chong, S. C. Foo, and I.M.S.K. Ilankoon, "Analysis of direct and indirect quantification methods of CO2 fixation via microalgae cultivation in photobioreactors: A critical review," *Renewable and Sustainable Energy Reviews*, 2021. [Online]. Available: https://www.sciencedirect.com/science/article/pii/S1364032120308637. [Accessed: Dec. 8, 2024]

[84] "Benefits of Heresite HVAC Coatings," *TCW Group*. [Online]. Available: https://www.mytcwgroup.com/post/benefits-heresite-hvac-coatings. [Accessed: Dec. 15, 2024]

[85] F. Aprilliani, E. Warsiki, and A. Iskandar, "Kinetic studies of potassium permanganate adsorption by activated carbon and its ability as ethylene oxidation material," *Research Gate, 2018*. [Online]. Available: https://www.researchgate.net/publication/324250891_Kinetic_studies_of_potassium_permanganate_adsorption_by_activated_carbon_and_its_ability_as_ethylene_oxidation_material. [Accessed: Dec. 19, 2024]

[86] J. L. Perry and M. J. Kayatin, "Trace Contaminant Control Design Considerations for Enabling Exploration Missions," *International Conference on Environmental Systems*, 2015. [Online]. Available: https://ttu-ir.tdl.org/server/api/core/bitstreams/14e65dc5-1d36-4fbb-be54-82aa718225e9/content. [Accessed: Jan. 05, 2024]

[87] G. Howell, "*Aerospace Fluid Component Designers' Handbook Vol. 1*," 1964. [Online]. Available: https://ntrl.ntis.gov/NTRL/dashboard/searchResults/titleDetail/AD447995.xhtml. [Accessed: Jan. 07, 2024].

[88] E. J. Olguín and G. Sánchez-Galván, "Heavy metal removal in phytofiltration and phycoremediation: the need to differentiate between bioadsorption and bioaccumulation," *New Biotechnology*, 2012. [Online]. Available: https://www.sciencedirect.com/science/article/pii/S1871678412001227. [Accessed: Jan. 08, 2024].

[89] N. S. Mian, S. Fletcher, A. P. Longstaff, and A. Myers, "The significance of air pockets for modelling thermal errors of machine tools," *University of Huddersfield*, UK, 2013. [Online]. Available: https://eprints.hud.ac.uk/id/eprint/16917/1/NSMIAN_Lamdamap_2013-.pdf. [Accessed: Jan. 12, 2024].

[90] "Air Flow," *Tomato Growing*. [Online]. Available: https://www.tomatogrowing.co.uk/airflow. [Accessed: Jan.15, 2024].

[91] G. Nestler, "Axial- oder Radialventilator?," *iVENTILATOREN*, July 02, 2018. [Online]. Available: https://www.iventilatoren.de/axial-oder-radialrohrventilator-x31386. [Accessed:

Jan.15, 2024].

[92] "Opakair ProSafe," *Camfil*. [Online]. Available: https://www.camfil.com/de-de/produkte/general-ventilation-filters/compact-filter_-box-type/opakair/opakair-prosafe-_-66271. [Accessed: Jan.15, 2024].

[93] "Absolute VGxL & VGxxL ProSafe," *Camfil*. [Online]. Available: https://www.camfil.com/de-de/produkte/epa-hepa-und-ulpa-filter/kompaktfilter-(kastenform)/absolute-v/absolute-vgxl--vgxxl-prosafe-_-42767. [Accessed: Jan.19, 2024].

[94] "Catalog Centrifugal Fans EC RadiPac," *Mouser Electronics*. [Online]. Available: https://www.mouser.com/datasheet/2/120/Catalog_Centrifugalfans_EC_RadiPac_EN-2940384.pdf. [Accessed: Jan.20, 2024].

[95] T. Kozai, Smart Plant Factory: The Next Generation Indoor Vertical Farms. *Springer* Singapore, 2018. [Online]. Available: https://link.springer.com/book/10.1007/978-981-13-1065-2. [Accessed: Jan.22, 2024].

[96] "LUKA Handbook," *LUKA*, 2022. [Online]. Available: https://www.luka.nl/cms/public/files/2022-06/luka-handboek-2022-06-eng-.pdf. [Accessed: Jan.25, 2024].

[97] Detrell, Gisela. "Chlorella Vulgaris Photobioreactor for Oxygen and Food Production on a Moon Base-Potential and Challenges." *Frontiers in Astronomy and Space Sciences*. 2021 [Online]. Available: https://www.researchgate.net/publication/353402576_Chlorella_Vulgaris_Photobioreactor_for_Oxygen_and_Food_Production_on_a_Moon_Base-Potential_and_Challenges [Accessed: Mar. 26, 2025].

[98] Hany M.R. Abdel-Latif, Saeed El-Ashram, Sevdan Yilmaz, Mohammed A.E. Naiel, Zulhisyam Abdul Kari, Noor Khalidah Abdul Hamid, Mahmoud A.O. Dawood, Joanna Nowosad, Dariusz Kucharczyk. "The effectiveness of Arthrospira platensis and microalgae in relieving stressful conditions affecting finfish and shellfish species: An overview," 2022. *Science Direct* [Online]. Available: https://www.sciencedirect.com/science/article/pii/S2352513422001314 [Accessed: Mar. 25, 2025].

[99] 9D PerlaAqua . *Aquisense* [Online]. Available: https://aquisense.com/products/water-treatment/pearl-aqua/ [Accessed: Mar. 26, 2025].

[100] "Science in Space: Week of July 10, 2023 – Plant Science" *NASA* 2023 Online]. Available: https://www.nasa.gov/missions/station/iss-research/science-in-space-week-of-july-10-2023-plant-science/ [Accessed: Mar. 26, 2025].

[101] "Guidelines for Noise and Vibration Levels for the Space Station" *NASA* 1987 Online. Available: https://ntrs.nasa.gov/api/citations/19870014729/downloads/19870014729.pdf [Accessed: Mar. 26, 2025].

[102] "PSYCHROMETRIC CHART" ***UNIVERSIDAD POLITÉCNICA DE MADRID*** **Online. Available: https://upload.wikimedia.org/wikipedia/commons/1/1c/Psychrometric_chart_%28altitude_0%2C_750%2C_1500%2C_2250%2C_3000_m%29.pdf [Accessed: Mar. 26, 2025]**

Annex

1.1. Blower

Normbrecher
mit Standardmaßen.

Der neue RadiPac macht vieles besser.
Um jeder Einbausituation gerecht zu werden,
gibt es die Radialventilatoren in verschiedenen
Ausführungen – Sie haben die Wahl.

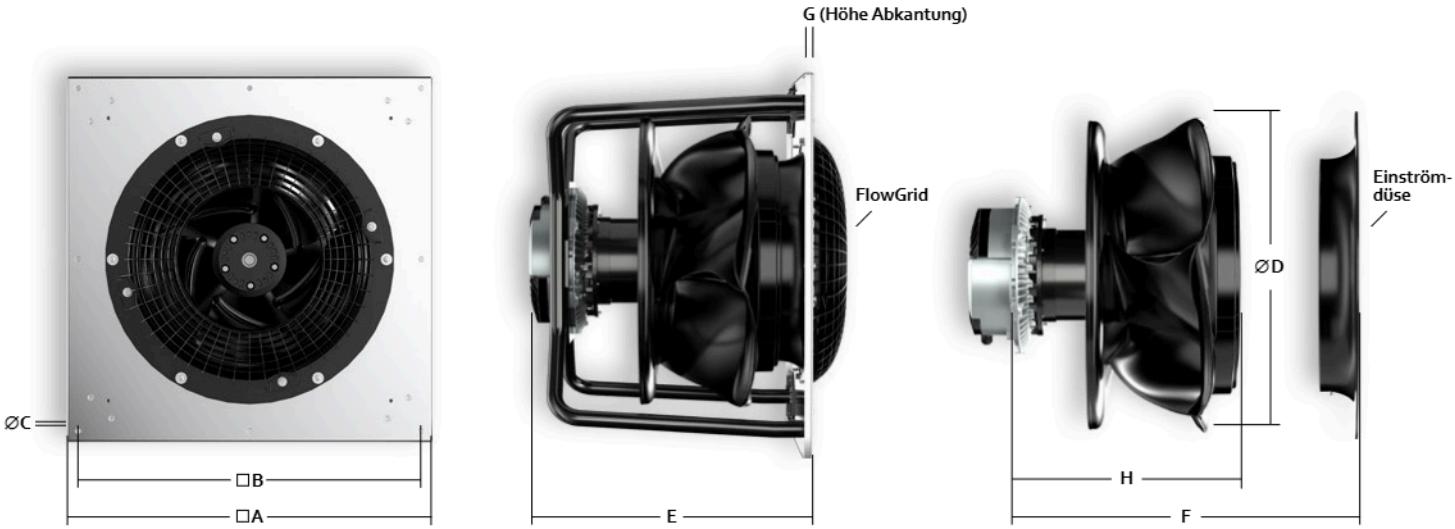

Abmessungen

Baugröße	□A	□B	ØC	ØD	E*	F	G	H	Einströmdüse Bestellnummer	FlowGrid Bestellnummer
280	380	330	11	289	245	202	15	172	8217102230	20280-2-2957
310	390	340	11	325	380	314	15	281	8217102242	25310-2-2957
355	450	400	11	364	396	330	15	292	8217102240	00400-2-2957
400	500	450	11	409	445	354	15	313	8217102241	00400-2-2957
450	560	510	11	458	493	402	15	362	8217102239	35505-2-2957
500	590	540	11	514	550	461	15	414	8217102238	35505-2-2957
560	710	660	11	577	571	481	15	430	8217102237	50710-2-2957
630	790	740	11	647	601	511	15	455	8217102236	00630-2-2957

*ohne Überstand der Schrauben
Daten beziehen sich auf die leistungsstärkste Ausführung.
Alle Angaben in mm. Datenblätter erhalten Sie auf Anfrage. Angaben ohne Gewähr.

Kurz oder Standard?
In der Standardversion ist der Motor komplett aus dem Strömungsbereich herausgezogen. Bei der Kurzversion taucht der Motor in das Laufrad ein. Dadurch sind die Ventilatoren kompakter, bieten aber dennoch eine deutliche Leistungssteigerung im Vergleich zu den Vorgängermodellen.

Mit oder ohne Tragspinne?
Beide RadiPac Varianten gibt es als Motor-Laufrad-Kombination oder als einbaufertige Plug & Play Lösung in einer kompakten Tragspinnenkonstruktion zur einfachen Wandmontage. Die Tragplatten sind dabei so dimensioniert, dass sich der Platz auf einer Europalette bestmöglich ausnutzen lässt. Das spart Transportkosten und verbessert den CO_2-Fußabdruck.

Einfacher Ventilatortausch
Durch steigende Energiekosten und den immer wichtiger werdenden Umweltgedanken rechnet sich oft der Austausch alter Ventilatoren, denn der neue RadiPac spart langfristig Kosten und Ressourcen. Dank seiner Leistungsdichte ist ein Retrofit mit dem neuen RadiPac ohne aufwändige Designänderungen möglich.

Leistung auf den Betriebspunkt gebracht.

Die gezeigten Daten basieren auf echten Leistungsmessungen, die auf modernsten Kammerprüfständen durchgeführt werden. Gemessen wird die gesamte Ventilator-Einheit, bestehend aus Motor, Steuerungselektronik und Laufrad bei unterschiedlichen Lastzuständen. So erhalten wir verlässliche Daten und Sie können sich bereits bei der Auswahl der Ventilatoren auf die Erreichung dieser Werte verlassen. Somit sind böse Überraschungen bei der Inbetriebnahme der Ventilatoren ausgeschlossen.

Die gemessenen Daten bilden die Basis für das auf Anfrage erhältliche Auslegungsprogramm FanScout. Mit dieser Software lassen sich die zu erwartenden Betriebskosten berechnen oder auch eine Lebenszyklus-Kostenbetrachtung durchführen.

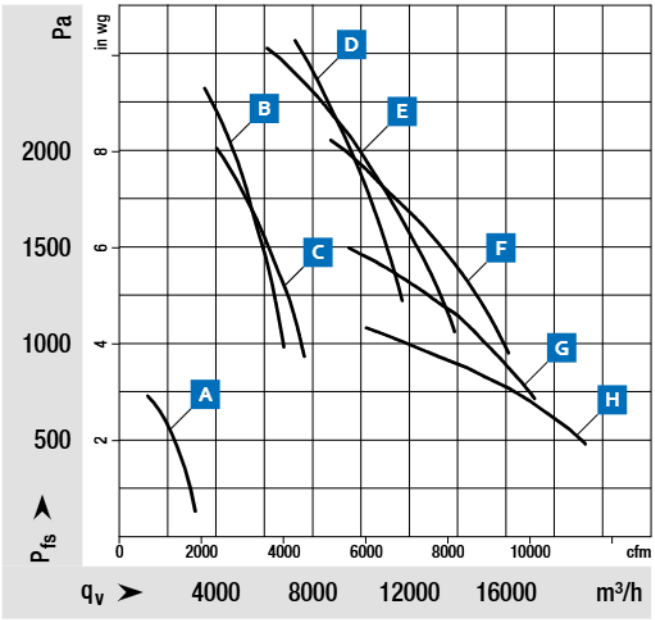

Das Kennfeld zeigt die maximale Luftleistung je Baugröße.

Nenndaten

Baugröße		K-Modul Type	Bestellnummer K-Modul	Max. Motor	Nennspannungsbereich	Frequenz	Drehzahl	Max. Aufnahmeleistung	Max. Aufnahmestrom	Zul. Umgebungstemperatur
					VAC	Hz	min⁻¹	kW	A	°C
280	A	VBH0280CSNGS	8300100482	M3G074DF	1~ 200–277	50/60	3.130	0,50	2,0	–25...+40
310	B	VBH0310CTRLS	8300100104	M3G112GA	3~ 380–480	50/60	4.560	2,75	4,3	–25...+40
355	C	VBH0355CTRLS	8300100087	M3G112GA	3~ 380–480	50/60	3.800	2,75	4,3	–25...+40
400	D	VBH0400CTTLS	8300100128	M3G150FF	3~ 380–480	50/60	3.690	4,50	6,9	–25...+40
450	E	VBH0450CTTPS	8300100075	M3G150IF	3~ 380–480	50/60	3.430	6,30	9,9	–25...+40
500	F	VBH0500CTTRS	8300100068	M3G150NA	3~ 380–480	50/60	2.840	6,21	9,6	–25...+40
560	G	VBH0560CTTRS	8300100101	M3G150NA	3~ 380–480	50/60	2.370	6,50	10,0	–25...+40
630	H	VBH0630CTTRS	8300100048	M3G150NA	3~ 380–480	50/60	1.910	5,85	9,0	–25...+40

Daten beziehen sich auf die leistungsstärkste Ausführung.
Datenblätter erhalten Sie auf Anfrage. Technische Änderungen vorbehalten.

1.2. Fans

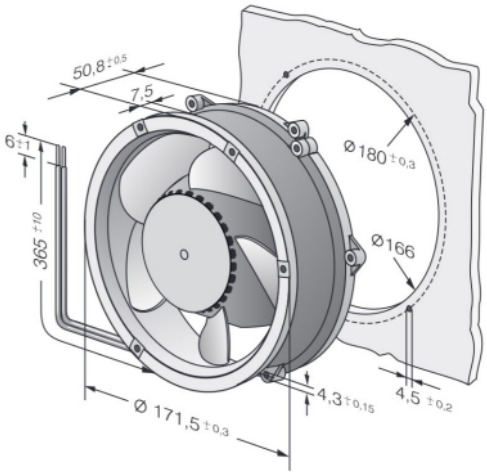

ebm-papst St. Georgen GmbH & Co. KG
Hermann-Papst-Str. 1
D-78112 St. Georgen
Phone +49 (0) 7724 81-0
Fax +49 (0) 7724 81-1309
info2@de.ebmpapst.com
www.ebmpapst.com

Nenndaten

Typ	DV 6224	
Nennspannung	VDC	24
Nennspannungsbereich	VDC	16 .. 28
Drehzahl	min^{-1}	4300
Leistungsaufnahme	W	40,0
Min. Umgebungstemperatur	°C	-20
Max. Umgebungstemperatur	°C	75
Volumenstrom	m^3/h	540
Schallleistungspegel	B	7,1
Schalldruckpegel	dB(A)	63

mb = Max. Belastung · mw = Max. Wirkungsgrad · fb = Freiblasend · kv = Kundenvorgabe · kg = Kundengerät
Änderungen vorbehalten

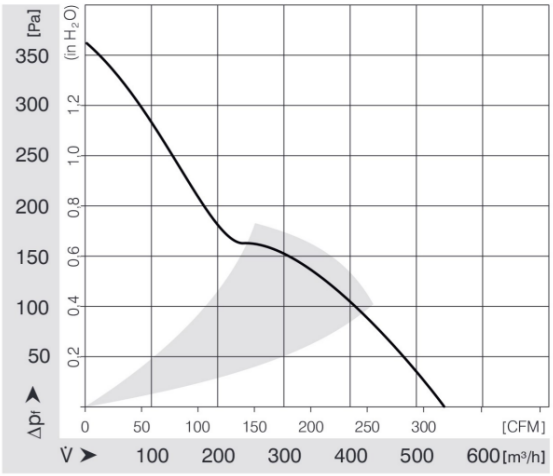

Technische Beschreibung

Masse	0,820 kg
Abmessungen	172 Ø x 51 mm
Material Laufrad	Glasfaserverstärkter Kunststoff PA
Material Gehäuse	Aluminium. Gehäuse mit Erdungsöse für Schraube M4 x 8 (TORX).
Förderrichtung	Über Stege blasend
Drehrichtung	Links, auf Rotor gesehen
Lagerung	Kugellager
Lebensdauer L10 bei 40 °C	90000 h
Lebensdauer L10 bei max. Temperatur	40000 h
Anschlussleitung	Einzellitzen AWG 22, TR 64, abisoliert und verzinnt.
Motorschutz	Geschützt gegen Verpolung und Blockieren.
Blockierschutz	Elektronische Blockiersicherung, mit elektronischer Motorstrombegrenzung in der Anlaufphase und bei blockiertem Rotor.
Zulassung	VDE, CSA, UL, CE
Option	Tachosignal, Alarmsignal

1.3. UV-C Lights

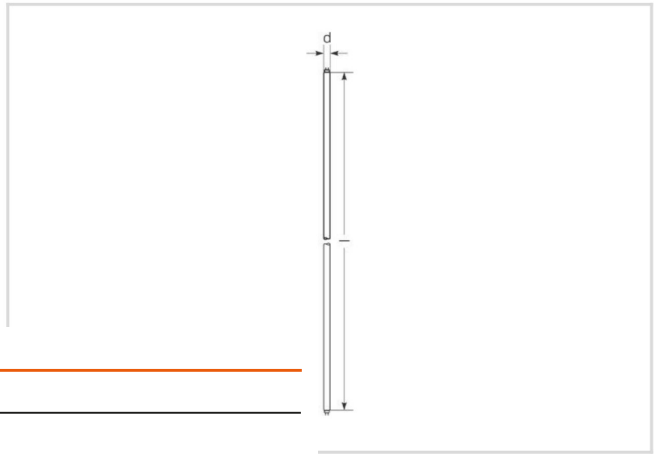

Lebensdauer

Mittlere Nennlebensdauer	10800 h

Spezifikation

Durchmesser	26 mm
Gesamtlänge	438 mm
Brennstellung	beliebig
Lampenform	T8
Ausführung	klar
Sockel	G13

Allgemeine Daten

Artikel Nr.	34319470
Bestellzeichen	NL-T8 UV 25W/254 G13 RO
EAN-Faltschachtel	4058075502628
Versandeinheit in Stk.	25
EAN Umkarton (Versandeinheit)	4058075502635
Brutto-Gewicht Versandeinheit in kg	2.192
Länge Versandeinheit in m	0.47
Breite Versandeinheit in m	0.15
Höhe Versandeinheit in m	0.15
Produktgewicht	70 g
Produktstatus	Aktiv

Elektrische Parameter

Lampenleistung	25.0 W
Lampenspannung	220-240 V

Lichttechnische Parameter

Art der UV-Strahlung	UV-C
UV-Leistung	8.2 W

1.4. Pre-filter and HEPA Filter

VORTEILE

- Hygienisches Produkt nach VDI 6022 und EN ISO846
- Geprüft auf Lebensmittelsicherheit nach EC 1935:2004
- Frei von BPA, Formaldehyd und Phtalaten
- Geprüfte Beständigkeit gegenüber Dekontaminations- und Reinigungsprozessen
- Vollständig veraschbar für optimiertes Abfallmanagement
- ProSafe-zertifiziert für Biowissenschaft, Lebensmittel- und Getränkeindustrie
- Für sehr hohe Strömungsgeschwindigkeiten (bis zu 3,5 m/s)
- Robuster und luftdichter Rahmen
- Leichtester Kompaktfilter

Anwendung	Kompaktfilter für Lüftungsanlagen mit hohem Luftvolumenstrom
Rahmen	ABS Kunststoff
Dichtung	Polyurethan
Medium	Glasfaser
Abstandshalter (Separator)	Schmelzkleber

EN 13053	
Maximaler Volumenstrom	1,1 x Volumenstrom
Max Temperatur (°C)	70°C
Relative Luftfeuchtigkeit (max.)	100%

Art.-Nr.	Typ	Filterklasse	ISO16890	Abmessungen BxHxT (mm)	Volumenstrom/Druckdifferenz (m^3/h/Pa)	Filterfläche (m^2)	Frachtgewicht (kg)
OPR3622131001	OPR-G6-610x305x292-P-PS	M6	ePM10 70%	610x305x292	2050/100	10.9	4.9
OPR6622121001	OPR-G6-610x610x292-P-PS	M6	ePM10 70%	610x610x292	4500/100	22.0	7.7
OPR3722131001	OPR-G7-610x305x292-P-PS	F7	ePM1 55%	610x305x292	2050/110	10.9	4.9
OPR6722121001	OPR-G7-610x610x292-P-PS	F7	ePM1 55%	610x610x292	4500/110	22.0	7.7
OPR3822131001	OPR-G8-610x305x292-P-PS	F8	ePM1 70%	610x305x292	2050/120	10.9	4.9
OPR6822121001	OPR-G8-610x610x292-P-PS	F8	ePM1 70%	610x610x292	4500/120	22.0	7.7
OPR3922131001	OPR-G9-610x305x292-P-PS	F9	ePM1 80%	610x305x292	2050/130	10.9	4.9
OPR6922121001	OPR-G9-610x610x292-P-PS	F9	ePM1 80%	610x610x292	4500/130	22.0	7.7

Absolute VGXL, XXL ProSafe

Vorteile

- 23% Energieersparnis gegenüber dem Marktdurchschnitt
- Robuster und luftdichter Rahmen
- VDI 6022 konform
- Komponenten mikrobiell inert nach DIN EN ISO 846
- Getestet für Food Contact nach EC 1935:2004
- Bisphenol-A-, phthalat-, formaldehydfrei
- Chemisch beständig gegen Inaktivierungs- & Reinigungsverfahren
- Optimiertes Abfallmanagement: kompakt, leicht und voll veraschbar
- Niedrigstes Gewicht in der Branche
- Leckagefreie Bauweise, maschinell getestet
- Optimierter, berührungsarmer Wartungssack-Filterwechsel, Bag-in/ Bag-out (BIBO)

Anwendung: Luftfilter für Zuluft- und Prozessluft-Anwendungen mit hohen Volumenströmen
Ausführung: Boxfilter in V-Form
Rahmen: ABS Kunststoff mit ergonomischem Griff
Dichtung: Polyurethan, endlos geschäumt
Medium: Glasfaser
Abstandshalter (Separator): Schmelzkleber
Vergussmasse: Polyurethan
Filterklasse & Abscheidegrad gem EN 1822 @ MPPS: E10 E10 (≥85%), E11 (≥95%), E12 (≥99,5%), H13 (≥99,95%), H14 (≥99,995%)
Empfohlene Enddruckdifferenz: 2x Anfangsdruckdifferenz
Maximale Enddruckdifferenz: 600 Pa
Maximale Temperatur: 70°C
Relative Luftfeuchtigkeit (max): 100%
Einbaumöglichkeit: FKB, 4N, CamCube, CamBox, CamSafe
Bemerkungen: Erfüllt die **ProSafe**** Anforderungen

Art. Nr.	Typ	Filter-klasse	Abmessungen BxHxT (mm)	Volumenstrom (m^3/h)	Druckdifferenz (Pa)***	Filterfläche (m^2)	Fracht-gewicht (kg)
ABV3022131001	VGXL10-610x305x292-P-PS	E10	610x305x292	1500/1800	150/190	10,9	4,9
ABV6022121001	VGXL10-610x610x292-P-PS	E10	610x610x292	3400/4000	150/190	22,0	7,7
ABV3032131001	VGXXL10-610x305x292-P-PS	E10	610x305x292	2300	210	14,9	5,3
ABV6032121001	VGXXL10-610x610x292-P-PS	E10	610x610x292	5000	210	30,2	8,5
ABV3122131001	VGXL11-610x305x292-P-PS	E11	610x305x292	1500/1800	170/210	18,9	5,7
ABV6122121001	VGXL11-610x610x292-P-PS	E11	610x610x292	3400/4000	170/210	38,3	9,3
ABV3222131001	VGXL12-610x305x292-P-PS	E12	610x305x292	1500/1800	180/220	18,9	5,7
ABV6222121001	VGXL12-610x610x292-P-PS	E12	610x610x292	3400/4000	180/220	38,3	9,3
ABV3322131001	VGXL13-610x305x292-P-PS	H13	610x305x292	1500/1800	200/240	20,5	5,8
ABV6322121001	VGXL13-610x610x292-P-PS	H13	610x610x292	3400/4000	200/240	41,6	9,6
ABV3332131001	VGXXL13-610x305x292-P-PS	H13	610x305x292	2300	400	20,5	5,8
ABV6332121001	VGXXL13-610x610x292-P-PS	H13	610x610x292	5000	400	41,6	9,6
ABV3422131001	VGXL14-610x305x292-P-PS	H14	610x305x292	1500	250	20,5	5,8
ABV6422121001	VGXL14-610x610x292-P-PS	H14	610x610x292	3400	250	41,6	9,6
ABV3432131001	VGXXL14-610x305x292-P-PS	H14	610x305x292	1800	310	20,5	5,8
ABV6432121001	VGXXL14-610x610x292-P-PS	H14	610x610x292	4000	310	41,6	9,6

* Nicht verfügbar mit Dichtsitzdichtung
** Alle Zertifikate und weitere Informationen unter www.camfil.com/prosafe
*** Druckdifferenz: ± 10 %

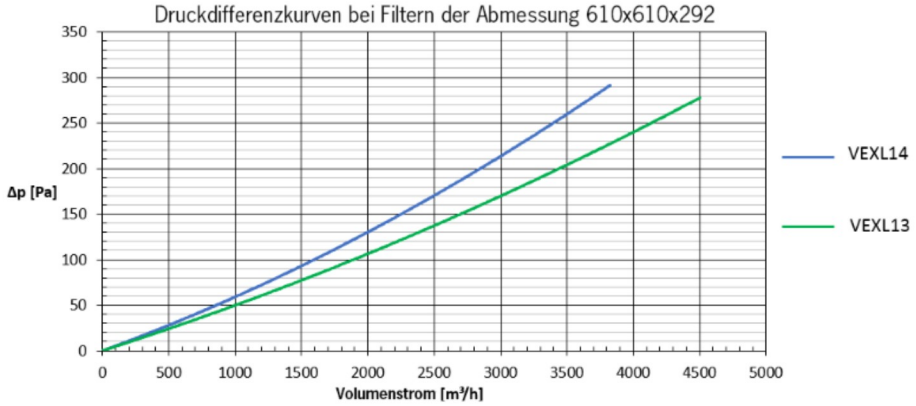

1.5. Modelling of Evapotranspiration

```
#!/usr/bin/env python3
import numpy as np
import matplotlib.pyplot as plt
# Psychrometric Functions
def saturation_pressure(T):
    return 0.6108 * np.exp((17.27 * T) / (T + 237.3))
def humidity_ratio(T, RH, P):
    p_sat = saturation_pressure(T)
    p_v = RH * p_sat
    return 0.622 * p_v / (P - p_v)
def moist_air_enthalpy(T, w):
    return 1.005 * T + w * (2501 + 1.86 * T)
# Crop ET Simulation Setup
crop_parameters = {
    'tomatoes': {
        'total_days': 120,
        'stages': [
            {'name': 'Establishment', 'start': 1,   'end': 10,  'Kc_start': 0.4,  'Kc_end': 0.4},
            {'name': 'Development',   'start': 11,  'end': 30,  'Kc_start': 0.4,  'Kc_end': 1.15},
            {'name': 'Mid-season',    'start': 31,  'end': 90,  'Kc_start': 1.15, 'Kc_end': 1.15},
            {'name': 'Late season',   'start': 91,  'end': 120, 'Kc_start': 1.15, 'Kc_end': 0.9}
        ]
    },
    'peppers': {
        'total_days': 100,
        'stages': [
            {'name': 'Establishment', 'start': 1,   'end': 8,   'Kc_start': 0.4,  'Kc_end': 0.4},
            {'name': 'Development',   'start': 9,   'end': 25,  'Kc_start': 0.4,  'Kc_end': 1.1},
            {'name': 'Mid-season',    'start': 26,  'end': 70,  'Kc_start': 1.1,  'Kc_end': 1.1},
            {'name': 'Late season',   'start': 71,  'end': 100, 'Kc_start': 1.1,  'Kc_end': 0.85}
        ]
    },
    'cucumbers': {
        'total_days': 80,
        'stages': [
            {'name': 'Establishment', 'start': 1,   'end': 7,   'Kc_start': 0.35, 'Kc_end': 0.35},
            {'name': 'Development',   'start': 8,   'end': 20,  'Kc_start': 0.35, 'Kc_end': 1.05},
            {'name': 'Mid-season',    'start': 21,  'end': 55,  'Kc_start': 1.05, 'Kc_end': 1.05},
            {'name': 'Late season',   'start': 56,  'end': 80,  'Kc_start': 1.05, 'Kc_end': 0.8}
        ]
    },
    'leafy_greens': {
```

```
        'total_days': 30,
        'stages': [
            {'name': 'Establishment', 'start': 1,  'end': 3,   'Kc_start': 0.3,  'Kc_end': 0.3},
            {'name': 'Development',   'start': 4,  'end': 10,  'Kc_start': 0.3,  'Kc_end': 0.8},
            {'name': 'Mid-season',    'start': 11, 'end': 20,  'Kc_start': 0.8,  'Kc_end': 0.8},
            {'name': 'Late season',   'start': 21, 'end': 30,  'Kc_start': 0.8,  'Kc_end': 0.5}
        ]
    }
}
def get_crop_coefficient(crop_name, day):
    params = crop_parameters[crop_name]
    for stage in params['stages']:
        if stage['start'] <= day <= stage['end']:
            if stage['Kc_start'] == stage['Kc_end']:
                return stage['Kc_start']
            else:
                fraction = (day - stage['start']) / (stage['end'] - stage['start'])
                return stage['Kc_start'] + fraction * (stage['Kc_end'] - stage['Kc_start'])
    return params['stages'][-1]['Kc_end']
def simulate_evapotranspiration(crop_name, base_ET0, ambient_pressure, area):
    total_days = crop_parameters[crop_name]['total_days']
    days = np.arange(1, total_days + 1)
    ET0_adjusted = base_ET0 * (101.3 / ambient_pressure)
    kc_values = np.array([get_crop_coefficient(crop_name, day) for day in days])
    daily_ET = ET0_adjusted * kc_values  # mm/day per m²
    cumulative_ET = np.cumsum(daily_ET)
    daily_ET_area = daily_ET * area   # liters/day
    total_water_loss = cumulative_ET[-1] * area  # liters
    return days, kc_values, daily_ET, cumulative_ET, daily_ET_area, total_water_loss
# Detailed HVAC Load Simulation
def simulate_HVAC_loads_detailed(days, daily_ET_area, equipment_load_kw=11, volume=87,
                                 T_set=14, RH_set=0.45, P=70):
    density = 0.83  # kg/m³
    m_da = density * volume  # kg of air
    h_fg = 2501  # kJ/kg latent heat of vaporization
    w_set = humidity_ratio(T_set, RH_set, P)
    h_set = moist_air_enthalpy(T_set, w_set)
    Q_eq_hour = equipment_load_kw * 3600  # kJ/h
    sensible_hourly_kWh = Q_eq_hour / 3600  # kWh/h
    sensible_daily = sensible_hourly_kWh * 24  # kWh/day
    water_added_hourly = daily_ET_area / 24  # kg/h (1 liter ≈ 1 kg)
    delta_w = water_added_hourly / m_da       # kg/kg per hour
    latent_hourly_kWh = (water_added_hourly * h_fg) / 3600  # kWh/h
    latent_daily = latent_hourly_kWh * 24  # kWh/day
    sensible_heating = np.zeros_like(days, dtype=float)
```

```
    sensible_cooling = np.full_like(days, sensible_daily, dtype=float)
    latent_cooling = (daily_ET_area * h_fg) / 3600  # kWh/day
    water_condensed = daily_ET_area.copy()  # liters/day
    return (sensible_heating, sensible_cooling, latent_cooling, water_condensed,
            Q_eq_hour, m_da, water_added_hourly, delta_w, latent_hourly_kWh, w_set, h_set)
# CO₂ Uptake Simulation
def simulate_CO2_uptake(crop_name, area, uptake_rate=10, photoperiod=12):
    total_days = crop_parameters[crop_name]['total_days']
    days = np.arange(1, total_days + 1)
    # Daily CO₂ uptake in mol/m²/day = uptake_rate * seconds in photoperiod / 1e6
    daily_uptake_mol = uptake_rate * 3600 * photoperiod / 1e6
    # Convert moles to grams (CO₂ molar mass ≈ 44.01 g/mol)
    daily_uptake_g = daily_uptake_mol * 44.01
    cumulative_uptake_g_m2 = days * daily_uptake_g  # g/m² cumulative uptake
    cumulative_uptake_total_g = cumulative_uptake_g_m2 * area
    cumulative_uptake_total_kg = cumulative_uptake_total_g / 1000.0
    return days, cumulative_uptake_total_kg, daily_uptake_g
# Main Simulation Loop
def main():
    # Parameters for ET and HVAC simulations.
    base_ET0 = 6.0         # mm/day under standard pressure (~101.3 kPa)
    ambient_pressure = 70  # kPa
    area = 23.5            # m²
    equipment_load_kw = 11 # kW
    volume = 87            # m³
    # Desired indoor conditions (setpoints)
    temperature_setpoint = 14  # °C
    humidity_setpoint = 45    # %
    RH_fraction = humidity_setpoint / 100.0
    w_set = humidity_ratio(temperature_setpoint, RH_fraction, ambient_pressure)
    h_set = moist_air_enthalpy(temperature_setpoint, w_set)
    sat_press = saturation_pressure(temperature_setpoint)
    print("Indoor Air Setpoint Conditions:")
    print(f"  Temperature: {temperature_setpoint} °C")
    print(f"  Relative Humidity: {humidity_setpoint}%")
    print(f"  Saturation Vapor Pressure at {temperature_setpoint} °C: {sat_press:.2f} kPa")
    print(f"  Humidity Ratio (w_set): {w_set:.4f} kg water/kg dry air")
    print(f"  Moist Air Enthalpy (h_set): {h_set:.2f} kJ/kg dry air")
    print("=" * 70)
    # List of crops to simulate.
    crops = ['tomatoes', 'peppers', 'cucumbers', 'leafy_greens']
    # Create a figure for the ET-related plots.
    n_crops = len(crops)
    fig_et, axes_et = plt.subplots(n_crops, 2, figsize=(14, 4 * n_crops))
    fig_et.subplots_adjust(hspace=0.5, wspace=0.5)
```

```
    # Loop through each crop.
    for i, crop in enumerate(crops):
        # --- ET Simulation ---
        days, kc, daily_ET, cum_ET, daily_ET_area, total_water_loss = simulate_evapotranspiration(
            crop, base_ET0, ambient_pressure, area
        )
        # Plot crop coefficient.
        ax1 = axes_et[i, 0]
        ax1.plot(days, kc, 'g-', linewidth=2)
        ax1.set_title(f"{crop.capitalize()} – Crop Coefficient (Kc)")
        ax1.set_xlabel("Day")
        ax1.set_ylabel("Kc")
        ax1.grid(True)
        # Plot daily and cumulative ET (per m²).
        ax2 = axes_et[i, 1]
        ax2.plot(days, daily_ET, 'b-', label="Daily ET (mm/m²)", linewidth=2)
        ax2.plot(days, cum_ET, 'r--', label="Cumulative ET (mm/m²)", linewidth=2)
        ax2.set_title(f"{crop.capitalize()} – Evapotranspiration")
        ax2.set_xlabel("Day")
        ax2.set_ylabel("ET (mm)")
        ax2.legend()
        ax2.grid(True)
        # --- Detailed HVAC Loads Simulation ---
        (sensible_heating, sensible_cooling, latent_cooling, water_condensed,
         Q_eq_hour, m_da, water_added_hourly, delta_w, latent_hourly_kWh, w_set_calc, h_set_calc) = simu-
late_HVAC_loads_detailed(
            days, daily_ET_area, equipment_load_kw, volume,
            T_set=temperature_setpoint, RH_set=RH_fraction, P=ambient_pressure
        )
        # Create a figure for HVAC energy loads for this crop.
        fig_hvac, (ax_hvac1, ax_hvac2) = plt.subplots(2, 1, figsize=(10, 8))
        fig_hvac.suptitle(f"{crop.capitalize()} – HVAC Energy Loads and Water Condensation", fontsize=14)
        fig_hvac.subplots_adjust(hspace=0.5)
        ax_hvac1.plot(days, sensible_heating, 'm-', label="Sensible Heating (kWh/day)", linewidth=2)
        ax_hvac1.plot(days, sensible_cooling, 'b-', label="Sensible Cooling (kWh/day)", linewidth=2)
        ax_hvac1.plot(days, latent_cooling, 'c-', label="Latent Cooling (kWh/day)", linewidth=2)
        ax_hvac1.set_xlabel("Day")
        ax_hvac1.set_ylabel("Energy (kWh/day)")
        ax_hvac1.legend()
        ax_hvac1.grid(True)
        ax_hvac2.plot(days, water_condensed, 'g-', linewidth=2)
        ax_hvac2.set_xlabel("Day")
        ax_hvac2.set_ylabel("Water Condensed (liters/day)")
        ax_hvac2.set_title(f"{crop.capitalize()} – Daily Water Condensed")
        ax_hvac2.grid(True)
```

```
# --- Detailed HVAC Variables Graphs ---
fig_detail, axs = plt.subplots(3, 1, figsize=(10, 12))
fig_detail.suptitle(f"{crop.capitalize()} – Detailed HVAC Variables (Averaged Hourly)", fontsize=14)
axs[0].plot(days, water_added_hourly, 'b-', linewidth=2)
axs[0].set_title("Average Hourly Water Added (kg/h)")
axs[0].set_xlabel("Day")
axs[0].set_ylabel("Water Added (kg/h)")
axs[0].grid(True)
axs[1].plot(days, delta_w, 'r-', linewidth=2)
axs[1].set_title("Increase in Humidity Ratio (Δw, kg/kg)")
axs[1].set_xlabel("Day")
axs[1].set_ylabel("Δw (kg/kg)")
axs[1].grid(True)

axs[2].plot(days, latent_hourly_kWh, 'c-', linewidth=2)
axs[2].set_title("Average Latent Load per Hour (kWh/h)")
axs[2].set_xlabel("Day")
axs[2].set_ylabel("Latent Load (kWh/h)")
axs[2].grid(True)
plt.tight_layout(pad=3)
# --- CO₂ Uptake Simulation ---
# Assuming a constant net CO₂ uptake rate of 10 μmol·m⁻²·s⁻¹ over a 12-hour photoperiod.
days_CO2, cumulative_CO2_kg, daily_uptake_g = simulate_CO2_uptake(crop, area, uptake_rate=10, photoperiod=12)
# Plot cumulative CO₂ uptake.
fig_CO2, ax_CO2 = plt.subplots(figsize=(10, 5))
ax_CO2.plot(days_CO2, cumulative_CO2_kg, 'k-', linewidth=2)
ax_CO2.set_title(f"{crop.capitalize()} – Cumulative CO₂ Uptake (kg) over Growth Cycle")
ax_CO2.set_xlabel("Day")
ax_CO2.set_ylabel("Cumulative CO₂ Uptake (kg)")
ax_CO2.grid(True)
# --- Summary Printout for the Crop ---
total_sensible_heating = np.sum(sensible_heating)
total_sensible_cooling = np.sum(sensible_cooling)
total_latent_cooling = np.sum(latent_cooling)
total_water_condensed = np.sum(water_condensed)
net_power_usage = total_sensible_cooling + total_latent_cooling
# Average detailed HVAC values:
avg_water_added_hourly = np.mean(water_added_hourly)
avg_delta_w = np.mean(delta_w)
avg_latent_hourly_kWh = np.mean(latent_hourly_kWh
# Compute total CO₂ uptake (kg) for the crop.
total_CO2_uptake = cumulative_CO2_kg[-1]
adjusted_ET0 = base_ET0 * (101.3 / ambient_pressure)
print(f"Crop: {crop.capitalize()}")
print(f"  Total growth cycle: {days[-1]} days")
```

```
        print(f"  Adjusted ET0: {adjusted_ET0:.2f} mm/day")
        print(f"  Total water loss (ET): {total_water_loss:.2f} liters (over {area} m²)")
        print("  HVAC Loads (over the cycle):")
        print(f"    Sensible Heating: {total_sensible_heating:.2f} kWh (assumed 0, as cooling restores {temperature_setpoint} °C)")
        print(f"    Sensible Cooling: {total_sensible_cooling:.2f} kWh (equipment load removal)")
        print(f"    Latent Cooling:   {total_latent_cooling:.2f} kWh (for water removal to maintain RH ≤ {humidity_set-point}%)")
        print(f"    Total Water Condensed: {total_water_condensed:.2f} liters")
        print(f"    Net HVAC Energy Usage: {net_power_usage:.2f} kWh (over the growth cycle)")
        print("")
        print("  Detailed HVAC Variables (averaged hourly):")
        print(f"    Equipment Load per Hour: {Q_eq_hour:.0f} kJ/h ({equipment_load_kw:.2f} kW)")
        print(f"    Indoor Air Mass: {m_da:.2f} kg")
        print(f"    Average Water Added per Hour: {avg_water_added_hourly:.4f} kg/h")
        print(f"    Average Increase in Humidity Ratio (Δw): {avg_delta_w:.4f} kg/kg")
        print(f"    Average Latent Load per Hour: {avg_latent_hourly_kWh:.4f} kWh/h")
        print("")
        print(f"  CO₂ Uptake:")
        print(f"    Daily CO₂ Uptake per m²: {daily_uptake_g:.2f} g/m²/day")
        print(f"    Total CO₂ Uptake over the Growth Cycle: {total_CO2_uptake:.2f} kg (for {area} m²)")
        print("-" * 70)
    plt.tight_layout(pad=3)
    plt.show()
if __name__ == '__main__':
    main()
```

1.6. Dehumidifier

Project	New project
Reference	
Notes	

Performance Data		**Heating**	**Cooling**
Model	CFK 315-3-2,5		
Art. no	210825		
Capacity	kW	11.0	10.6

Air Side Data		**Heating**	**Cooling**
Atmospheric Pressure / Altitude	Pa / m	101325.00 / 0.00	
Volumetric Flow	m³/h	1000	1000
Mass Flow	kg/h	1221.30	1162.55
Density	kg/m³	1.22	1.16
Surface Velocity	m/s	1.46	1.46
Air Inlet Temperature	°C	15.0	27.0
Inlet Humidity	%	45.0	85.0
Air Outlet Temperature	°C	47.2	15.2
Outlet Humidity	%	7.1	100.0
Pressure Drop	Pa	20	35

Fluid Side Data		**Heating**	**Cooling**
Fluid	-	Water	Water
Mixture Rate	%	0	0
Volumetric Flow	m³/h	1.93	1.82
Inlet / Outlet Temperature	°C	60.0 / 55.0	4.0 / 9.0
Mass Flow	kg/h	1901.4	1821.1
Density	kg/m³	983.16	999.92
Velocity	m/s	1.97	1.85
Pressure Drop	kPa	61.2	64.2

Heat Exchanger Data		
Tube Volume	l	2.1
Tube Material	-	Copper
Fin Material	-	Aluminium

Dimensions

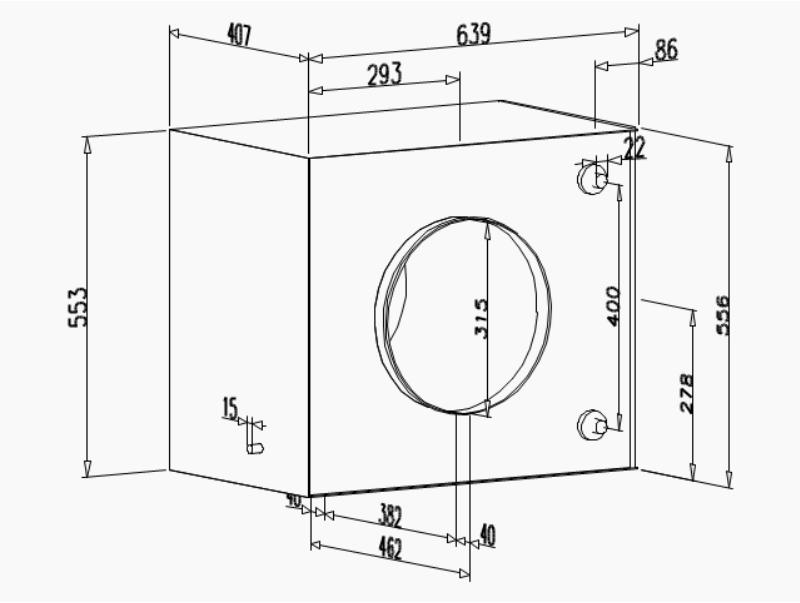

VEAB Heat Tech AB
281 33 Hässleholm
Sweden

Visitor address
Stattenavägen 50
Delivery address
Ängdalavägen 4

Phone
+46 451 485 00

veab@veab.com
www.veab.com

1.7. Gyroid Dehumidifier Code

```
#!/usr/bin/env python3
import math
import numpy as np
import matplotlib.pyplot as plt
from skimage import measure
# Functions
def saturation_pressure(T_C):
    return 0.611 * 10**(7.5 * T_C / (T_C + 237.3))
def reynolds_number(rho, v, d_h, mu):
    return (rho * v * d_h) / mu
def gyroid_hydraulic_diameter(epsilon, specific_surface_area):
    return 4 * epsilon / specific_surface_area
def gyroid_pressure_drop(reynolds, L_tube):
    #Constants from [65]
    a = 0.0086
    b = 1.594
    # pressure drop using the power law correlation
    return a * (reynolds ** b) * (L_tube / 0.04)
def gyroid_coolant_pressure_drop(m_dot_cool, rho_water, mu_water, D_tube, L_tube, t_wall, channel_gap, L_cell,c_f=2,
complexity_factor=1.7):
    #basic parameters
    vol_flow_rate = m_dot_cool / rho_water
    #surface area and flow geometry
    unit_cells_count = (D_tube**2 * np.pi/4 * L_tube) / (0.5*(L_cell**3))
    surface_area = (3.1 * (L_cell**2) * unit_cells_count)*0.92
    flow_area = surface_area * channel_gap
    hydraulic_diameter = 4 * channel_gap
    #flow characteristics
    velocity = vol_flow_rate / flow_area
    reynolds = (rho_water * velocity * hydraulic_diameter) / mu_water
    #friction factor
    f = 64 / reynolds if reynolds < 2300 else 0.316 * reynolds**(-0.25)
    #pressure drop
    path_length = L_tube *c_f
```

```
    dp_base = (f * path_length * rho_water * velocity**2) / (2 * hydraulic_diameter)
    dp_total = dp_base * complexity_factor
    return {
        'vol_flow_rate': vol_flow_rate,
        'unit_cells_count': unit_cells_count,
        'surface_area_m2': surface_area,
        'pressure_drop_pa': dp_total,
        'pressure_drop_kpa': dp_total / 1000,
        'reynolds_number': reynolds,
        'flow_regime': 'Laminar' if reynolds < 2300 else 'Turbulent',
        'hydraulic_diameter_mm': hydraulic_diameter * 1000,
        'flow_velocity_m_s': velocity,
        'flow_area_m2': flow_area,
        'path_length_m': path_length,
        'friction_factor': f
    }
# 1. AIR COOLING CALCULATIONS
# Given air conditions:
air_flow_rate_m3h = 1000            # m^3/h
air_flow_rate = air_flow_rate_m3h / 3600.0
T_air_in = 27.0                     # °C
RH_air_in = 0.85                    # %
T_air_out = 16.0                    # °C
RH_air_out = 0.45                   #%
# Cooling load
Q_cooling = 20100.0                 # W
# 2. Heat Exchanger Parameters
# Overall heat transfer coefficient
U_improved = 120.0                  # W/m^2*K
# Coolant conditions:
T_cool_in = 5.0                     # °C
T_cool_out = 13.0                   # °C
deltaT_cool = T_cool_out - T_cool_in  # °C
# Log–mean temperature difference for counter–flow:
deltaT_hot  = T_air_in - T_cool_out   # °C
deltaT_cold = T_air_out - T_cool_in    #°C
```

```
if abs(deltaT_hot - deltaT_cold) < 1e-6:
    LMTD = deltaT_hot
else:
    LMTD = (deltaT_hot - deltaT_cold) / math.log(deltaT_hot / deltaT_cold)
# Required total heat-transfer area:
A_required = Q_cooling / (U_improved * LMTD)
print("--- COMPACT HEAT EXCHANGER SIZING ---")
print(f"Assumed LMTD: {LMTD:.2f} °C")
print(f"Required exchanger surface area: {A_required:.1f} m^2")
print(f"deltaT_hot: {deltaT_hot:.1f} °C")
print(f"deltaTcold: {deltaT_cold:.1f} °C")
print(f"LMTD: {LMTD:.1f} °C")
# 3. VPD
e_sat_27 = saturation_pressure(T_air_in)   # kPA
e_sat_14 = saturation_pressure(T_air_out)    # kPa
VPD_in = e_sat_27 * (1 - RH_air_in)   # kPa
VPD_out = e_sat_14 * (1 - RH_air_out)  # kPa
print("\n--- VAPOUR PRESSURE DEFICIT ---")
print(f"e_sat_27: {e_sat_27:.3f} kPa")
print(f"e_sat_14: {e_sat_14:.3f} kPa")
print(f"Inlet VPD: {VPD_in:.3f} kPa")
print(f"Outlet VPD: {VPD_out:.3f} kPa")
# 4. Coolant Flowrate
cp_water = 4180.0     # J/(kg*K)
rho_water = 1000.0    # kg/m^3
# Energy balance: Q = m_dot * cp * ΔT  =>  m_dot = Q / (cp * ΔT)
m_dot_cool = Q_cooling / (cp_water * deltaT_cool)   # kg/s
Q_cool_vol = m_dot_cool / rho_water                 # m^3/s
print("\n--- COOLANT FLOW RATE ---")
print(f"m_dot_cool: {m_dot_cool:.3f} kg/s")
print(f"deltaT_cool: {deltaT_cool:.1f} °C")
print(f"Q_cooling: {Q_cooling:.1f} W")
print(f"Required coolant mass flow rate: {m_dot_cool:.3f} kg/s")
print(f"Volumetric flow rate: {Q_cool_vol*1000:.2f} L/s  (or {Q_cool_vol*3600:.1f} m^2/h)")
# 5. Gyyroid Heat exchanger
D_tube = 0.50        # m
```

```
A_tube = math.pi * (D_tube/2)**2  # m^2
print("\n--- CYLINDER GEOMETRY ---")
print(f"Cylinder cross-sectional area: {A_tube:.3f} m^2")
#gyroid periodicity
L_cell = 0.045   # m
print(f"\nChosen gyroid unit cell periodicity: {L_cell*1000:.1f} mm")
# unit cell parameters
A_cell = 3.1 * (L_cell**2)    # m^2
cell_volume = 0.5 * (L_cell**3)        # m^3
S_v = A_cell / cell_volume      # Specific surface area [m^2/m^3]
print(f"A_cell: {A_cell:.7f} m^2")
print(f"cell_volume: {cell_volume:.7f} m^3")
print(f"Achieved specific surface area: {S_v:.3f} m^2/m^3")
# gyroid volume required  needed for heat-transfer area:
V_gyroid = A_required / S_v     # m^3
# compute the tube length needed when filling the tube with the gyroid:
L_tube = V_gyroid / A_tube      # m
print(f"\nTotal gyroid volume required: {V_gyroid:.3f} m^3")
print(f"Computed tube length (fully packed): {L_tube:.3f} m")
if L_tube <= 1.2:
    print("Design target met: Tube length is within 1.2 m.")
else:
    print("Warning: Tube length exceeds 1.2 m; further compaction needed.")
L_tube_safe = 1.1 * L_tube
# 6. Porosity and channel volume
t_wall = 0.0015        # m (mm)
channel_gap = 0.003    # m (mm)
t_total = (2*t_wall) + channel_gap
L_cell_cm = L_cell * 100       #  m to cm.
t_wall_cm = t_total * 100      #  m to cm.
c = (t_wall_cm * math.pi) / L_cell_cm
solid_fraction = 0.65 * c
epsilon = 1 - solid_fraction
V_wall = V_gyroid * solid_fraction       # m^3
V_channel = V_wall / 2
print(f"Level-set parameter c: {c:.4f}")
```

```
print(f"solid_fraction (volume fraction): {solid_fraction:.4f}")

print(f"Porosity (void fraction): {epsilon:.4f}")

print(f"Estimated solid (wall) volume: {V_wall:.4f} m^3")

print(f"Estimated channel (internal) volume: {V_channel:.4f} m^3")

# 7. Air pressure drops using [65]

# air properties

mu_air = 1.8e-5       # Pa*s for air

rho_air = 0.0825       # kg/m^3

# hydraulic diameter for air

d_h_air = gyroid_hydraulic_diameter(epsilon, S_v)

#effective flow area and velocity

A_air_eff = epsilon * A_tube  # m^2

v_air = air_flow_rate / A_air_eff #m/s

#reynolds number for air

Re_air = reynolds_number(rho_air, v_air, d_h_air, mu_air)

#pressure drop for air

deltaP_air = gyroid_pressure_drop(Re_air, L_tube)

print("\n--- AIR SIDE PRESSURE DROP---")

print(f"Hydraulic diameter: {d_h_air*1000:.2f} mm")

print(f"Effective air flow area: {A_air_eff:.4f} m^2")

print(f"Average air velocity in porous medium: {v_air:.3f} m/s")

print(f"Air Reynolds number: {Re_air:.1f}")

print(f"Estimated air pressure drop: {deltaP_air:.2f} Pa")

# coolant hydraulic diameter

d_h_cool = gyroid_hydraulic_diameter(epsilon, S_v)

# 8. Coolant pressure drop

mu_water = 0.001  # Pa*s

coolant_result = gyroid_coolant_pressure_drop(m_dot_cool, rho_water, mu_water, D_tube, L_tube_safe, t_wall, chan-
nel_gap, L_cell)

print("\n--- COOLANT SIDE PRESSURE DROP ---")

print(f"Coolant hydraulic diameter: {coolant_result['hydraulic_diameter_mm']:.2f} mm")

print(f"path length: {coolant_result['path_length_m']:.2f} m")

print(f"Coolant flow_area: {coolant_result['flow_area_m2']:.3f} m^2")

print(f"Coolant flow velocity: {coolant_result['flow_velocity_m_s']:.3f} m/s")

print(f"Coolant Reynolds number: {coolant_result['reynolds_number']:.1f}")

print(f"Flow regime: {coolant_result['flow_regime']}")
```

```
print(f"Estimated coolant pressure drop: {coolant_result['pressure_drop_pa']:.2f} Pa")
print(f"Unit Cell Count: {coolant_result['unit_cells_count']:.1f}")
print(f"Surface_area_m2: {coolant_result['surface_area_m2']:.1f}")
print(f"vol_flow_rate: {coolant_result['vol_flow_rate']:.4f} m^3/s")
print(f"friction_factor: {coolant_result['friction_factor']:.4f}")
# 9. weight of gyroid structure
Weight_gyroid = (V_wall * 2750) / 2
print("\n--- GYROID STRUCTURE WEIGHT ---")
print(f"Estimated gyroid structure weight: {Weight_gyroid:.3f} kg")
# 9. coolant check
# coolant residence time in the exchanger:
residence_time = V_channel / Q_cool_vol  # secs
print("\n--- COOLANT ACCOMMODATION CHECK ---")
print(f"Coolant channel volume: {V_channel:.4f} m^3")
print(f"Coolant volumetric flow rate: {Q_cool_vol:.6f} m^3/s")
print(f"Resulting coolant residence time: {residence_time:.2f} s")
if residence_time > 0.1:
    print("The channel volume is ample relative to the coolant flow rate.")
else:
    print("Warning: The coolant residence time is very short; channel volume may be insufficient!")
# Creating a 3D plot of the gyroid surface
n_points = 100
x = np.linspace(0, L_cell, n_points)
y = np.linspace(0, L_cell, n_points)
z = np.linspace(0, L_cell, n_points)
X, Y, Z = np.meshgrid(x, y, z, indexing='ij')
X_scaled = 2 * np.pi * X / L_cell
Y_scaled = 2 * np.pi * Y / L_cell
Z_scaled = 2 * np.pi * Z / L_cell
F = np.sin(X_scaled) * np.cos(Y_scaled) + \
    np.sin(Y_scaled) * np.cos(Z_scaled) + \
    np.sin(Z_scaled) * np.cos(X_scaled)
verts, faces, normals, _ = measure.marching_cubes(F, level=0, spacing=(x[1]-x[0], y[1]-y[0], z[1]-z[0]))
fig = plt.figure(figsize=(10, 10))
ax = fig.add_subplot(111, projection='3d')
ax.plot_trisurf(verts[:, 0], verts[:, 1], faces, verts[:, 2],
```

```
            cmap='viridis', lw=1)
ax.set_xlabel("X [m]")
ax.set_ylabel("Y [m]")
ax.set_zlabel("Z [m]")
ax.set_title("Gyroid Minimal Surface (Unit Cell)")
plt.show()
R_tube = D_tube / 2
n_points_x = 100
n_points_y = 100
n_points_z = 100
x = np.linspace(-R_tube, R_tube, n_points_x)
y = np.linspace(-R_tube, R_tube, n_points_y)
z = np.linspace(0, L_tube, n_points_z)
X, Y, Z = np.meshgrid(x, y, z, indexing='ij')
F = np.sin(2 * np.pi * X / L_cell) * np.cos(2 * np.pi * Y / L_cell) + \
    np.sin(2 * np.pi * Y / L_cell) * np.cos(2 * np.pi * Z / L_cell) + \
    np.sin(2 * np.pi * Z / L_cell) * np.cos(2 * np.pi * X / L_cell)
mask = (X**2 + Y**2) <= (R_tube**2)
F_masked = F.copy()
F_masked[~mask] = 1.0
verts, faces, normals, _ = measure.marching_cubes(F_masked, level=0, spacing=(x[1]-x[0], y[1]-y[0], z[1]-z[0]))
fig = plt.figure(figsize=(12, 10))
ax = fig.add_subplot(111, projection='3d')
ax.plot_trisurf(verts[:, 0], verts[:, 1], faces, verts[:, 2],
            cmap='viridis', lw=1, alpha=0.9)
theta = np.linspace(0, 2 * np.pi, 50)
z_cyl = np.linspace(0, L_tube, 50)
Theta, Z_cyl = np.meshgrid(theta, z_cyl)
X_cyl = R_tube * np.cos(Theta)
Y_cyl = R_tube * np.sin(Theta)
ax.plot_surface(X_cyl, Y_cyl, Z_cyl, color='gray', alpha=0.3, edgecolor='none')
ax.set_xlabel("X [m]")
ax.set_ylabel("Y [m]")
ax.set_zlabel("Z [m]")
ax.set_title("Gyroid Structure Within Cylindrical Duct")
plt.show()
```

1.8. Heater

Size designation		CV 10	CV 12	CV 16	CV 20	CV 25	CV 31	CV 40
Diameter (∅ mm)		100	125	160*	200	250	315	400 **
Minimum air volume m³/h		43	70	110	170	270	415	690
Output	Voltage							
300 W	230 VAC 1-ph.		X[3]	X[2]				
400 W	230 VAC 1-ph.	X[3]						
600 W	230 VAC 1-ph.	X[3]	X[5]	X[3]	X[2]	X[1]		
900 W	230 VAC 1-ph.		X[7]	X[4]	X[2]	X[2]	X[1]	
1200 W	230 VAC 1-ph.		X[8]	X[5]	X[3]	X[2]	X[1]	
1500 W	230 VAC 1-ph.		X[9]	X[6]	X[3]	X[3]	X[2]	
1800 W	230 VAC 1-ph.		X[10]	X[6]	X[4]	X[3]	X[2]	
2100 W	230 VAC 1-ph.			X[7]	X[4]	X[3]	X[2]	
2700 W	230 VAC 1-ph.			X[8]				

Choose between 61 variants: CV31-90-3

3D 360° | 2D image | Dimensions

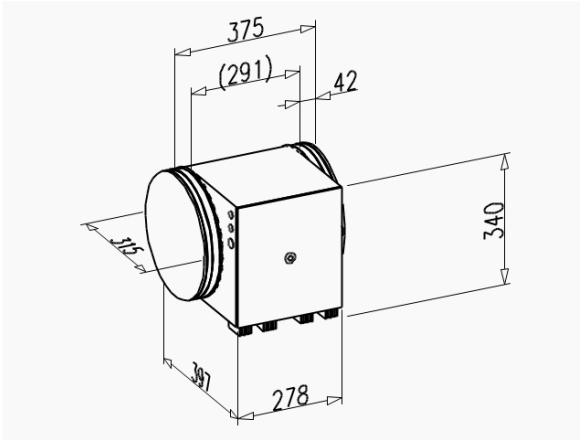

[1]= See pressure drop curve 1
[2]= See pressure drop curve 2
[3]= See pressure drop curve 3
[4]= See pressure drop curve 4
[5]= See pressure drop curve 5
[6]= See pressure drop curve 6
[7]= See pressure drop curve 7
[8]= See pressure drop curve 8
[9]= See pressure drop curve 9
[10]= See pressure drop curve 10
[11]= See pressure drop curve 11
[12]= See pressure drop curve 12

Pressure Drop Chart

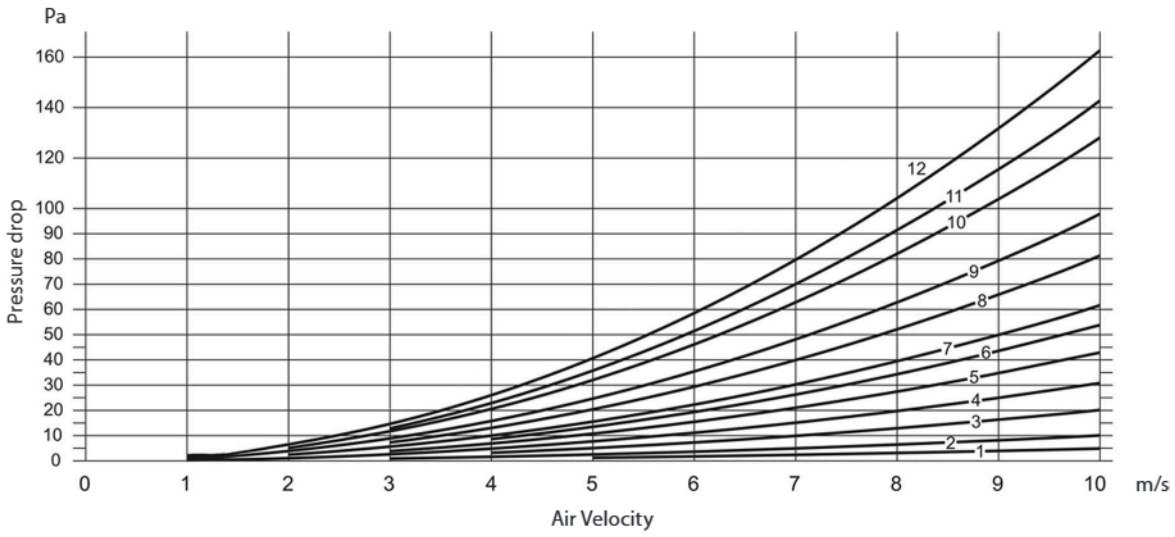

1.9. VOC filter

Summary

- **3-Stage Filtration:** Captures airborne particles as well as mold and bacteria and viruses.
- **VortexAir™ Technology:** Increases indoor air circulation and filtration efficiency.
- **AirSight™ Plus Technology:** Laser Dust Sensor scans surrounding air for airborne particles.
- **PM2.5 Display:** Displays the amount of airborne particles detected by the laser dust sensor.
- **ARC Formula™:** Helps neutralize household odors and pet smells.
- **QuietKEAP™ Technology:** Keeps noise levels as low as 24dB.
- **App Control:** Control settings, check filter life, receive real-time air quality updates and more.
- **Voice Control:** Connect air purifier to Amazon Alexa or Google Assistant™.
- **Air Quality Indicator Rings:** Indicates real-time air quality as Bad, Moderate, Good, or Very Good.

Product Specifications

Voltage: AC 120V, 60Hz

Rated Power: 38W

Effective Range: 403 ft^2 / 37 m^2

Dimensions: 10.8 x 10.8 x 20.5 in / 27.4 x 27.4 x 52 cm

Weight: 14.12 lb

Operating Conditions Temperature: 14°–104°F / -10°–40°C

Humidity: < 85% RH

Noise Level: 24–52dB

CADR: 260 CFM / 442 m^3/h

Standby Power: < 2W

1.10. Sensors

EE650

Air Velocity Sensor for HVAC Applications

The EE650 air velocity sensor is designed for accurate and reliable measurement in building automation and ventilation applications.

Innovative Design

The device employs an innovative air velocity sensing element, which operates on the thermal anemometer principle and is manufactured by E+E in state of the art thin-film technology. Due to its innovative design, the sensing element is very robust and highly insensitive to pollution, which leads to outstanding long-term performance.

User Configuration

For the EE650 with analogue output, the measuring range 0...10 / 15 / 20 m/s (0...2 000 / 3 000 / 4 000 ft/min), the output signal 4 - 20 mA or 0 - 10 V as well as the response time 1 or 4 seconds are selectable by jumpers.
The response time, the termination resistor and the bus address of the Modbus RTU version can also be easily set on the electronics board.

Installation and Adjustment

The enclosure design and the mounting flange included in the scope of supply allow for fast and easy installation.
EE650 adjustment, output scale setting and interface parameter selection can be easily performed using the free PCS10 Product Configuration Software and an optional stick.

EE650 for duct mounting

EE650 with remote probe

Dimensions

Values in mm (inch)

Duct mount

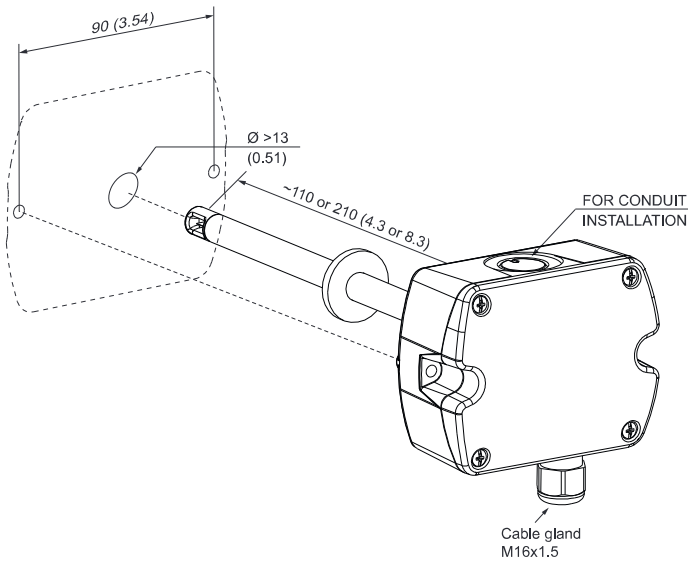

Remote probe

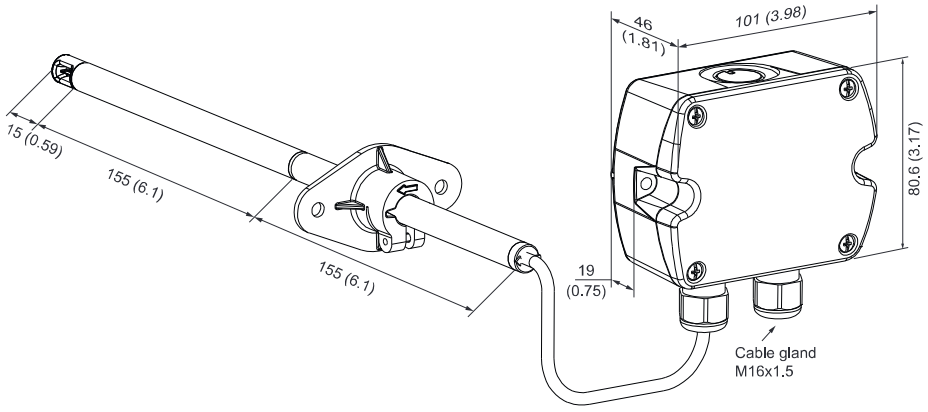

Mounting flange

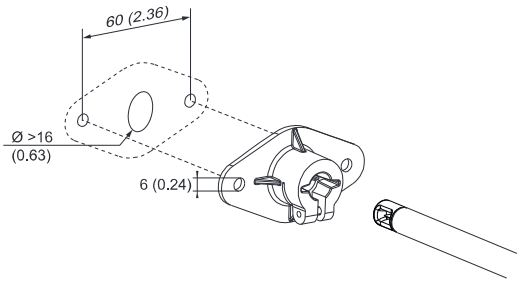

Technical Data

Measurands

Air Velocity (v)

Measuring range	0...10 m/s (0...2000 ft/min) 0...15 m/s (0...3000 ft/min) 0...20 m/s (0...4000 ft/min) (factory setting)
Accuracy[1)] from 0.2 m/s, @ 20 °C (68 °F), 45 %RH and 1 013 hPa (14.7 psi)	± (0.2 m/s (40 ft/min) + 3 % of m. v.) mv = measured value
Response time t_{90}, typ. @constant temperature, selectable via jumpers, only for analogue output	4 s (factory setting) down to 1 s

1) The accuracy statement includes the uncertainty of the factory calibration with an enhancement factor k=2 (2-times standard deviation). The accuracy was calculated in accordance with EA-4/02 and with regard to GUM (Guide to the Expression of Uncertainty in Measurement).

Outputs

Analogue

Air velocity v measuring range selectable via jumpers, only for analogue output	0 - 10 V 4 - 20 mA (3-wire, factory setting)	$0 < I_L < 1$ mA $R_L \leq 500\ \Omega$	I_L = load current R_L = load resistance

Digital

Digital interface	RS485 (EE650 = 1 unit load)
Protocol **Factory settings** **Supported Baud rates** **Measured data types**	Modbus RTU 9600 Baud, parity even, 1 stop bit, Modbus address 65 9600, 19200 and 38400 FLOAT32 and INT16

General

Power supply class III USA & Canada: Class 2 supply necessary		24 V AC/DC ±20 %	
Current consumption, max.		**AC supply**	**DC supply**
	Analogue output	170 mA	70 mA
	RS485	120 mA	50 mA
Electrical connection		Screw terminals max. 1.5 mm² (AWG 16)	
Cable gland		M16x1.5	
Humidity working range		5...95 %RH, non-condensing	
Temperature working range	**Probe** **Electronics** **Storage**	-25...+50 °C (-13...+122 °F) -10...+50 °C (+14...+122 °F) -30...+60 °C (-22...+140 °F)	
Enclosure material		Polycarbonate (PC), UL94V-0 approved	
Protection rating	**Enclosure** **Remote probe**	IP65 / NEMA 4X IP20	
Electromagnetic compatibility		EN 61326-1 FCC Part15 Class A	EN 61326-2-3 ICES-003 Class A Industrial environment
Conformity		CE UKCA	

EE850

CO_2 and Temperature Sensor for Duct Mounting

The EE850 combines CO_2 and temperature (T) measurement in an innovative enclosure. It is ideal for demand controlled ventilation and building automation. With a CO_2 measuring range of up to 10 000 ppm and a T working range of -20...+60 °C (-4...+140 °F), the EE850 can be employed also in demanding climate and process control applications.

Long-Term Stability

The EE850 incorporates the E+E dual wavelength NDIR CO_2 sensor, which compensates for ageing effects, is highly insensitive to pollution and offers outstanding long term stability.

High Measurement Accuracy

A multiple point CO_2 and T factory adjustment procedure leads to excellent CO_2 measurement accuracy over the entire T working range.

Functional Design

Installed into a duct, a small amount of air flows through the divided probe to the CO_2 sensing cell located inside the sensor enclosure and back into the duct. The T sensing element is placed inside the probe. The functional enclosure facilitates easy and fast mounting of the sensor with closed cover.

Analogue, Digital and Passive T Outputs

The CO_2 and T measured data is available on analogue outputs. Additionally, the RS485 interface supplies all values via Modbus RTU protocol.

Easy Configuration and Adjustment

An optional stick and the free PCS10 Product Configuration Software facilitate the configuration and adjustment of the EE850.

EE850 duct mount

Dimensions

Values in mm (inch)

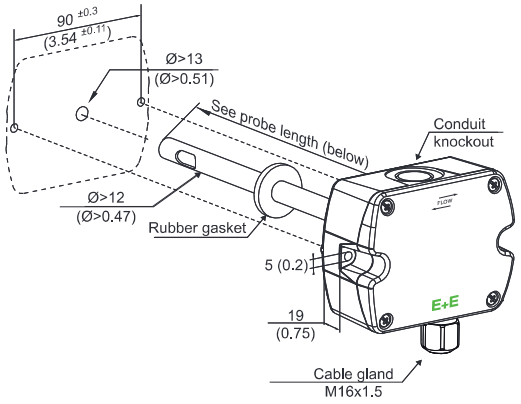

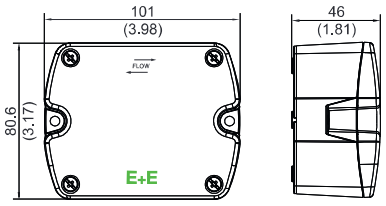

Mounting flange

(Included in the scope of supply)

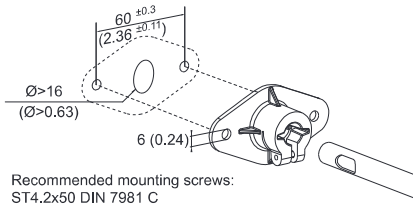

Recommended mounting screws:
ST4.2x50 DIN 7981 C

Probe length

L200:

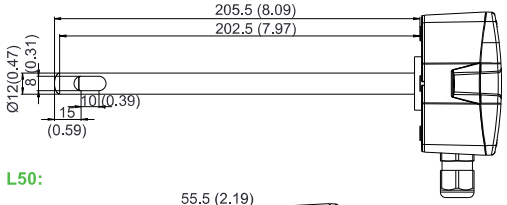

L50:

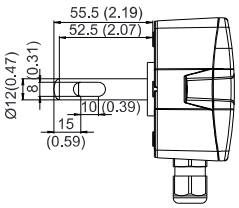

Technical Data

Measurands

CO_2

Measurement principle	Dual wavelength non-dispersive infrared technology (NDIR)
Measuring range	0...2 000 / 10 000 ppm
Accuracy @ 25 °C (77 °F) and 1 013 mbar (14.7 psi) **0...2 000 ppm** **0...10 000 ppm**	 < ±(50 ppm +2 % of measured value) < ±(100 ppm +5 % of measured value)
Temperature dependency, typ. in the range of -20...+45 °C (-4...+113 °F)	±(1+ CO_2 concentration [ppm] / 1 000) ppm/°C ± 0.556 * (1+ CO_2 concentration [ppm] / 1 000) ppm/°F
Response time t_{63}, typ.	<100 s at 3 m/s (590 ft/min) air speed in the duct
Measuring interval	Approx. 15 s
Calibration interval Recommended under normal operating conditions in building automation.	>5 years

Temperature (T)

Measuring range	-20...+60 °C (-4...+140 °F)
Accuracy @ 20 °C (68 °F)	±0.3 °C (±0.5 °F)
Response time t_{63}	<50 s

Outputs

Analogue

T: according to ordering guide	0 - 10 V	-1 mA < I_L < 1 mA	I_L = load current
CO_2 **0...2 000 / 10 000 ppm**	0 - 10 V 4 - 20 mA	-1 mA < I_L < 1 mA R_L < 500 Ω	 R_L = load resistance

T sensor passive

2-wire-connection	T sensor type according to order code, see ordering guide
Wire resistance (terminal - sensor), typ.	0.4 Ω

Digital

Digital Interface	RS485 (EE850 = 1/10 unit load)
Protocol **Factory settings** **Supported Baud rates** **Measured data types**	Modbus RTU Baud rate acc. to order code, parity even, 1 stop bit, Modbus address 67 9 600, 19 200 und 38 400 FLOAT32 and INT16

Technical Data

General

Power supply class III USA & Canada: Class 2 supply necessary, max. voltage 30 V DC	24 V AC ±20 % 15 - 35 V DC
Current consumption, typ.	15 mA + output current
Peak current, max..	350 mA for 0.3 s (analogue output) 150 mA for 0.3 s (RS485 interface)
Minimum air speed in the duct, min.	1 m/s (196 ft/min)
Electrical connection	Screw terminals max. 2.5 mm^2 (AWG 14)
Cable gland	M16x1.5
Working and storage conditions	-20...+60 °C (-4...+140 °F) 0...95 %RH, non-condensing
Enclosure material	Polycarbonate (PC), UL94 V-0 approved
Protection rating **Enclosure** **Probe**	IP65 / NEMA 4X IP20
Electromagnetic compatibility	EN 61326-1 EN 61326-2-3 Industrial environment FCC Part15 Class A ICES-003 Class A
Conformity	EN 45545-2 (HL3) CE UKCA
Configuration and adjustment	PCS10 Product Configuration Software (free download) and USB-C configuration stick

Ordering Guide

	Feature	Description	Code	
			EE850-	
Hardware Configuration	Model	CO_2	M10	
		CO_2 + T		M11
	CO_2 measuring range	0...2000 ppm	HV1	
		0...10000 ppm	HV3	
	Output	0 - 10 V	A3	A3
		4 - 20 mA	A6	
		RS485	J3	J3
	T sensor passive[1]	Without T sensor		No code
		Pt1000 DIN A		TP3
	Probe length	50 mm (1.97")	L50	
		200 mm (7.87")	No code	No code
Setup Analogue Outputs[1]	Output 2 measurand	Temperature T [°C]		No code
		Temperature T [°F]		MB2
	Output 2 scaling low	0		No code
		Value - within the range -20...60 °C		SBL*Value*
	Output 2 scaling high	50		No code
		Value - within the range -20...60 °C		SBH*Value*
Setup RS485[3]	Protocol	Modbus RTU[2]	P1	
	Baud rate	9600	BD5	
		19200	BD6	
		38400	BD7	

1) Not with RS485 output (J3) or 50 mm probe length (L50) / T-Sensor details see www.epluse.com/R-T_Characteristics.
2) Factory setting: Parity even, 1 stop bit; Modbus Map and communication setting: See User Manual and Modbus Application Note at www.epluse.com/ee850.
3) Not with analogue output A3 und A6.

Technical Data

Configurability

Device	DIP switches	PCS10
Analogue output without auto-zero	✓	✓
Analogue output with auto-zero	✓	✓
Digital interface without auto-zero	✓	✓
Digital interface with auto-zero	✓	✓

Configuration options see above or manual at www.epluse.com/ee600.

Ordering Guide

	Feature	Description	Code		
			EE600-		
Hardware configuration	Measuring range[1]	0...1 000 Pa (0...4 inch WC, 0...10 mbar, 0...1 kPa)	HV52		
		0...10 000 Pa (0...40 inch WC, 0...100 mbar, 0...10 kPa)	HV53		
		±1 000 Pa (±4 inch WC, ±10 mbar, ±1 kPa)			HV54
		±10 000 Pa (±40 inch WC, ±100 mbar, ±10 kPa)			HV55
	Output	4 - 20 mA (2-wire)			A6
		Analogue (voltage and current output)	A7		
		RS485		J3	
	Display	Without display	No code		
		Display with backlight	D2		
		Display without backlight			D1
	Auto-zero	Without auto-zero	No code		
		Auto-zero	AF8		
Software setup	Protocol	Modbus RTU[2]		P1	
	Baud rate	9 600		BD5	
		19 200		BD6	
		38 400		BD7	

1) Measuring ranges 0...25 % / 50 % / 75 % / 100 % FS, selectable with DIP switches at analogue output or PCS10.
2) Factory setting: Even parity, 1 stop bit; Modbus Map and communication setting: See User Manual and Modbus Application Note at www.epluse.com/ee600.

Values in mm (inch)

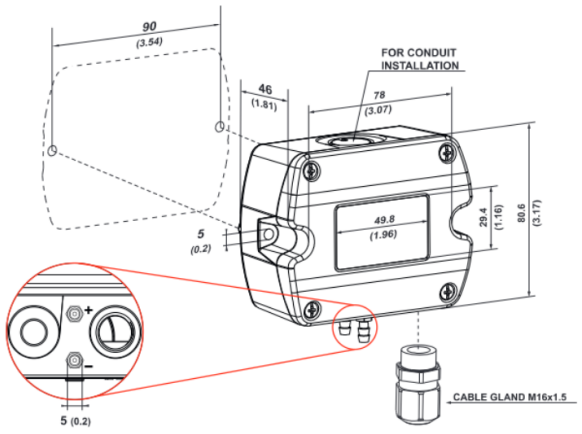

Pressure fittings Ø5 (0.2)
\+ high pressure
\- low pressure

Pressure connection set is included in the scope of supply.

Technical Data

Measurands

Differential Pressure (Δp)

Measurement principle	Piezoresistive, no flow-through
Measuring range	
4 - 20 mA (2-wire) output	±1 000 Pa (±4 inch WC) ±10 000 Pa (±40 inch WC)
Voltage and current output / RS485	0...1 000 Pa (0...4 inch WC) 0...10 000 Pa (0...40 inch WC)
Analogue scaling	
4 - 20 mA (2-wire) output	±250 / ±500 / ±750 / ±1 000 Pa..... field selectebale with DIP switches[1)] ±2 500 / ±5 000 / ±7 500 / ±10 000 Pa.... field selectebale with DIP switches[1)]
Voltage and current output	0...250 / 500 / 750 / 1 000 Pa..... field selectebale with DIP switches[2)] 0...2 500 / 5 000 / 7 500 / 10 000 Pa ..... field selectebale with DIP switches[2)]
with PCS10	Configurable within max. measuring range
Accuracy @ 20 °C (68 °F), incl. hysteresis, non-linearity and repeatability	±0.5 % fs fs = full scale (1 000 Pa or 10 000 Pa)
Temperature dependency, typ.	<0.03 % from fs/K
Response time t_{90}	
Analogue output[1,2)]	50 ms / 500 ms / 2 s / 4 s field selectable with DIP switches Configurable from 0.05 to 30 s with PCS10
Digital interface[3)]	Configurable from 0.5 to 30 s with PCS10
Auto-zero interval	
Factory setting	24 h
4 - 20 mA (2-wire) output	Configurable from 90 min to 7 days with PCS10. Can be disabled.
Voltage and current output / RS485	Configurable from 10 min to 7 days with PCS10. Can be disabled.
Long-term stability	<0.5 % fs/year fs = full scale (1 000 Pa or 10 000 Pa)
Overload limits **1 000 Pa fs**	±10 000 Pa
10 000 Pa fs	±80 000 Pa

1) Factory setup A6: measuring range ±100 % fs; response time t_{90}: 50 ms; displayed unit: Pa; other ranges upon request.
2) Factory setup A7: measuring range 0...100 % fs; response time t_{90}: 50 ms; displayed unit: Pa; display backlight: on; other ranges upon request.
3) Factory setup RS485: response time t_{90}: 500 ms; displayed unit: Pa; display backlight: on.

Calculated measurands

		Unit
Level Indicator	LI	cm
		inch
Volume flow	V'	m^3/h
		l/s
		m^3/s
		ft^3/min
Air velocity	v	m/s
		ft/min
Filter contamination level	FCL	%

Technical Data

Outputs

Analogue

4 - 20 mA (2-wire) output	$R_L \leq 500\ \Omega$		R_L = load resistance
Voltage and current output[1)]	0 - 5 V or 0 - 10 V and 0 - 20 mA or 4 - 20 mA (3-wire)	-1 mA < I_L < 1 mA $R_L \leq 500\ \Omega$	I_L = load current R_L = load resistance

1) Voltage and current output signals available simultaneously at the spring loaded terminals (factory setup: 0 - 10 V / 4 - 20 mA). Settings selectable with DIP switches.

Digital

Digital interface	RS485 (EE600 = 1/2 unit load)
Protocol **Factory settings** **Supported Baud rates** **Data types for measuring values**	Modbus RTU Baud rate see order information, parity even, 1 stop bit, Modbus address 43 9600, 19200 and 38400 FLOAT32 and INT16

General

Power supply class III USA & Canada: Class 2 supply necessary, max. voltage 30 V DC			
4 - 20 mA (2-wire) output	15 - 35 V DC		
Voltage and current output / RS485	15 - 35 V DC or 24 V AC ±20 %		
Current consumption, typ. @ 0 Pa (0 psi) / 24 V DC		**Analogue output**	**Digital interface**
	Without display	23 mA	8 mA
	Display with backlight	49 mA	29 mA
	Display without backlight and 4 - 20 mA (2-wire)	According to output current, max. 20 mA	
Electrical connection **Analogue output**	Spring-loaded terminals, max. 1.5 mm^2 (AWG16)		
Digital interface	Screw terminals, max. 2.5 mm^2 (AWG14)		
Cable gland	M16x1.5		
Display	Graphic, with backlight		
Selectable units on display with **analogue output via DIP switch**	Pa, kPa, mbar, kPa		
analogue output and digital interface via PCS10	Pa, kPa, mbar, kPa, inch WC, m^3/h, m^3/s, ft^3/min, l/s m/s, ft/min, %		
Humidity range	0...95 %RH, non-condensing		
Temperature range **Operation**	-20...+60 °C (-4...+140 °F) / -20...+50 °C (-4...+122 °F) with display		
Storage	-40...+70 °C (-40...+158 °F) / -20...+60 °C (-4...+140 °F) with display		
Enclosure **Material**	Polycarbonate, UL94 V-0 (with display UL94 HB) approved		
Protection rating	IP65 / NEMA 4X		
Electromagnetic compatibility	EN 61326-1 Industrial environment FCC Part15 Class A ICES-003 Class A		
Shock and vibration	Tested according to EN 60068-2-64 and EN 60068-2-27		
Conformity	CE UKCA		

2 SPECIFICATIONS

Analytical Performance

Measuring range Typical Maximum	**in units of hPa** 0-1000 hPa 0-2000 hPa	**in units of %O_2** 0-100% O_2 (gas)
Accuracy* @ 10°C – 40°C	±0.2 hPa at 10 hPa ±5 hPa at 200 hPa ±20 hPa at 1000 hPa	±0.02% O_2 at 1% O_2 ±0.5% O_2 at 20% O_2 ±2% O_2 at 100% O_2
Accuracy* @ -10°C – 60°C	±1 hPa at 10 hPa ±10 hPa at 200 hPa	±0.1% O_2 at 1% O_2 ±1% O_2 at 20% O_2
Resolution*	±0.1 hPa at 10 hPa ±1 hPa at 200 hPa ±5 hPa at 1000 hPa	±0.01% O_2 at 1% O_2 ±0.1% O_2 at 20% O_2 ±0.5% O_2 at 100% O_2
Detection limit	0.1 hPa	0.01% O_2
Response time (t_{63})	<2 sec.	
Drift	typ. <1% O_2 / year**	
Max. number of measurements	>500 million ***	
Lifetime	typ. >5 years ***	
Warm-up time	3 min (reduced accuracy during warm-up)	
Internal atmospheric pressure sensor measurement range	300 – 1100 mbar (measured through the venting capillary at the backside of the housing)	

* given for factory calibration. Units of %O_2 given for 1013 mbar ambient air pressure.
** at 21% O_2, 25°C, 1013 mbar ambient gas pressure, protected from direct sunlight. The drift can be significantly increased after the exposure to elevated temperature >60°C or to specific chemicals (refer to section 3).
*** at 21% O_2, 25°C, 1013 mbar ambient gas pressure, protected from direct sunlight.

Note, the FDO2 outputs oxygen partial pressure pO (hPa). The unit volume percent oxygen (%O_2) is given here only for convenience. If the air pressure P at the oxygen sensing membrane is identical to the air pressure at the venting capillary on the backside of the housing, then the measurement of the internal pressure sensor can be used for converting pO into units of %O_2 by the formula:

$$\text{volume percent oxygen}[\%O_2] = 100 \times pO[\text{hPa}] / P[\text{hPa}]$$

FDO2
Optical Oxygen Sensor

Environment

Temperature range during operation	-10 to 60°C
Temperature range during storage	-40°C to 60°C
	Note: Exposure to temperatures >60°C might lead to increased drift of the oxygen measurement within the next weeks.
Humidity	Backside: Non-condensing Sensing Membrane: Dew point must not be within the membrane
Maximum absolute pressure	20 bar
Maximum differential pressure	3 bar

Interface

Supply Voltage	3.3 – 5.0 V DC **
Standby / Peak Currents	ca. 8 mA / 40 mA *
Energy Consumption per Measurement	ca. 1-2 mAs
Communication Interface	3.0 V UART (max. 3.3 V)
Connector	Molex 560020-0420

* inrush currents after power up can be higher

Mechanical

Dimensions	Ø 28,5 mm x 28 mm
Weight	10,5 g
Mounting Thread	M16 x 1
Housing Material	Polycarbonate
Conformity to RoHS directive	RoHS compliant, lead free

** WARNING:

If the supply voltage is below 3.3 V DC (e.g. 3.0 V DC), the digital interface of the sensor can be still working, but the oxygen readings might show significant deviations from the real oxygen values. It is on the user's authority to supervise the supply voltage and to discard the oxygen readings, if the supply voltage falls below 3.3 V DC.

3 CROSS-SENSITIVITY AND CHEMICAL COMPATIBILITY

The following table shows the compatibility and possible cross sensitivities to some important chemical substances at a given concentration range. An “X” under “OK” indicates compatibility. “Cross-Sensitivity” indicates that the oxygen measurement is influenced by this substance. “Damage” indicates that this substance might physically damage the FDO2 (marked in red).

Substance	Concentration	OK	Cross-Sensitivity	Damage	Comment
Moisture	0-100%	X			
CH_4	<20%	X			
Cl_2			X	X	
CO	<20%	X			
CO_2	<20%	X			
H_2S	< 1%	X			
NO	< 1%	X			1.
NO_2			X	X	2.
N_2O	< 1%	X			
Inorganic acids / bases	< 1%	X			
"Methanol, Ethanol, Isopropanol, Formic Acid, Acetic Acid"	< 0.1%v	X			3.
"Methanol, Ethanol, Isopropanol, Formic Acid, Acetic Acid"	> 0.1%v		X		4.
Ethylene oxide			X		5.
Other volatile organic compounds			(X)	(X)	6.

Comments:

1. NO may form NO_2 in presence of oxygen.
2. Ca. 5-10 times more sensitive to NO_2 than to oxygen. Slow degradation over time.
3. 0.1%v in gas corresponds approximately to the vapor pressure above a 0.5-1% solution in water at 25°C.
4. Recalibration after conditioning at constant substance levels might be possible.

Concept

GASERA ONE PULSE can be configured for several applications and it measures up to 9 gases plus H_2O in one instrument. Gases are measured selectively by choosing up to 10 optical filters with narrow spectral bands for target and interfering gases.

Advanced multi-component analysis

In the unique analysis method several mid-IR spectral regions can be used for analysing each gas component with minimal cross-sensitivity. Unlike in conventional NDIR systems, the analysis in GASERA ONE PULSE is based on a chemometric least squares fit of sample response to calibration data providing unmatched selectivity.

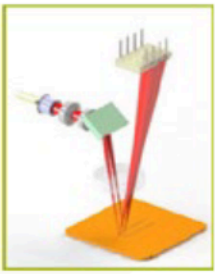

Ultra-sensitive patented optical cantilever microphone

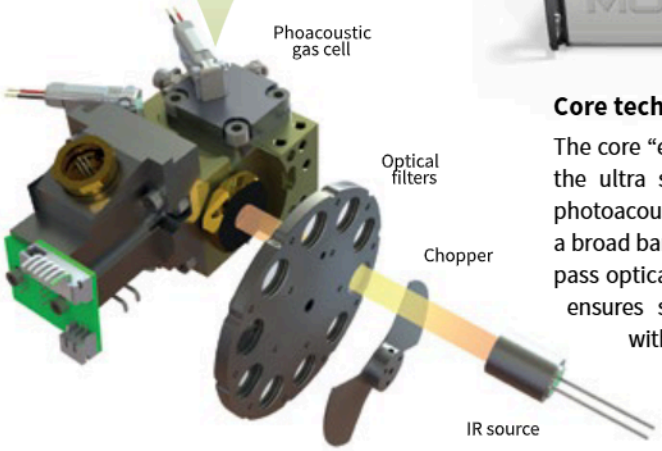

Available options

MULTIPOINT SAMPLER enhances the monitoring capabilities by increasing the number of sample inlets up to 12. In addition, it performs automated sampling from multiple points.

Core technology

The core “engine” is based on combining the ultra sensitive cantilever enhanced photoacoustic detection technology with a broad band IR source and narrow band-pass optical filters. This unique approach ensures stable and reliable operation with high sensitivity and wide dynamic range. Extremely versatile by design, GASERA ONE PULSE can measure down to trace levels of almost any gas that absorbs infrared light.

Features include

- Multiple gases analyzed simultaneously
- ppb to sub-ppm detection limits
- Response time user configurable from 15 seconds to a few minutes
- Wide dynamic range and stable operation
- No consumables
- Low sample volume (few ml)
- Built-in gas exchange system
- Recommended re-calibration interval of 12 months
- User configurable monitoring tasks
- Intuitive user interface
- Built-in display presents results both numerically and graphically
- Gas cell stabilized to 50 °C and 850 mbar to avoid drifts due to changes in environmental conditions

Measurable gases include

- Anesthetics: desflurane, enflurane, isoflurane, sevoflurane etc.
- Greenhouse gases: CF_4, C_2F_6, R13, R-134a, CO_2, N_2O etc.
- Tracer gases: SF_6, R-134a, HFO-1234yf
- Hydrocarbons: CH_4, C_2H_2, C_2H_4, C_2H_6 etc.
- Inorganics: CO, CO_2, H_2O, N_2O, NF_3, NH_3, SF_6, SO_2
- VOCs: acetone, benzene, ethanol, formaldehyde, methanol, toluene, xylenes etc.

Application examples

Animal husbandry

Monitoring emissions from livestock, individual animals and air quality in animal shelters.

Fume hood performance testing

Leak testing from fume hoods using SF_6.

Greenhouse gases research

Measuring GHG emissions from air, soil and water in situ to evaluate the climatic effects.

Occupational health and safety

Measuring toxic gas leakage from industry.

Photocatalysis

Measuring several gases in photocatalytic equipment performance evaluation.

Refrigerant leakage

Monitoring refrigerant leakage from HVAC systems.

SF_6 leakage

SF_6 leak detection in power utilities and switchgear manufacturing.

Soil analysis

Evaluation of N_2O and NH_3 emissions from soil due to fertilization

Tracer gases

Measuring air exchange using tracer gases.

Waste anesthetic gases

Monitoring the levels of anesthetic gases such as fluranes and N_2O in hospital operating theatres.

GASERA ONE PULSE

General

- 19” 3U (unit) housing for both table top and rack mount operation
- Dimensions: 48,4 cm W x 13,9 cm H x 44 cm D (19.1 in W x 5.5 in H x 17.3 in D)
- Weight: approx 13 kg
- Built-in computer with a 7” WSVGA display
- Data storage capacity sufficient for at least 1 year of continuous monitoring of a full set of gases with the shortest sampling interval
- Total internal gas volume 30 ml
- 2 gas connections in the rear including 2 sample input connections equipped with user changeable filters for dust and small particles
- Electrical connections:

  Input voltage: 90...264 Vac, 47...63 Hz

  Input power: 75 W max.
- Interface: Ethernet, USB and optionally Serial over USB, current message or voltage message. Supports MODBUS and AK-protocol.

Standards

- Complies with the Low Voltage Directive 2014/35/EU, EMC Directive 2004/108/EC and ROHS 2 directive 2011/65/EU

Measurement specifications

- Response time: 15 seconds to few minutes depending on user configurable channel integration time (C.I.T.) and gas exchange routine.
- Detection limit: gas and light source dependent. Typically from sub-ppb to sub-ppm
- Dynamic range: typically 5 orders of magnitude (i.e. 100 000 times the detection limit)
- Repeatability: less than 1 % of measured value in operational conditions at the calibration concentration
- Accuracy: limited by the calibration gas accuracy at the calibration concentration. Typically 2–5 %
- Temperature stability: ambient temperature change within the operational temperature range will not cause drift
- Pressure stability: Sample gas pressure change within the pressure range will not cause drift

Environment

- Operational conditions:

  Temperature range: 0 °C – +40 °C

  Humidity: below 90% RH, non-condensing

  Pressure range: ambient level

  Dust/water resistance: IP20 (IEC 529)
- Storage conditions:

  Temperature range: -20 °C – +60 °C
- Sample gas conditions:

  Temperature: 0 – +49 °C

  Humidity: non-condensing, maximum relative humidity 80% for temperatures up to 35°C, decreasing linearly to 35% relative humidity at 49°C

  Pressure: 750 mbar...1050 mbar

  Gas flow: approx 0.6 liters/minute during the gas exchange.

  Particulates < 1 μm

Gasera Ltd. | Lemminkäisenkatu 59, 20520 Turku, FINLAND | sales@gasera.fi